EXPERIMENTAL STUDIES ON PORE SCALE MULTIPHASE FLOW IN HOMOGENEOUS AND HETEROGENEOUS MICROMODELS USING MICRO-PIV

A Thesis

Submitted in Partial Fulfillment of the Requirements for

the Award of the Degree of

DOCTOR OF PHILOSOPHY

By

MD NAJRUL HAQUE

(Reg. No. 146103050)

DEPARTMENT OF MECHANICAL ENGINEERING

INDIAN INSTITUTE OF TECHNOLOGY GUWAHATI

GUWAHATI – 781 039, INDIA

September, 2022

Declaration

I hereby certify that the work presented in this dissertation entitled 'Experimental Studies on Pore Scale Multiphase Flow in Homogeneous and Heterogeneous Micromodels Using Micro-PIV,' is utterly performed by myself, else stated, under the supervision of Professor Ujjwal K. Saha and Professor Anugrah Singh. Any part of this work has not earlier been submitted for the award of any degree, diploma, associate-ship, fellowship or its equivalent to any University or Institution.

Date: September 16, 2022

Md Najrul Haque
Registration No. 146103050
Department of Mechanical Engineering
Indian Institute of Technology Guwahati
Guwahati-781039

Certificate

It is certified that the work delineated in the thesis entitled 'Experimental Studies on Pore Scale Multiphase Flow in Homogeneous and Heterogeneous Micromodels Using Micro-PIV,' submitted by Md Najrul Haque, a student in the Department of Mechanical Engineering, Indian Institute of Technology Guwahati, India, for the Award of the Degree of Doctor of Philosophy has been carried out under our supervision. This research work has not been submitted previously elsewhere for the award of any other degree or diploma.

Ujjwal K. Saha
Professor
Department of Mechanical Engineering
Indian Institute of Technology Guwahati
Guwahati-781039

Anugrah Singh
Professor
Department of Chemical Engineering
Indian Institute of Technology Guwahati
Guwahati-781039

Acknowledgements

I would like to acknowledge the contribution to this work of a number of people, whose support and assistance played a key role in my research in the past years.

I would like to thank my advisors, Professor Ujjwal K. Saha and Professor Anugrah Singh for their assistance and guidance in research and for their remarkable support in case of experimental difficulties.

Furthermore, I would like to thank my doctoral committee members for all the preparation work and organization, which gave me new inspiration and motivation for this work.

I am very grateful to IIT Guwahati for giving me this great and unique opportunity and financial support to pursue my Doctorate degree in the department of mechanical engineering. Also special thanks to CIF lab, IIT Guwahati for providing the experimental facilities. I want to thank Mr. Ganesh Kamble, Jost engineering, Dantec dynamics, for his selfless elaborated advice during the experiments.

Finally, I want to thank my family for their incredible support during my research studies. Your help, patience and love made it a lot easier to do my research and finish my studies. Mother, father, my wife and my siblings and all the family members, thanks for being with me in good as well as in hard times!

Md Najrul Haque

Abstract

The increasing demands for oil, water, and food produced in an environmentally sound manner have placed emphasis on the manner of their production, a major part of which is concerned with flow through porous media. The movement of materials through porous media is of interest in many disciplines: in chemical engineering-adsorption, petroleum engineering-displacement of oil with gas, water and miscible solvents; in hydrology movement of trace pollutants in water systems, recovery of water for drinking and irrigation, salt water encroachment into fresh water reservoirs; in soil physics movement of water, nutrients, and pollutants into plants; in biophysics-life processes such as flow in the lung and the kidney.

Micromodels are useful tool to study the fluid flow behavior in porous media at micron scale that is relevant to the petroleum recovery. During the last 30 years, micromodels have found to be the most precious tool, which allow the observation of fluid flow and transport at the micron scale in many processes related to chemical, biological, and physical fields of engineering. The number of research projects that employ microfluidic devices has expanded the application of this technique to more innovative fields of study over recent decades. Oil and gas production, a multidisciplinary industrial field, has benefited from the opportunities that microfluidic devices provide to study microscale processes, such as adhesion, interfacial tension (IFT) alteration and multiphase pore scale transportation. Obtaining a deeper understanding through the micromodel visualization experiments, the governing factors that influences the flow behavior inside porous media can be understood effectively.

Micro-fluidic devices have been designed and used to investigate immiscible fluid-fluid displacement processes. Due to their optically transparent nature, such devices allow direct visualization of pore scale events using light microscopy. In this thesis, we focus on imaging multiphase flow phenomena at the pore scale within specifically designed micro-models using optical microscopy. The flow channel designs have been selected to investigate fundamental questions relating to fluid displacement mechanisms.

The diversity of proposed micromodel research and the associated requirements have led researchers to develop new methodologies, materials and techniques to overcome challenges attributed to micromodel visualization experiments. In this work, the fundamentals of steady flow through porous media: it discusses single-fluid flow, multi fluid immiscible flow,

including the effects of heterogeneity, non-uniformity, and anisotropy of media in the form of fracture and multi porosity.

First, this research tries to adopt an alternative procedure of fabrication of micromodel, which is simple and cost effective method compared to the traditional techniques like optical lithography, soft lithography and etching method. This modified procedure offers increased flexibility in size and network pattern as well as a significant reduction in the material, time and operation costs. Next, the fabricated prototype is applied in both single phase and two-phase flow visualization studies to verify the applicability and reliability of the features under the specified experimental conditions.

Following the fabrication of a suitable PDMS micromodel, this thesis will present the processing/analysis of the visual data in micromodel experiments. In this section, an image processing MATLAB tool (PIV lab, version 1.41) is used that quantifies the flow field. The availability of advanced image processing functions and the simplicity of working with PIV lab, provide the unique opportunity to implement it that quantifies the visual observations during PDMS micromodel test and single-phase and two-phase flow studies.

Contents

ABSTRACT v-vi

CONTENTS vii- ix

NOMENCLATURE x-xi

LIST OF FIGURES xii- xiii

1 INTRODUCTION 1-10

1.1 Motivation 1

1.2 The Porous Medium 1

1.3 Basic Concepts 2

1.3.1 Porosity, absolute porosity and effective porosity 2

1.3.2 Pore size distribution 3

1.3.3 Permeability 4

1.3.4 Fluid saturation 5

1.3.5 Surface and interfacial tension 5

1.3.6 Capillary pressure 6

1.3.7 Multiphase flow of immiscible fluids in porous media 7

1.3.8 Basic concept of Capillary number 8

1.4 Present Objective 9

1.5 Layout of the Thesis 10

2 POROUS MICROMODELS AND THEIR APPLICATIONS 11-34

2.1 Historical Development of Micromodels 11

2.1.1 Perfectly regular models 11

2.1.2 Partially regular models 12

2.1.3 Fractal patterns 12

2.1.4 Irregular patterns 12

2.1.5 Hele-Shaw and glass-beads models 13

2.2 Micromodel Fabrication and Imaging Techniques 15

2.2.1 Micromodel materials 15

2.2.2 Micromodel fabrication process 17

2..2.2.1 Optical lithography 17

2.2.2.2 Etching method 18

2.2.2.3 Chemical or wet etching 19

2.2.2.4 Plasma or laser etching 20

2.2.2.5 Stereo-lithography 21

2.2.2.6 Soft lithography 22
2.2.3 Micromodel imaging methods 24
2.2.3.1 A microscope-camera visualization setup 24
2.2.3.2 Direct visualization with a camera 25
2.2.3.3 Photo-luminescent Volumetric Imaging (PVI)-Confocal microscopy 25
2.2.4 Application of micromodels in studying two-phase flow displacement processes 28
2.3 Significance of 2-D Micromodels 29
2.4 Summary and Scope of Research 30

3 FLOW VISUALIZATION IN POROUS MICROMODELS 35-63
3.1 Introduction 35
3.2 Materials and Methods 39
3.2.1 Creation of homogeneous micromodel 40
3.3 Experimental Setup 42
3.4 Result and Discussion 44
3.4.1 Micro-PIV measurement 44
3.4.2 Velocity field 48
3.4.3 Effect of orientation 50
3.4.4 Creation of heterogeneous porous media 54
3.4.5 Creation of dual porosity micromodel 55
3.4.6 Effect of discontinuity on fluid flow 58
3.5 Investigation of Velocity Field in Porous Micromodels 59
3.6 Summary 63

4 FLOW VISUALIZATION AND MEASUREMENTS IN FRACTURED MICROMODELS 64-85
4.1 Introduction 64
4.2 Materials and Methods 67
4.2.1 Method of fabrication 68
4.2.2 Experimental setup 69
4.3 Results and Discussion 70
4.3.1 Flow visualization and micro-PIV measurements 70
4.3.2 Single-phase flow observation 73
4.3.3 Two-phase flow mechanisms using micro-PIV technique 78
4.3.4 Instabilities in the imbibition process 79
4.3.5 Recirculation 83
4.4 Summary 84

5 CONCLUSIONS AND FUTURE SCOPE 86-88

5.1 Conclusions 86

5.1.1 Findings of porous micromodel experiments 86

5.1.2 Findings of fractured micromodel experiments 87

5.2 Future Work 88

REFERENCES 89-101

LIST OF PUBLICATIONS 102

Nomenclature

Abbreviations

CAD	Computer-aided design
CCD	Charged Couple Device
COC	Cyclic Olefin Copolymer
EOR	Enhanced Oil Recovery
FFT	Fast Fourier Transform
IFT	Interfacial tension
LDV	Laser Doppler Velocimetry
LIGA	Lithographie, Galvanoformung, Abformung; German for Lithography, Electroplating, Moulding
μCP	Micro contact printing
μTM	Micro-transfer moulding
Nd:YAG	Neodymium-doped yttrium aluminium garnet
PDMS	Polydimethylsiloxane
PMMA	Polymethylmethacrylate
PIV	Particle Image Velocimetry
REM	Replica moulding
SAMIM	Solvent-assisted micro-moulding
SEM	Scanning Electron Microscope
SL	Stereo-lithography
UV	Ultraviolet light
WAG	Water-alternating-gas

Notations

A	Flow area
b	Width of the fracture
d	Depth of the micromodel
D	Diameter of the cylindrical pillars of the micromodel
k	Permeability of the porous medium
l	Length of the fracture
L	Length of porous matrix region of the micromodel
P_c	Capillary pressure
P_{nw}	Molecular pressure in the non-wetting phase
P_w	Molecular pressure in the wetting phase
ΔP	Pressure difference between two fluid phases
Q	Flow rate
Re	Reynolds number
s	Maximum distance between two cylindrical pillars
S_h	Hydrocarbon saturation
S_w	water saturation
t	Minimum distance between two cylindrical pillars (Throat)
W	Width of the porous region of the micromodel

Greek Symbols

φ_a	Absolute porosity
φ_e	Effective porosity
μ	Fluid viscosity
μ_A	Viscosity of the displacing phase
μ_B	Viscosity of the displaced phase
ρ_A	Density of the displacing fluid
ρ_B	Density of the displaced fluid
σ	Interfacial tension between the two fluids

List of Figures

Figures No.	Caption	Page No.
1.1	Schematic shape of pore and pore throat	4
1.2	Illustration of surface tension	6
2.1	Image of micromodel with a partially regular pattern (Tsakiroglou and Avraam 2002)	12
2.2	Lateral view of a glass bead micromodel (Corapcioglou and Fedirchuk, 1999)	14
2.3	Schematic cross-section of the network used by Lenormand et al. (1983)	15
2.4	Schematic presentation of a bottom-up stereo-lithography system with scanning laser (Melchels et al., 2010)	22
2.5	The experimental setup for PVI (Montemagno and Gray, 1995)	26
2.6	Schematic description of a typical micro-PIV hardware implementation (Wereley and Meinhart, 2005)	27
2.7	The basic setup for confocal microscopy (Semwogerere and weeks, 2005)	28
3.1	Schematic diagram of (a) homogeneous porous medium, (b) dual porosity system where a porous medium is adjacent to another porous medium, and (c) a dual porosity system with a horizontal fracture.	36
3.2	Image of the (a) master pattern, (b) enlarged view of the small region	40
3.3	(a) Schematic description of steps for fabricating the micromodel, (b) enlarged view of the cylindrical pillars of the micromodel	42
3.4	Details of (a) Experimental setup, (b) image of the micromodel and (c) enlarged view of a part of the homogeneous porous micromodel	43
3.5	Schematic diagram of a micro-PIV setup	45
3.6	Image of the fabricated micromodel with highlighted locations where velocity fields are obtained	46
3.7	Image of the fluorescent particles at different sections of the micromodel	47
3.8	Velocity vector map of the micromodel at the three locations (along the red line) corresponding to the images shown in Figure 3.6	48
3.9	Velocity profile for the three flow rates at each three section of the micromodel along the red line shown in Fig. 3.6	49
3.10	Schematic of two different orientations (a) pattern A and (b) pattern B in porous section of the micromodel	50
3.11	Images of micromodels at the two different orientations for (a, b) 61 % and (c, d) 54% porosity	51
3.12	Schematic diagram of experimental setup used for pressure difference measurement between inlet and outlet	51
3.13	Variation of flow rate with pressure drop for (a) 61% and (b) 54% porosity micromodel	52
3.14	Streamlines at two arbitrary locations of (a) pattern A, and (b) pattern B for 61% porosity micromodel	52
3.15	Streamlines at two arbitrary locations of (a) pattern A and (b) pattern B for 54% porosity micromodel	53
3.16	Velocity contours at two arbitrary locations of (a) pattern A and (b) pattern B for 61 % porosity micromodel	53
3.17	Velocity contours at two arbitrary locations of (a) pattern A and (b) pattern B for 54 % porosity micromodel	53

3.18	Image of the (a) dual porosity pattern, (b) dual porosity micromodel and (c) enlarged view at the interface of the micromodel	55
3.19	Dual porosity micromodel with highlighted locations where velocity fields are obtained	56
3.20	Velocity vector map at locations corresponding to the image shown in Fig. 3.17	57
3.21	Dual porosity micromodel with fracture along the fluid flow	58
3.22	Dual porosity fractured micromodel with highlighted locations where measurements are performed	58
3.23	Velocity vector map at locations corresponding to the image shown in Fig. 3.20	59
3.24	Micromodel images having different porosity (a) micromodel A (61%), (b) micromodel B (45%) and (c) micromodel C (54%)	60
3.25	Sample image of the micromodel with highlighted locations where velocity field is obtained	60
3.26	Velocity vector map at the two locations corresponding to the image shown in Fig. 3.25 for micromodel A	61
3.27	Velocity vector map at the two locations corresponding to the image shown in Fig. 3.25 for micromodel B	61
3.28	Velocity vector map at locations corresponding to the image shown at the highlighted locations shown in Fig. 3.25 for micromodel C	62
3.29	Flow rate vs pressure drop for different porosity micromodels	62
4.1	(a) Image of the porous plate having circular holes (holes along the marked cross strips are covered to get the desired fracture), (b) enlarged view of circular hole	67
4.2	Steps of the fabrication of the fractured micromodel	69
4.3	(a) Experimental setup, (b) image of the fractured micromodel and (c) enlarged view at the junction of the two fractures	70
4.4	Experimental setup used for micro-PIV experiment	72
4.5	Basic steps of PIV analysis to get the velocity flow field	73
4.6	Image of the micromodel with highlighted locations where velocity field was obtained for flow rate 100 µl/min	73
4.7	Image of the micromodel with highlighted locations where velocity field was obtained for flow rate 1000 µl/min	73
4.8	Image of the fluorescent particles at various locations of the micromodel as highlighted in Fig. 4.6	75
4.9	Velocity contour map of the micromodel at various locations as highlighted in Fig. 4.6 for flow rate 100 µl/min	77
4.10	Velocity contour map of the micromodel at various locations as highlighted in Fig. 4.7 for flow rate 1000 µl/min	78
4.11	Image of the micromodel with highlighted locations where velocity field was obtained for two-phase immiscible flow (flow rate =1000 µl/min)	79
4.12	Image of the fluorescent particles at various locations of the micromodel as highlighted in Fig. 4.11	80
4.13	Velocity contour map of the micromodel at various locations as highlighted in Fig. 4.11 for two-phase immiscible flow (flow rate =1000 µl/min)	82
4.14	Velocity vector contours showing oscillating movement	83
4.15	Image of tracer particles for the trapped wetting phase	83
4.16	(a) Velocity vector field for circulating motion and (b) streamline image at the corresponding location	84

Chapter 1

Introduction

1.1 Motivation

Fluid flow and displacement processes of multiphase fluids inside porous media occur in many subsurface systems. It has vast applications in numerous fields of science and engineering such as petroleum engineering, hydrology, geothermal energy development, waste disposal and medical science. Over the years, enormous research investigations have been exclusively dedicated to understand the multiphase flow and transport phenomena inside the porous and fractured media. Many significant multidisciplinary research have been carried out and these studies have advanced an understanding with the passage of time. In the past few years, many quantitative approach and models have been developed and successfully implemented to understand, describe and predict the multiphase flow physics at micron scale. Mathematical and numerical modelling have matured over the time and are being routinely implemented to investigate the flow dynamics and to optimize the field project design and operation. In many cases, it would not have been possible without the development of these approaches.

Flow visualization experiments are reliable and practical tools to get the better insight of these phenomena that helps in developing various numerical models. However, performing experiments in field scale has many obstacles that can be overcome by performing experiments on prototype of porous media in the laboratories. Visualizing the fluid flow in soils and geomaterials is a challenging task as these real materials are not transparent to visible light and these materials do not allow visualization experiments. Therefore, most of the experimental analysis are based on the visualization of flow phenomena in artificial porous medium, also known as micromodels, owing an aim to characterize the dynamics of flow mechanism at pore scale.

1.2 The Porous Medium

In our day-to-day life, whether it is in nature or in manmade technology, porous media are found everywhere. Apart from few materials, almost all the substances are porous in nature up to some extent. For material to be considered as porous medium, it must contain spaces or pores

between the solid boundaries. These pores normally retains some fluid such as air, water or mixture of oil and other fluids. In addition, these void spaces should be interconnected up to some extent so that fluids can enter through one face of a sample of material and emerge on the other side.

Flow through porous media has important applications in the subsurface phenomena such as ground water hydrology, waste water management, filtration technology and oil recovery processes. On the other hand, it has also application in medical sciences such as tissue engineering and drug delivery system. To understand the insight of the flow phenomena it is important to understand the basic engineering and the fluid properties of these porous substances.

1.3 Basic Concepts

Flow through porous media is a very complicated process and the fluid flow pattern in this domain is not comparable with that of flow through pipes or conduits. In case of pipe flow, it is rather easy to calculate the flow field as a function of pressure, however, in porous media flow, we encounter tortuous paths that makes the measurement of fluid flow more complex.

The understanding of fluid flow in porous media has been evolved throughout the years with the development of experimental, analytical and numerical analysis. Since the beginning, physicist, hydrologists and engineers have performed various experiments to understand the flow behavior of various fluids as it flows through a pack of sand beads to fused Pyrex glass. Based on these analyses, researchers have tried to formulate various laws and correlation, which can be used to deliver analytical prediction for similar systems.

Flow and transport of various fluids in porous media is a dynamic process and flow is driven by the energy that can be stored within the porous system (such as reservoir) or can be supplied by outside external agency. To estimate the distribution of fluid flow inside the porous media and to calculate the movement of fluids, a number of physical properties are required. These parameters are necessary to understand, as these are needed for deriving flow-governing equations of multiphase fluids in porous media. Some of the important parameters are discussed below.

1.3.1 Porosity, absolute porosity and effective porosity

The geomaterial or rock texture comprises of solid grains of numerous size and shape and its pore structure is very complicated. The passage connecting these pore structures serve as pathway to transport fluids or it may store the fluids forming storage pores. In reservoir

engineering, porosity is the most important rock properties. It is a measure of free void space available for the storage of hydrocarbon and other fluids. Porosity (φ) is defined as the ratio of pore volume to the total volume (bulk volume). Mathematically, it can be represented as

$$\varphi = \frac{Pore\ Volume}{bulk\ volume} = 1 - \frac{Grain\ volume}{Bulk\ volume} \tag{1.1}$$

$$Bulk\ volume = Grain\ volume + Pore\ volume \tag{1.2}$$

It is important to understand that all the voids are not interconnected. In the geomaterials like rock structures, sediments were deposited and the rocks were formed over geological times. Due to which, some of the developed void spaces become isolated from others and this leads to two different types of porosity viz., absolute porosity and effective porosity.

Absolute porosity is defined as the ratio of total void space present inside the porous material to the bulk volume of the whole sample material. A rock or porous material may have considerable porosity but still it may lack pore connectivity for the passage of fluid. Mathematically, the absolute porosity (φ_a) it is defined as

$$\varphi_a = \frac{Total\ pore\ volume}{Bulk\ volume} = \frac{Bulk\ volume - Grain\ volume}{Bulk\ volume} \tag{1.3}$$

However, it is important to understand that in case of flow through porous media only the interconnected pores are of interest as they create connecting pathways for the passage of various fluids. Hence, the concept of effective porosity (φ_e) arises and it is defined as the ratio of interconnected pore volume to the bulk volume of the sample porous material.

$$\varphi_e = \frac{Interconnected\ pore\ volume}{Bulk\ volume} \tag{1.4}$$

In engineering calculations, effective porosity is used as it counts only the pore space that is internally connected.

1.3.2 Pore size distribution

Pore size or pore space cannot be defined with a unique definition as these pore spaces are comprised of irregular network of pores. Every method of pore size determination defines a pore size in terms of a pore model, which is best suited to the quantity measured in the particular experiment. There is the same situation for the definition of void space. Therefore, for simplicity, these void spaces are usually restricted to the pore space enclosed between the solid boundaries. However, terms are defined and used to further distinguish the pore spaces

according to their sizes. The narrow constrictions that interconnect relatively larger spaces are called pore throats or pore necks, with pore throats being the more common term. While the relatively larger pore spaces are called pore bodies, node pores or bulge pores, with pore bodies being the most commonly used term. Figure 1.1 shows the geometric shape of a pore.

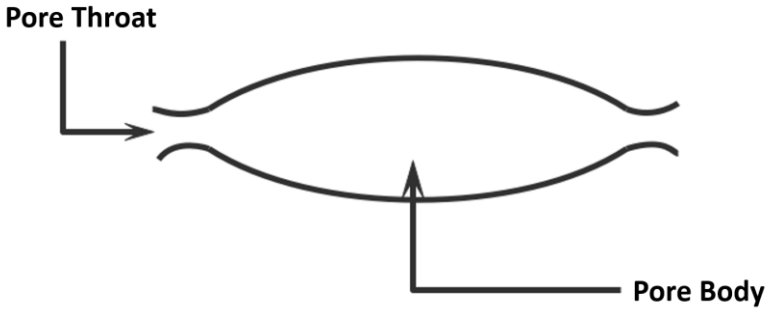

Figure 1.1: Schematic shape of pore and pore throat

1.3.3 Permeability

Permeability of a porous medium is defined as that property using which the ability and capability of porous medium to transmit fluid can be estimated. It is the measure of capacity of the porous medium such as reservoir rock to transmit various fluid through its interconnected network of pores. The permeability, *k*, is a very important property because it controls the directional movement and the flow rate of the fluids in the porous region. This characterization was first defined mathematically by Henry Darcy in 1856. Mathematically, it is defined by Darcy's law, which can be expressed as

$$Q = -\frac{k\Delta PA}{\mu L} \tag{1.5}$$

where Q is the flow rate, $\frac{\Delta P}{L}$ is the pressure gradient causing the flow, A is the flow area and μ is the fluid viscosity.

If the pores are filled with only one fluid phase, then the permeability can be termed as absolute permeability. It is an intrinsic property, as the magnitude of the absolute permeability does not depend on the type of fluid present in the void space. When the pore spaces in the porous medium are occupied by more than one fluid, the permeability measured is the effective permeability of the porous medium for that particular fluid. Effective permeability is the ability of the rock to transmit fluid in presence of other immiscible fluids. Absolute permeability is a rock property and therefore, varies at different locations and even at the same location with the flow directions. It is strongly correlated to porosity since the interconnections and orientations

of pores are important to fluid flow. Usually, for a reservoir rock the permeability values ranges from 1 mD to 1000 mD.

1.3.4 Fluid saturation

In porous materials such as in reservoir rock, both hydrocarbon and water coexists. In most of the oil formation phenomena it is believed that the formation was fully saturated with water prior to the oil migration and trapping in the formation. The less dense hydrocarbons are considered to migrate to positions of hydrostatic and dynamic equilibrium by displacing the initial water. However, the oil will not displace all the water originally occupied by these pores. Thus, saturation is defined as that fraction (or percent) of the pore volume occupied by a particular fluid (oil, gas, or water). This property is expressed mathematically by the following relationship:

$$Fluid\ saturation = \frac{total\ volume\ of\ the\ fluid}{pore\ volume} \tag{1.6}$$

The pore spaces in reservoir rocks are occupied by fluids. In petroleum reservoirs, the fluids are usually water and hydrocarbons. The relative volumes of water and hydrocarbons in the pore volume of the reservoir rock are designated as saturations. Water saturation in the reservoir rock is the fraction of the pore volume occupied by water. By the same definition, hydrocarbon saturation in the reservoir rock is the fraction of the pore volume occupied by hydrocarbons. The sum of the water and hydrocarbon saturations in the reservoir rock is equal to unity (Ahmed, 2019). This relationship can be expressed simply as:

$$S_h + S_w = 1 \tag{1.7}$$

where S_h and S_w shows the hydrocarbon saturation and water saturation respectively.

1.3.5 Surface and interfacial tension

In multiphase flow system, when two immiscible fluids are in contact, then it becomes necessary to take into account of forces that arise at the interface between the two fluids. When these two fluids are liquid and gas, then a force known as surface tension describes the force acting at the interface. It is a surface property of a liquid that helps the liquid to resist any external force at the surface. Due to which the surface behaves like an elastic membrane. Whenever two immiscible liquids meet each other, the force developed at the interface is known as interfacial tension.

The cohesive forces among the liquid molecules are responsible for the development of the surface tension force. In the bulk of the liquid, each molecule is pulled equally in every direction by neighboring liquid molecules, resulting in a net force of zero. However, the molecules present at the surface do not have surrounding molecules in all the sides. Because of which, the molecules present at the liquid surface experiences an unbalanced force and consequently they are pulled inwards. This creates an internal pressure and it forces the molecules at the surface to contract to minimal area. Due to this unbalanced force, the surface behaves like an elastic membrane with a measurable tension, i.e., surface/interfacial tension. Figure 1.2 depicts the pictorial description of surface tension.

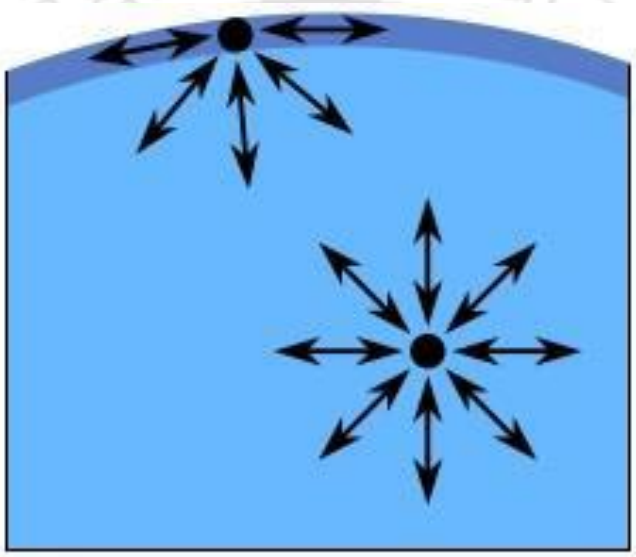

Figure 1.2: Illustration of surface tension

A certain extent of work is needed to displace a liquid molecule from within the body of the liquid through the interface. This amount of work is usually known as free surface energy of that liquid. Therefore, it can be defined as the work necessary to create a new unit area of the surface. The surface or interfacial tension has the units of force per unit of length.

1.3.6 Capillary pressure

Capillary pressure is a major parameter in reservoir rock system that controls the distribution of fluid inside porous media. Whenever two immiscible fluids come in contact in capillary like tubes, capillary pressure arises and it becomes observable. In a capillary tube, when two immiscible fluids exits simultaneously, a clear interface arises between them due to the interfacial tension effects. The interface is a curved surface and the pressure on the concave side is always higher than that of convex side. This pressure difference is known as capillary

pressure. In the presence of two immiscible fluids, one of them preferentially wets the tube surface and it is called the "wetting" fluid, the other fluid is the "non-wetting" fluid.

The tiny pores in reservoir rock are similar to the small capillary tubes. The capillary pressure also comes into play whenever two immiscible fluids come in contact inside a porous medium. The interface between the two fluids will be curved if one fluid is more wetting than the other. Capillary pressure, denoted P_c, is defined as the molecular pressure difference across this interface.

$$P_c = P_{nw} - P_w \tag{1.7}$$

where P_{nw} and P_w is molecular pressure in the non-wetting and the wetting phase, respectively.

1.3.7 Multiphase flow of immiscible fluids in porous media

Immiscible flow and displacement of multiple-phase fluids in porous media are of fundamental importance to many problems relating to underground natural resource recovery and storage projects, or waste disposal and contamination transport evaluation. Immiscible flow of multiple-phase fluids through porous media, as compared with single-phase flow, is much more complicated and its effects are yet to be understood thoroughly in many areas due to the complex interactions of different fluid phases in porous media. Multiphase flow through porous media deals with the problems of flow through porous media when two or more fluid phases exist simultaneously in the pore space and these phases are separated by clear interface.

In porous medium such as in reservoirs, most of the gas or oil are recovered by displacing it through the injection of water or other fluids. The displacement could be in the form of solution gas drive, gas cap expansion, water influx from aquifers or injection of water and/or gas. Solution-gas drive, gas cap expansion, and water influx from aquifers are essentially natural processes that supply energy to the reservoir for hydrocarbon recovery. Gas and water injection are designed and installed to artificially supply energy to the reservoir and thereby improve hydrocarbon recovery. It is important to understand the fundamental processes that occur when reservoir fluids are displaced immiscibly by gas or water.

When multiple immiscible fluids exist within pores of porous media under reservoir conditions, one liquid (water or oil) preferentially wets the solid surface. Wettability is defined as the ability of a liquid to maintain contact with a solid surface when the two are brought together in the presence of other immiscible fluids. The degree of wetting (wettability) is determined by a force balance between adhesive and cohesive forces, estimated in terms of contact angles.

Therefore, wettability is determined by rock minerals, fluid composition, and saturation history. Wettability has significant impact on fluid saturation distribution as well as oil recovery in reservoirs. Note that under natural conditions, natural gas is always a non-wetting phase. Two processes closely related to multiphase flow and displacement are imbibition and drainage. Imbibition is a fluid flow process in which the saturation of the wetting phase increases and the non-wetting phase saturation decreases, i.e., using a wetting fluid to displace a non-wetting fluid. In contrast, drainage is the process of a wetting phase fluid being displaced by a non-wetting phase.

When a porous medium containing non-wetting phase comes in contact with a wetting phase, the wetting phase spontaneously displaces some portion of the non-wetting phase. This phenomenon is known as spontaneous or free imbibition. However, when this process is controlled externally by regulating the capillary pressure or by constant feed pump, it is known as forced imbibition. When a wetting phase is drained out of the pores either under the influence of gravity or by a force exerted by non-wetting phase under pressure is known as drainage process.

1.3.8 Basic concept of Capillary number

Whenever more than one immiscible fluid phase exists during flowing through a porous medium, the flow behavior is mainly determined by three major forces. These three forces are capillary, viscous and gravity force. The relative importance of viscous force and capillary force can be expressed by a factor is known as capillary number. It is a dimensionless group that analyze the fluid flow by characterizing the ratio of viscous forces to interfacial tension forces. It is usually denoted by Ca. The capillary number is usually expressed as

$$Capillary\ number, Ca = \frac{velocity\ \times viscosity}{Interfacial\ Tension} \tag{1.8}$$

Therefore, for a multiphase flow system, if $Ca >> 1$, then viscous forces dominates over interfacial tension forces. On the other hand if $Ca << 1$, viscous forces are negligible compared to interfacial forces. Capillary numbers are large for high speed flows and low for low speed flows. When the value of capillary number is lower than 10^{-5}, the flow regime is determined by capillary forces (Iqbal and Satter, 2016).

1.4 Present Objectives

Understanding the dynamics of immiscible multiphase fluid flows in porous media is relevant to a multitude of fields in science and engineering. Applications include, among others, mass transfer in porous catalysis, mobilization of trapped hydrocarbon in enhanced oil recovery and, more recently, membrane-based fuel cells and geological carbon sequestration. In such applications, processes are driven by the injection/suction of a certain fluid phase into/from a porous domain saturated with another fluid, resulting in a moving fluid-fluid interface. Understanding the fundamental physics of these interactions is extremely important for the realization of predictive models capable of assessing the efficiency of fluids injection and the concomitant impact on its local and reservoir-scale migration. Considerable progress has been made over the last few decades to develop a theoretical framework based upon the qualitative observations of front migration and meniscus dynamics.

However, direct measurements of either the pressure or fluid velocity field near the fluid-fluid interface are lacking due to the difficulties associated with collecting direct datasets in a solid porous matrix with a complex geometry. These physical quantities embody the most valuable information for understanding the physics of the front displacements and are necessary to validate numerical models developed to reproduce the behavior of such multi-liquid systems. This lack of experimental and field flow measurements is thus hampering the development of robust numerical models and limiting their predictive ability. In particular, to our knowledge, experimental investigations reporting the quantification of multi-liquid flow velocity distributions with high spatial resolution at the pore scale are limited. Based on the study of literature, the following objectives are aimed at the present research work:

- *Adoption of a noble method to fabricate two-dimensional homogeneous porous micromodels in PDMS having different pore network patterns.*
- *Adoption of a noble method to fabricate two-dimensional heterogeneous porous micromodels in PDMS having different pore network patterns.*
- *Ensuring the assurance of experimental reliability and applicability of these fabricated micromodels by performing single-phase experiments and quantification of the flow field using micro-PIV method.*
- *Microscale investigation of multiphase fluid in fractured micromodels to assess the flow behavior on a pore scale and simultaneous quantification of the velocity distribution in a multi-liquid system using micro-PIV method.*

1.5 Layout of the Thesis

The present thesis has been organized by concentrating on the improvement in the design and efficient methodology for the fabrication of various micromodels. Chapter 1 offers the motivation behind the work in the field of micromodel fabrication methods and a brief introduction of basic parameters related to the fluid flow in porous media. Chapter 2 introduces the basic history related to the various fabrication technology and visualization methods adopted to quantify and qualify the flow field at microscale. Chapter 3 discusses a noble method that tries to modify and combines the recent advances involved in soft lithography micromodel fabrication method to offer a low-cost and cost efficient alternative procedure. This modified procedure offers increased flexibility in size and network pattern as well as a significant reduction in the material, time and operation costs. Next, both the fabricated prototype of homogeneous and heterogeneous micromodels are applied in a single-phase flow visualization study to check the experimental applicability and reliability of the proposed features under the specified experimental conditions. Following the fabrication of fractured micromodel, Chapter 4 describes the fabrication of 2-D fractured micromodel, microscale investigation of random peculiarities are observed and velocity of the flow field is quantified using micro-PIV. Chapter 5 summarizes the conclusions and some future scopes.

Chapter 2

Porous Micromodels and Their Applications

2.1 Historical Development of Micromodels

A micromodel is regarded as an artificial portrayal of a porous medium comprised of a network of connected pores made of a transparent material. Micromodels have opened up a broad range of opportunities for various research areas that investigate the physics of multiphase fluid movements at minute scale. Thus, using these micromodels it becomes possible to study and to gain information regarding pore scale flow events up to the considerable extent. Due to its numerous applications in chemical, biological and other important fields, researchers were motivated to develop new fabrication methods and use different substrate materials to overcome fabrication challenges and to reach different experimental approaches.

Over the years, the methodologies adopted to fabricate micromodels have been improved considerably. At the start, early micromodels had simple and plain porous network structure. Since 1980s, with the development of new computer based application software, it has become possible to fabricate micromodels containing complex network patterns.

With the passage of time, the use of micromodels as visualization tool in various multidisciplinary studies has been increasing to understand the fluid flow mechanism in further details. The application of micro-models has increased over the past several decades, especially with regard to visualize the processes relating to enhanced oil recovery (EOR) and other oil recovery processes. The basic geometry of micromodels can be categorized as follows. The four main categories that are mainly used to classify micromodels based on the geometry and topology of the porous medium are described below.

2.1.1 Perfectly regular models

In perfectly regular micromodels, the geometry of the pore body such as depth, width and distance between the pores are constant throughout the whole network domain. However, minor variation can occur due to the manufacturing process. One example of perfectly regular

micromodel can be seen in the works of Corapcioglu et *al*. (1997) that was to visualize and quantify solute transport in porous media.

2.1.2 Partially regular models

In partially regular micromodels, the cross section of pore body and pore throat is same. However, their dimensions vary along the porous domain. Pore size distributions are taken from statistical distribution and it may be correlated or uncorrelated. The use of these kind of models can be seen in the works of Sbragaglia et al. (2007); Tsakiroglou and Avraam (2002) (Figure 2.1); and Chen and Wilkinson (1985).

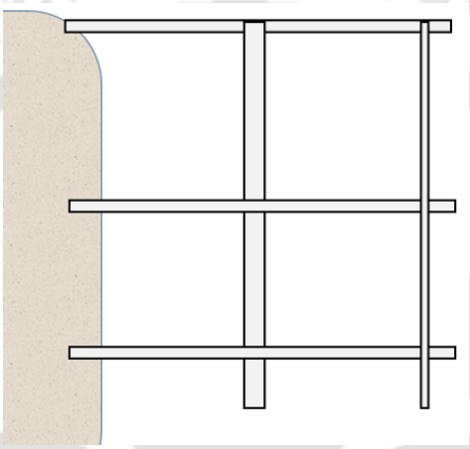

Figure 2.1: Image of micromodel with a partially regular pattern (Tsakiroglou and Avraam 2002)

2.1.3 Fractal patterns

The geometry of the flow network in these porous micromodels is based on fractals. The pattern may be correlated spatially or not. The fractural pattern in these micromodels may be seen as irregular pore network, but actually the pattern of the flow networks are created in such a way that it follows the rules of percolation theory. Micromodels having these kind of pattern can be seen in the works of Cheng et al. (2004), Nolte and Pyrak-Nolte (1991), Nolte et *al.* (1989), and Pyrak-Nolte et *al.* (1988). For flow to happen at least 50 % porosity is required in case of a correlated network, while in case of uncorrelated network it requires 60% porosity. If the porosity is less than these limits, then no connected path across the micro model can be achieved.

2.1.4 Irregular patterns

In this category, pore networks are randomly oriented in the entire micromodel and the pore distribution is not spatially correlated while their sizes are chosen from a single statistical

distribution. Heiba et *al.* (1992) and Blunt and King (1991) have used Delaunay triangulation methodology to generate the pattern that can replicate flow network patterns analogous to real porous media.

2.1.5 Hele-Shaw and glass-beads models

Hele Shaw micromodel is one of the first of its kind, which was used by the Chuoke et *al.* (1959) to perform two-phase immiscible displacement experiments. They presented both theoretical and experimental evidences for the existence of macroscopic instabilities in displacement of a fluid by another immiscible fluid. These micromodels are very simple in geometry as they are made of two parallel glass plate and a gap is maintained between the two plates to create the pore space. It becomes a glass bead micromodel, when the maintained gap is filled with glass or quartz sphere beads. The first such type of micromodel was used by Alfred Chatenever and John C. Calhoun in 1952 at the University of Oklahoma. They termed it as an observation cell, which was a single layer of glass spheres packed between the two flat glass plates. They found that using more than one layer of glass spheres would make difficulties in the flow observation process and to distinguish one phase from the other. The packing of the glass beads within the model resulted in an approximately rhombic pattern and the packing of beads give the pore space a complex structure that makes it extremely difficult for the observation of flow phenomena. During the experimental analysis, Chatnever and Calhoun used different flow cells.

This micro-model was comprised of a Lucite base, a compression cover, an observation window, and a gasket. A glass plate was molded into the Lucite base in a press to make an all-glass matrix composed of a glass top, glass spheres, and a glass base. The observation window was, in fact, the top cover of the cell. The spheres that were packed inside the cell formed a single-layered rhombic pattern of pore network.

In Hele-Shaw and glass beads micro-models, fluids were introduced into the model through a hole in the center of one plate (Sandnes et *al.* 2007), or at the ends of the parallel plates (Tallakstad et *al.* 2009; Tóth et *al.* 2007; Lovoll et *al.* 2005; Corapcioglou and Fedirchuk 1997). Figure 2.2 shows the side view of a glass bead micro-model from Corapcioglou and Fedirchuk (1999).

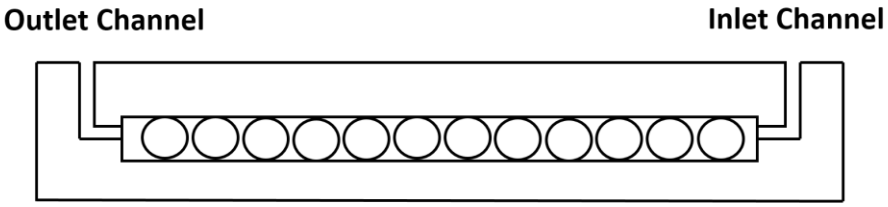

Figure 2.2: Lateral view of a glass bead micromodel (Corapcioglou and Fedirchuk, 1999)

In principle, Hele–Shaw and glass-beads micro-models are easy to make. However, the use of optical microscopy poses a problem. The three-dimensional nature of the model makes it difficult, or sometimes impossible, to visualize the distribution of fluids under the level of the largest bead diameter. As such, much information cannot be recorded when optical means are employed.

As observing the flow physics inside the packing of beads is extremely complicated, Fatt et *al.* (1956) proposed a two-dimensional regular flow network made of different radii cylindrical glass tubes that enhances the visualization of flow phenomena. During their experiments, four different network patterns viz. single hexagonal, square, double hexagonal and triple hexagonal are used.

Mattax and Kyte (1961) fabricated the first etched glass micromodel and was able to capture the motion of fluid interface in more detail. The fabricated micromodel comprises of network of interconnected capillary grooves etched into a glass plate. The glass was coated with a thin layer of wax above which the pattern network was drawn with the help of a stylus. Then the exposed area of the glass slide containing the pore network pattern was etched using hydrofluoric acid (HF). After the completion of etching process, the wax is removed and the open side of the glass slide containing the pore network is fused with another glass plate in an annealing oven. Finally inlet and outlet holes are created by drilling the glass slide. It was a very good approach to observe and visualize flow behaviour. The main drawbacks of such micromodels was the formation of concave shaped pore walls during the etching process and use of wax limits the capacity of design pattern. A further development of the micromodel was achieved by Davis and Jones (1968). They worked on the drawbacks and limitations of the micromodel and came up with a new fabrication technique. They replaced the wax material with a photoresist layer due to which it becomes possible to etch any black and white pattern on the glass plate. Later this methodology was refined by McKellar and Wardlaw (1982) and it is still used to fabricate etch glass micromodel. They added an additional copper-silver layer between the photoresist and the glass plate. This copper-silver layer is resistant to hydrofluoric

acid and can be easily removed by other solvents. Furthermore, the photoresist is still able to bond easily to the copper-silver layer. The copper or silver layer can either be directly applied to the glass plate, or instead a piece of mirror can be used once the backing has been removed, revealing the copper/silver layer.

Lenormand et *al.* (1983) further advanced in the fabrication process and fabricated a resin micromodel. The manufacturing process was also eased and previous limitation relating to poor visualization at pore scale difficulty in data interpretation in the packs of beads are also overcome. Using this kind of resin moulding technique, they were able to produce micromodels having throats of rectangular cross section, which is suitable for the better observation and analysis (Figure 2.3).

Hornbrook et *al.* (1991) produced the first silicon micromodels, which were almost identical to original Berea sandstone. Geometrical and topological properties as well as wettability and pore roughness were close to an original core sample. Micromodel pore structure was based on a thin section of a Berea sandstone. With a scanning electron microscope (SEM), a high-resolution photograph was taken and digitally processed. The drawback of this technique was that the SEM captured only a very little portion of the thin section. Hence, the edges of the photograph had to be processed to loop this unit cell image together and to produce the definite matrix area.

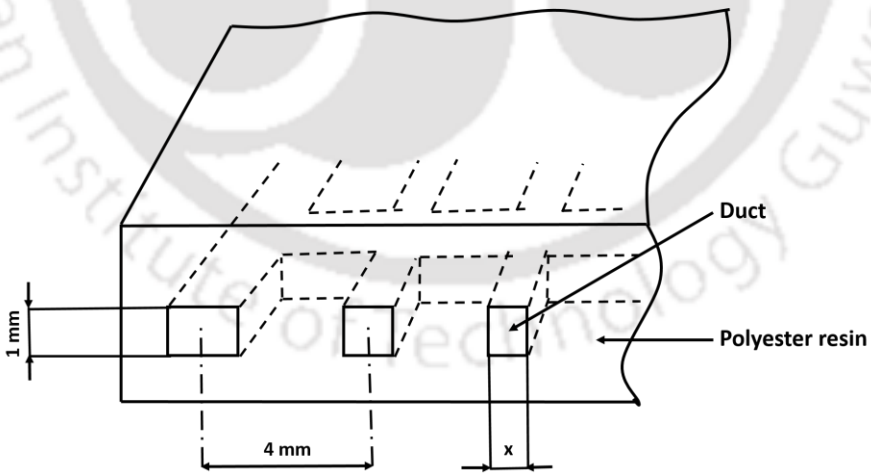

Figure 2.3: Schematic cross-section of the network used by Lenormand et *al.* (1983)

2.2 Micromodel Fabrication and Imaging Techniques

2.2.1 Micromodel materials

After adopting the design of the pore network, micromodels are fabricated. The prime properties of the materials required to fabricate the micromodels are that it should be fabricated

from transparent and rigid materials where the grooves of pore network can be embedded analogous to the structure of real porous media. Over the years, various materials have been used to fabricate porous micromodels.

Since, the beginning, the glass and quartz has been extensively used for the fabrication of micromodels. Starting from the era of Hele Shaw and glass bead micromodels, use of these materials are quite common in the fabrication process. It was very easy to construct these micromodels using glass of quarts beads of definite dimension at a relatively higher accuracy. Due to the easiness, low cost in the construction of micromodels these micromodels at that time gained immense of popularity. However, visualization along the layer of beads was very challenging and complicated and it creates many obstacles/problems during visualization process. In later stage, new methodologies are evolved and glass micromodels were fabricated using chemical etching method. Though it is an economical process, this process can not be carried out in regular laboratory environment due to use of acids. In addition, the micromodels should be handled carefully, as it may get broken easily. Glass micromodels are tough and rigid, due to which it can withstand high pressure. As the entire micromodel is made of glass, it retains same wetting properties within the micromodel, which is suitable for multiphase flow experiments.

Etching process also can be used to replicate pore network in silicone substrates. However, a micromodel made of entire silicon cannot be used for optical visualization experiments, as the material is translucent. Therefore, after engraving the pore network, the open side containing the grooves is sealed with a transparent material like glass. Another issue is that, the final version of the silicone micromodel experiences two different wetting properties, as it is made of two materials and this affects the fluid flow in two-phase flow studies.

The most popular material used to fabricate micromodels are the soft polymeric materials. Among them Polymethylmethacrylate (PMMA) and Polydimethylsiloxane (PDMS) are the widely used polymers. PMMA is an acrylic thermoplastic material and a good alternative of glass. It is not as hard as glass and can be etched easily with chemical solution, using ions or using laser radiation. Polydimethylsiloxane is softer than PMMA and PDMS micromodels are economical and can be fabricated easily in normal laboratory. However, a master pattern containing pore network is required and this has to make in clean environment. Using this mater pattern, pore network is replicated in the soft materials and in such a way; many micromodels can be fabricated from a single master pattern. However some disadvantages are also can be

observed during the use of these micromodels. These micromodels react with some chemicals and can absorb it. Due to which, it may get deform that consequently damages the pore network features. In addition, micromodels made of these soft materials cannot withstand high pressure and may get deformed at a pressure less than 100 Kpa (Eddings et *al*., 2008) which results in breaking the micromodel (in case of PMMA) or it can damage the bonding features (in case of PDMS).

2.2.2 Micromodel fabrication process

With the development of computer generated digital design tools, it has now become possible to fabricate a wide variety of more complex 2D and 3D micromodels (Tsakiroglou and Avraam 2002). Various fabrication techniques are discussed below.

2.2.2.1 Optical lithography

At present, the common method of fabricating micromodels is the optical lithography technique that transfers the predesign geometric pattern from a mask to a photoresist layer on the substrate like silicon wafer or glass. Specific features like pore geometry, pore size and pore nos. and other minute dimensions cannot be created using simple methods as used in Hele Shaw and glass bead micromodels. Optical lithography has gain immense of popularity due to its ability to produce any kind of complicated small dimension flow network analogous to irregular or fractal patterns.

Since 1980, the principles of photolithography were used (Thompson et *al.* 1994, 1983). The detailed fabrication process is reported in many literatures (Cheng et *al*. 2004; Giordano and Cheng 2001). In this methodology, the design of the flow network is made digitally. The flow network pattern design can be based on statistical distribution or also can be made without spatial correlation of the pores. Then the design of the flow network is printed on a transparent material. Transparent material imprinted with the flow network is known as mask. The next process involve as the transfer of this design into the micromodel substrate material. But it is performed through a series of steps.

The chosen substrate has to be cleaned perfectly and then a layer of thin layer of polymeric material, known as photo-resist is applied on the surface of the substrate. The most commonly used photoresist material is SU-8. The photoresist material is spin coated over the substrate material to get the uniform thickness layer over the entire surface of the substrate material. The spinning condition such as rotation speed, spinning duration and the material type determine the thickness of the final coated layer that in later stage become the final depth of the flow

network. Then the substrate is soft baked in order to harden the photo-resist (Cheng et *al*. 2004; Giordano and Cheng 2001).

In the next step, methodology is applied to transfer the flow network pattern from the mask to the photoresist material. For this purpose, the mask is projected on the photoresist using the ultraviolet light with the help of mask aligner. The photoresist area, which is exposed to the ultraviolet light, reacts with the developing solution. Later, the exposed area is removed which gives the flow network. After that, the open side of the flow network is covered with another glass plate to get the final applicable version of the micromodel. The covering glass plate is also coated with a photoresist layer that gives strength to the bonding of the two plates and gives uniform wetting properties throughout the micromodel. This methodology is relatively economical and easy to implement. However, creation of the flow network in the photoresist material produce another major problem. As these materials are photosensitive, exposure of light having wavelength near to ultraviolet range causes to the production of nitrogen gas. These bubbles of nitrogen gas grow in size with the passage of time and slowly damages the flow network. The production of these nitrogen bubbles are demonstrated in the work of Karadimitrio et *al.* (2013). One solution to this problem is to cut all the light emission which have wavelengths below 550 nm. In addition, optical filters can be used to block all the wavelengths below 550 nm. Though these methods are effective, yet experimental setup becomes expensive. Another difficulty occurs during the sealing of the micromodel, as the micromodels containing minute dimension flow network do not have enough surface areas for the bonding purpose.

2.2.2.2 Etching method

The first etched micro-model was constructed by Mattax and Kyte (1961). The fabrication technique is based on chemical reactions and the interaction of laser and plasma radiation with glass, silicon or polymer (Zhang et *al.* 2011, 2010; Gutierrez et *al.* 2008; Baouab et *al.* 2007; Jeong and Corapcioglou 2005; Lanning and Ford 2002; Weidman and Joshi 1993). However, with the passage of time procedures or various steps involved in etching process are developed and modified.

Many initial steps of this methodology is similar to that of optical lithography technique. The design of the flow network. Mattax and Kyte (1961) used a thin layer of wax over a glass plate above which the pattern network was drawn with the help of a stylus. Then the exposed area of the glass slide containing the pore network pattern was etched using hydrofluoric acid (HF).

However due to some limitations, this method is refined by Davis and Jones (1968) who replaced the wax material with a photoresist layer. In the late 1980s, with the development of computer application software it has become possible to design the flow network digitally and also the process involved in processes like mask creation are modified which can be seen in the optical lithography process. Now in the recent etching process, many steps like creation of design of the flow network and mask creation are similar to that of optical lithography. However, the main difference between these two methods is that in optical lithography, flow network is created in the photoresist material, while in etching method, one step is taken further and grooves of the flow network is produced on the substrate material itself. After the pattern is developed and exposed in the photoresist layer, the final flow network in the substrate is created using an etching method. Normally two etching methods are used which are discussed in the following section.

2.2.2.3 Chemical or wet etching

In chemical etching or wet etching, acids are used as etchants to etch the glass or silicon surface (Sirivithayapakorn and Keller 2003; Wan et *al*. 1996; Avraam et *al.* 1994; Hornbrook et *al*. 1991; Wegner and Christie 1983; McKellar and Wardlaw 1982). However, during etching process, the remaining area of the substrate covered by the photo-resist remains unaffected due to the use of acid.

The etching rate and time of exposure of the etchant determines the depth of penetration of the eroded flow network. Since the beginning of the development of micromodels, etching process has been widely used and popular method of fabricating micromodels. However, one of the major problem arises due to the use of etching process is that the pore walls of the flow network is not vertical instead slopping walls are generated. In addition, curvatures are found at the bottom of the pores as liquid acids are isotropic in nature and thus erode the glass substrate in all directions. These types of curvatures can be found in the microchannel constructed by wet etching method in the works of Iliescu et *al.* (2008). The formation of curvature can be found at the bottom walls and this curvature and the optical setup used to take the pictures create refraction, leaving no light to reach the camera's sensor. This effect hinders studying two-phase flow, especially if the optical visualization of fluids and their configuration in the network are important. One remedy would be to diffuse the illumination and increase the intensity of the light. Another effective solution is to use front-light illumination instead of backlight illumination. In this case, a strong contrast between the sample and the background is needed.

2.2.2.4 Plasma or laser etching

Another way for etching substrate materials like glass, silicon and other polymeric materials like PMMA is the use of electromagnetic radiation. The radiation can be supplied from a laser source or from a beam of ions. The latter method is called ion milling, when using a noble-gas plasma (Kolari et *al.* 2008; Durandet et *al.* 1990). The noble gas commonly used for this purpose is Ar+. Using an ion gun, ions bombard the uncovered area, and by transfer of momentum, begin removing atoms from the glass surface. The reactive ion etching process, apart from the photo-lithographic step, can be broken down in the following steps:

- generate etchant species (radicals or ions)
- reaction or momentum transfer with the Surface
- by-product desorption
- diffusion of by-product to bulk gas

Instead of ion milling, excimer (Basov et *al.* 1970) laser can be used to create the pattern on the glass substrate (Arnold et *al.* 1995). The technique is called LIGA (Lithographie, Galvanoformung, Abformung) and was introduced by Ehrfeld et *al.* (1996, 1994). The network pattern is directly formed on the substrate and the whole procedure is computer controlled.

Both procedures are very anisotropic, which means that the sloping effect at the walls is diminished. However, the control of the whole procedure is not easy. This procedure is usually reserved for very narrow and shallow channels. After the pattern has been created on the glass substrate, the inlet and outlet reservoirs are produced with wet etching techniques. A second glass plate, on which two holes are drilled for the input and output, is used to cover the micro-model.

The sealing of the micro-model can be done in two ways, both of which are common for both wet and dry etched micro-models. One way is the use of a muffle furnace, or high temperature oven (Avraam et *al.* 1994). This method is used mostly for micro-models that are multi-layered. The other method involves placing a thin layer of polymer (a few nano-meters thick) between the two glass plates and baking in a UV oven (Tsakiroglou and Avraam, 2002). Heating the model and simultaneous application of a light pressure will have the desired effect for glass/glass bonding. Silicon and glass bonding can be achieved by gentle heating (~400^{o}C) while applying an electric field across the silicon/glass sandwich to ensure good contact via the associated electrostatic force.

This method is known as field-assisted, or anodic, bonding (Giordano and Cheng 2001). Anodic bonding will work only for moderate operating pressures of a few atmospheres within the micro-model. Other methods should be used if larger pressure must be applied (Little 1982).

When the channels are deep and much narrow, it becomes difficult to get vertical walls and keep the roughness at the bottom of channel low. It is found that as the ratio of the depth to the width of the channels becomes larger, the quality of the channels becomes lower (Yeom et *al*. 2005). The surface roughness increases and we do not get a rectangular shape at the bottom. Although such channels are not common to two-phase flow in porous media, they are presented here as an extreme example of reactive ion etching.

The Reactive Ion Etching method is a complicated and difficult procedure and many things can go wrong. Etching itself is a subject of on-going research. Given our current knowledge, however, etching remains one of the best ways to make good quality micromodels. Especially when optical microscopy with back light illumination is employed, etching is perhaps the best alternative. In particular, the stability of glass with respect to its chemical and physical properties is highly appreciated.

2.2.2.5 Stereo-lithography

Stereo-lithography (SL) is a computer-based manufacturing process that was developed by Hull (1986). As described by Melchels et *al.* (2010), it is a solid freeform fabrication technique. Stereo-lithography is an additive fabrication process that allows the fabrication of parts using a computer-aided design (CAD) file. The manufacturing of 3-D objects by stereo-lithography is based on the spatially controlled solidification of a liquid resin by photo-polymerization. The setup consists of a computer-controlled laser beam or digital light projector, a computer-driven building stage with a platform, and a resin reservoir. The platform is initially placed just below the resin surface, according to the desired depth of the resin layer. The computer guides the laser beam to follow a path and illuminate a desired pattern on the resin surface. As a result of this, the resin in the pattern is solidified to a pre-specified depth, causing it to adhere to the support platform. After photo-polymerization of the first layer, the platform is lowered incrementally, allowing the built layer to be recoated with liquid resin. Each time, the pattern is cured (i.e. solidified) to form another layer. As the depth of curing is slightly larger than the platform step height, good adherence to the first layer is ensured (i.e., unreacted functional groups on the solidified structure in the first

layer polymerize with the illuminated resin in the second layer). These steps (i.e., the movement of the platform and the curing of a pattern in a layer of resin) are repeated until a solid, three-dimensional object of desired height is constructed. After draining and washing-off excess resin, the desired structure is obtained. In this structure, the conversion of reactive groups is usually incomplete, and post-curing with (stroboscopic) ultraviolet light is often employed to improve mechanical properties of the structures. In Figure 2.4, a schematic presentation of the process is presented.

Stereo-lithography is an effective way to make micro-models when the dimensions of the structure are not very small (larger than microns). Parts from a larger assembly (not micro-models but general structures) can be manufactured in one day and with great efficiency. The complexity of a flow network or a part of an assembly is not an issue. On the other hand, this procedure is quite expensive. Stereo-lithography micromodels have been used in studying flow (Crandall et *al.* 2009, 2008; Stoner et *al.* 2005). However, they are less popular when it comes to very small dimensions (micrometer scale) because of the spatial resolution of the process.

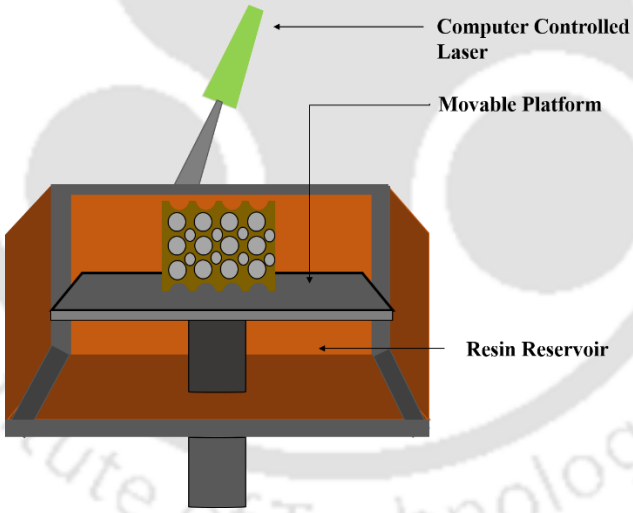

Figure 2.4: Schematic presentation of a bottom-up stereo-lithography system with scanning laser (Melchels et *al.* 2010)

2.2.2.6 Soft lithography

Soft lithography refers to methods for making structures using 'soft' materials like elastomeric stamps, moulds, and photo-masks (Wang et *al.* 2005; Rogers and Nusso 2005; Shor et *al.* 2004). It is mostly reserved to create very small, simple geometric structures, on the micro- and nano-scale (Park et *al.* 2009; Huh et *al.* 2007). Variations of soft lithography method include micro contact printing (μCP) (Xia and Whitesides, 1998), replica moulding

(REM) (Senn et *al.* 2010), micro-transfer moulding (μTM) (Xia and Whitesides, 1998), micro-moulding in capillaries (MIMIC) (Kim et *al.* 1996) and solvent-assisted micro-moulding (SAMIM) (Kim et *al.* 1997). These methods are particularly suitable for creating micro-scale structures, the scale of interest in two-phase flow, where soft lithography is most accurate.

One of the most widely used materials in soft lithography is PDMS, which is an elastomeric material. It is a liquid that is polymerized after mixing with a curing agent. The procedure for manufacturing a PDMS micro-model is explained in detail in Markov et *al.* (2010), Auset and Keller (2004) and Quake and Schere (2000). Usually, it consists of the following steps:

- The network of micro-model channels is created digitally. This network is printed on a transparency, which will be used as a mask in the next step.
- A silicon or glass wafer is spin-coated with photo-resist (positive or negative depending on the desired depth) to create a patterned silicon or glass wafer (called master) by using photo-lithography.
- The master wafer is put in a petri dish. Then, a mixture of liquid PDMS and curing agent is prepared. This mixture is then poured over the master wafer in the petri dish.
- The polymer is degassed under vacuum and then cured.
- After curing, the polymer is peeled from the master.
- The PDMS slab with the desired network is placed on a pre-cured thin slab of PDMS in order to close the network. Then it is exposed to ion plasma so that bonding can take place.

Soft lithography is widely used in two-phase flow studies. It is a method that produces detailed micro-models without severe production restrictions. However, one problem does arise. Because they are polymeric materials, their wetting properties may change with time. For instance, PDMS is initially hydrophobic, though not strongly. In the making of an all-PDMS micro-model, the two parts of the model are bonded with oxygen plasma. The treated PDMS becomes hydrophilic but the effect is not stable; it degrades with time and eventually recovers its hydrophobicity. This effect starts almost immediately after exposure, and it continues for hours, or even days, until the material reaches its initial condition (Murakami et *al*. 1998; Fritz and Owen, 1995). Thus, if hydrophilic behavior is needed, the micro-model must be used directly after its plasma treatment. An alternative treatment is to force the PDMS surface to

have specific wetting properties and become purely hydrophobic. This can be done with the application of a mixture of silane with ethanol (Zhou et *al.* 2010).

Another consideration is that the phases involved in the experiments will not make the material swollen or deformed. Gervais et *al.* (2006) studied the flow-induced deformation of PDMS models and provided a dimensionless number as a simple means of assessing whether deformation should be considered. This dimensionless number depends on the pressure drop along the network, the network's height and width, as well as the entry pressure of the features of the network. Depending on the value of this dimensionless number, deformation can be considered as important, or not.

2.2.3 Micromodel imaging methods

Since the start of use of micromodels, the main challenge that arises during the observation of fluid flow process is the adoption of proper optical configuration to perform visualization experiments. In multiphase flow experiments, estimation of fluid phase saturation and specific interfacial area are the main topic of interest. These measurements are done mainly by capturing the events optically in the form of videos or image frames. In addition, in dynamic experiments as the distribution of fluid phase change abruptly with time, visualization setup having high image acquisition facilities are required.

Chatenever and Calhoun (1952) performed two-phase experiment and obtained the image of fluid distribution using cine-photo-micrography technique. During the experiment, main optical components used are microscope and its accessories (lenses, mounts, etc.), a 16mm movie camera, a beam splitter, an arc illuminator, and an exposure meter.

It is obvious to mention that the bulk of the multiphase flow experiments are based on optical imaging techniques. The main chosen experimental setup that are used to capture the events related to the distribution of fluid phase during the experiments are discussed below.

2.2.3.1 A microscope-camera visualization setup

The optical apparatus associated with this kind of setup is very simple. The micromodel is placed under the objective piece of a microscope and the camera is fixed on the ocular of the microscope (Corapcioglu et *al.* 2009; Rangel German and Kovscek 2006; Vayenas et *al.* 2002; Keller et *al.* 1997). Then the camera is connected to a computer and the data generated by capturing the image frames are stored and acquired images are analyzed with proper image

processing software. By performing this kind of analysis, one can easily estimate average saturation of fluid phase and specific interfacial area (Chen et *al.* 2007; Cheng et *al.* 2004).

This technique is adopted whenever high resolution is required and minimum pore size is confined to one or two microns and parameters like interfacial area have to be calculated. However, for elongated and large micromodels, this experimental setup is not suitable as optical window of a microscope is limited in size. In addition, microscope can be focused on a specific area only and there is no provision to record area that lies outside the optical window. A remedy to this problem is to move the micromodel slowly to record the flow field at different positions. However, this leads to introduce unknown inertial forces in the micromodel and recorded image produce pore quality images as it is difficult to focus the camera all the time. This methodology is quite suitable for quasi-static experimental conditions.

2.2.3.2 Direct visualization with a camera

The principle of this method is similar to the method described in the section 2.2.3.1. However, the main difference between these two methods is that no microscope is used in this method and the camera directly captures the image frames (Hematpour et *al.* 2011; Chang et *al.* 2009). This provides the flexibility to handle the camera at various orientations and to acquire the images of flow events. Objective lens also can be added into the camera to magnify the field of view. Generally, this kind of setup without microscope is used when high resolution is not necessary. However, currently, cameras having high frame rate and having good resolutions are available and can be used to capture image frames. In addition, advanced image analysis software can be used for easy handling and data analysis. The other benefit of using this kind of setup is that the camera setup can be kept at a distance from the micromodel to reduce any vibration that affects the flow system. This kind of setup was used in the works of Chang et *al.* (2009), where experiments are performed in an acrylic micromodel and images were captured with a camera of resolution of 640 × 480 pixels in RGB format (Red, Green, Blue).

2.2.3.3 Photo-luminescent Volumetric Imaging (PVI) – Confocal microscopy

This method was first introduced by Montemagno and Gray (1995), where the porous micromodel was fabricated using quartz grains. The performed two phase immiscible experiments with fluids matching refractive indices to that of quartz particles (Budwig, 1994). During the experiment, the wetting phase was seeded with special fluorophores that helps in distinguishing the fluid-fluid interface. The fluid flow was illuminated by a planer laser source at successive planes and a CCD camera captured the fluorescent image frames. The images

were later processed and 3-D data sets were created to visualize the pore space and to get the location of fluid-fluid interfaces.

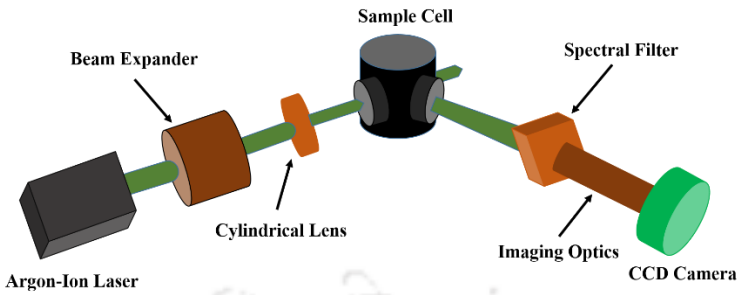

Figure 2.5: The experimental setup for PVI (Montemagno and Gray, 1995)

The experimental setup uses an Argon-ion laser (emission at 514.5 nm) as the source for illumination, CCD camera and other optical accessories to capture the flow events in the sample cell (Figure 2.5). A beam expander was used to increase the diameter of the Argon-ion laser beam from 1.5 mm to 25mm and cylindrical lens was used to convert the cylindrical beam into planer sheets. The laser sheet had a dimension of 15 mm width and 125 μm in the sample cell. When laser light falls in the fluorophores, it gets excited and emits light at higher wavelength. A spectral filter was used to block the unwanted wavelength of light and directs the permitted light into the camera. The data from the camera is transferred to a computer and later analysis with imaging software.

This methodology was later used by Zang (1998) during volumetric imaging of the multiphase flow dynamics in porous media. Stohr et *al.* (2003) used this methodology and performed three dimensional measurements of single phase flow at pore scale.

One of the significant application of fluorescent microscopy is micro-particle image velocimetry technique, which is used to investigate the fluid flow and transport phenomena at micron scale (Perrin et *al.* 2005; Shinahara et *al.* 2004). This methodology has been exclusively used to study pressure drive flows (Shinohara et *al.* 2004; Devasenathipathy et *al.* 2003; Sato et *al.* 2003; Meinhart et *al.* 1999), electro-osmotic flow (Devasenathipathy et *al.* 2002), and the fluid dynamics of blood capillaries in vivo (Sugii et *al.* 2002) and in vitro (Sugii and Okamoto 2004).

The working principle of micro-PIV is similar to that particle image velocimetry where micron sized particles are used as tracers and seeded to the working fluid and by tracing those particles velocity of the flow field is estimated (Keane and Andrian, 1992). An illustrative review of this

method in terms of its application and recent developments is reported by Lindken et *al.* (2009). A detailed description related to the various experimental components (Figure 2.6) needed during micro-PIV experiment has provided by Wereley and Meinhart (2005).

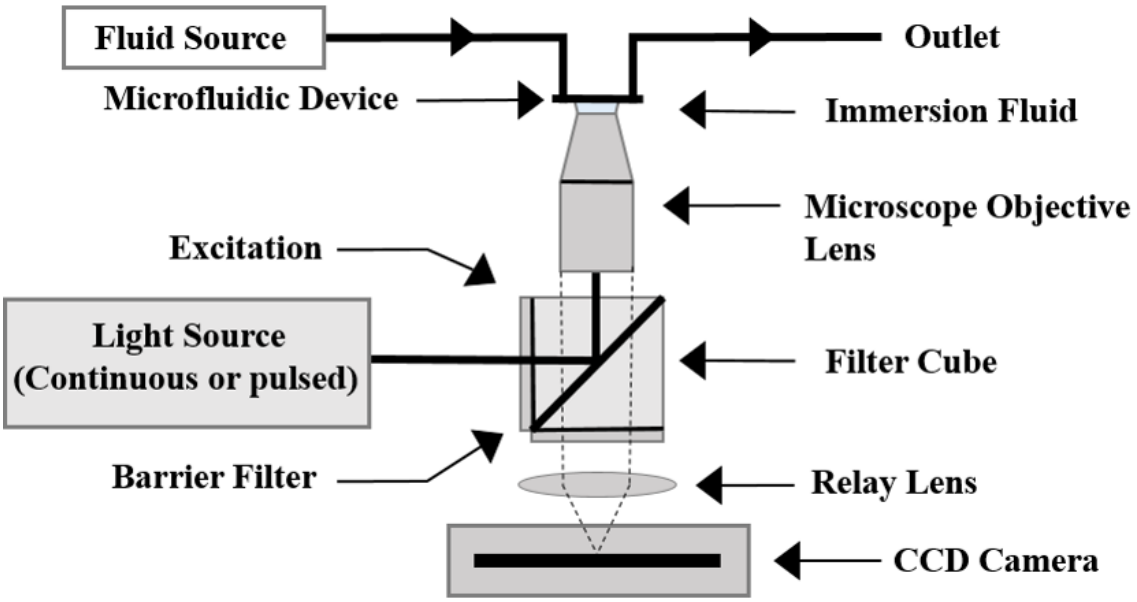

Figure 2.6: Schematic description of a typical micro-PIV hardware implementation (Wereley and Meinhart, 2005)

In this method of fluorescent microscopy, light source (laser) can be pulsed or continuous and the light being directed to a lens that converts it into plane sheets. When the laser light falls on these tracer particles, it gets excited and emits lights at higher wavelength. The optical filter also known as dichroic mirror attached to the optical system blocks the unwanted light and only permits the desirable wavelength of light to reach the sensor of the camera. In this way, two-dimensional images can be acquired. After capturing the images at definite time interval and analyzing the displacement of particles, the velocity of the whole field of view can be obtained. To obtain three dimensional image fluorescent microscopy can be combined with confocal microscopy.

Confocal microscopy is another technique that uses laser induced fluorescence technology. It is and point by point imaging method that provides good quality sharp images which may appear blurred when viewed under normal conventional microscope. Three dimensional images also can be constructed with the help of this technology by overlapping two-dimensional at successive layers. The patent of confocal microscopy was given by Marvin Minsky (1988). The fundamental concept of confocal microscopy (Figure 2.7) was provided by Semwogerere and Weeks (2005).

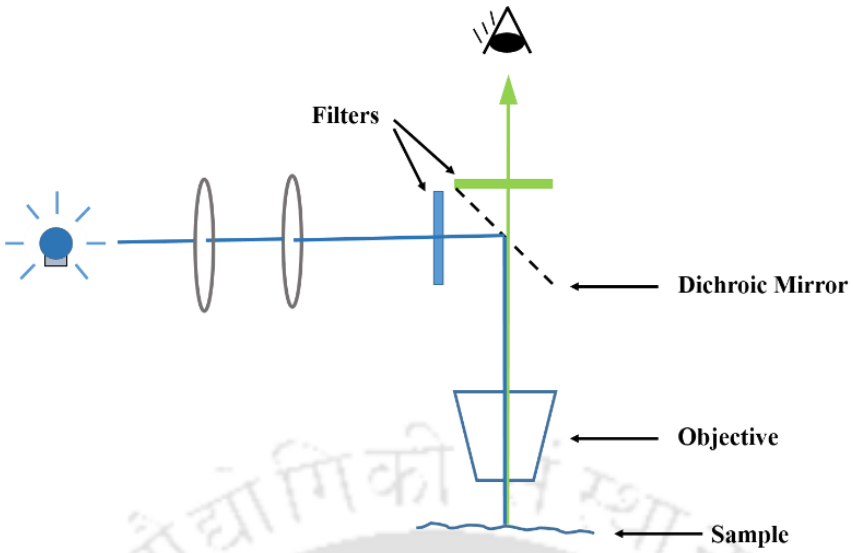

Figure 2.7: The basic setup for confocal microscopy (Semwogerere and Weeks, 2005)

A monochromatic light source such as laser is used as the light source that is reflected by an optical filter and directed on the sample specimen through objective lens. The working fluid is either dyed with fluorescent dye or seed with fluorescent particles. When these particles absorb the light, it gets excited and emits lights of higher wavelength. This emitted light is permitted by the dichroic mirror and the light from the light source is reflected back to the source. Thus, the field of view of the sample is visualized point wise in two dimensions. This methodology is very suitable for relatively slow and minute sized events that needs to be visualized preciously where conventional microscopy could not be used to get satisfactory results (Baumann 2007; Baumann and Werth 2004; Sirivithayapakorn and Keller 2003; Lindek et *al.* 1996; Hell et *al.* 1994; Wan and Wilson 1994).

2.2.4 Application of micromodels in studying two-phase flow displacement processes

Use of micromodels in studying flow and transport phenomena includes majorly immiscible displacement of two phases in porous media (Cottin et *al.* 2011; Dawe et *al.* 2010; Crandall et *al.* 2009; Corapcioglou et *al.* 2009; Chang et *al.* 2009; Tsakiroglou et *al.* 2007; Theodoropoulou et *al.* 2005; Tsakiroglou et *al.* 2003; Wan et *al.* 1996; Avraam et *al.* 1994; Chuoke et *al.* 1959). Flow mechanism such as viscous fingering, capillary fingering, snap off and the displacement processes related to imbibition and drainage have been also studied with the help of various micromodels (Zhang et *al.* 2011; Sharma et *al.* 2011; Romano et *al.* 2011; Gutiérrez et *al.* 2008; Lovoll et *al.* 2005; Jeong and Corapcioglu 2005; Ferer et *al.* 2004; Sugii and Okamoto 2004; Frette et *al.* 1997; Lenormand 1989, Lenormand et *al.* 1988; Mattax and Kyte 1961).

The earliest example of two-phase flow displacement experiments can be found in the works of Lenormand et *al.* (1983). They have fabricated channels in the shape of capillary duct using transparent polyester resin material. Meniscus displacement mechanism such as snap off or piston type motion are observed at different flow conditions.

Micromodels have been extensively used to study the mechanism involved in oil recovery from oil reservoirs in presence of gas and other fluid phases (Keller et *al.* 1997).

2.3 Significance of 2-D micromodels

Visualizing the fluid flow in soils and geomaterials is a challenging task as these real materials are not transparent to visible light. Fluid flow investigation in real porous material samples such as reservoir core are preferably used to gather macroscopic data like pressure drop, outlet fluid properties and saturation profiles (Askarinezhad et *al.* 2018). However, fluid and particle transport mostly occurs at pore scale, which can be considered as the smallest structural unit in actual reservoirs and so as to develop more efficient oil recovery methods, a deep understanding of insight of these flow phenomena is required. Thereby, these lab scale flooding experiments that uses real sample reservoir rock as core, lack flexibility for systematic research on the pore-scale aspects such as the effect of pore size, aspect ratio, pore-to-pore distance, pore-scale cascade of water-oil displacement events such as direct invasion, imbibition and snap-off. Therefore, using these models, direct visualization and quantitative description of pore scale behaviour of multiphase fluid-fluid interaction is still difficult, due to the complex 3-D geometry of the real porous media (e.g. subsurface rocks).

With the development of computer generated digital design tools, it has now become possible to fabricate a wide variety of more complex 2D and 3D micromodels (Tsakiroglou and Avraam 2002). With the passage of time, researchers are able to fabricate micromodels with microstructures (Folch et *al.* 1999) as well as with two-dimensional porous material representation, which are extensively used to perform visualization experiments (Conn et *al.* 2014; Fathollahi et *al.* 2019). These 2-D representations may consists of Hele-Shaw cells (Chuoke et *al.* 1959), small packed glass spheres sandwiched between two flat glass plate (Chatenever and Calhoun 1952), regular connected network of pores designed to investigate specific phenomenon (Blois et *al.* 2015), replicas of two-dimensional images of actual reservoir rocks (Kumar Gunda et *al.* 2011). Micromodels have been used as an effective qualitative and

quantitative tools to establish a better understanding of fluid flow patterns, fluid-fluid or fluid-solid interactions in pore throats and pore bodies of different porous materials at multiple length scales (mili, micro or nano scale) (Karadimitriou et *al.* 2012). These micromodels should contain at least one transparent side to allow visualization experiments.

Over the time, 3-D micromodels have been also tentatively fabricated to mimic 3D porous structure. Fand et *al.* (1987) and Kececioglu and Jiang (1994) constructed the porous medium in the form of packed beads to mimic complex natural porous media. Later, Bowden et *al.* (2010), Sen et *al.* (2012) and Krummel et *al.* (2011) represented the porous medium in the form packed beads and performed multiphase flow experiments. These kinds of models are limited to engineered porous media that contains random or orderly packed granular system and do not provide a realistic representation of actual pore connectivity. Therefore, in recent times, 2-D micromodels have been extensively used to investigate many common fluidic phenomena inside porous media related to enhanced oil recovery applications such as chemical water flooding (Mohammadzadeh et *al.* 2019), foam flooding (Conn et *al.* 2014), surfactant flooding (Kianinejad et *al.* 2014) and polymer flooding (Sedaghat et *al.* 2013), steam flooding (Lyu et *al.* 2018), capillary trapping/fingering (Geistlinger et *al.* 2016), foam coalescence (Almajid and Kovscek 2016) and fluid analysis such as the measurement of minimum miscibility pressure of CO_2 in crude oils (Zhang et *al.* 2011) due to the advantage of easy and clear visualization at the pore scale. Even though such models lack some three-dimensional aspects such as lesser connectivity compared to the 3-D skeleton of pore structure, they facilitate means to study micromechanics of displacement processes at the pore-scale.

2.4 Summary and Scope of Research

Understanding the physics of fluid flow inside complex porous structure is an extremely difficult task. The dynamics of immiscible multiphase flow is relevant to many science and engineering fields that includes mobilization of trapped hydrocarbon in enhanced oil recovery, geological carbon sequestration, membrane-based fuel cells etc. Fluid flow Investigation in real porous material samples, like membrane devices and oil displacement core-flood device are common. In these types of studies usually macroscale data like pressure drop, outlet fluid properties and saturation profiles are measured. However, using these models, direct visualization and quantitative description of pore scale behaviour of multiphase fluid-fluid interaction is still difficult, due to the complex 3-D geometry of the real porous media (e.g.

subsurface rocks). Although porous cores offer the advantages of realistic wettability and pore structure, they lack flexibility for systematic research on the pore-scale aspects such as the effect of pore size, aspect ratio, and pore-to-pore distance. They often envision a macro-scale prospective although micromodels are used in such investigations. For example, the effect of pore structure is often neglected and the pore-scale cascade of water-oil displacement events such as direct invasion, imbibition and capillary drainage, and snap-off are not analysed. However, direct measurement of fluid flow parameters such as velocity especially at pore level is difficult to obtain due to the opacity of these materials. Therefore, to perform the experimental analysis, artificial porous medium that mimics the porous structure, known as micromodels are created and developed time to time. In these micromodels, numerous visualization experiments are performed to get insight of fluid-fluid movement at pore scale.

Micromodels have been used as an effective qualitative and quantitative tools to establish a better understanding of fluid flow patterns, fluid-fluid or fluid-solid interactions in pore throats and pore bodies of different porous materials at multiple length scales (mili, micro or nano scale). With the passage of time, researchers are able to fabricate micromodels with microstructures as well as with two-dimensional porous material representation, which are extensively used to perform visualization experiments.

The most common method of fabricating micromodels is the lithography technique, which transfers the predesign geometric pattern from a mask to a photoresist layer on the substrate like silicon wafer or glass. The most commonly used lithography technique is the photolithography technique. This kind of fabrication process like photolithography and etching are costly and time consuming. The cost of the substrate material like silicon wafer is also very high that creates an obstacle to the researchers while studying the fluid flow behaviour in permeable media. Soft lithography is a method that is used to replicate the micro patterns on the surface of soft materials like elastomeric stamps using moulds and photo-masks. Among elastomeric stamps PDMS is the most commonly used material for the fabrication of micromodels. PDMS is a very low-cost material compared to the other substrates like silicon or glass that are used in traditional micro-fabrication methods. Due to the ease of bonding and excellent optical properties, PDMS is the most suitable material for micro fluidic devices. However, the fabrication of PDMS micromodels by soft lithography depends on a master with micrometric features that need to be made in a clean room using photolithography and microfabrication methods. In addition, the photolithography technique is comparatively

expensive, time-consuming and beyond the reach of many researchers. In order to overcome the shortage of micromodel and to fabricate low cost micromodel, new advances or enhanced strategies have been explored gradually to diminish the high expenses that come from using conventional photolithography technique.

The reviews of previous work have clearly suggested that several works had been done to understand the fluid-fluid interaction in porous materials. In earlier days, flow processes at the pore scale were investigated using 2D micromodels with a simple network geometry and imaged the interaction between two immiscible flowing fluids. Later, micromodels were constructed with a more complicated geometry. Since the 1980s, the flow pattern of micromodels has been computer generated and with the development of new techniques more complicated micromodel fabrication can be achieved which were based on the geometry and topology of the real porous medium. A number of attempts have been made to qualitatively characterize fluid–fluid interactions at the pore scale in 2D porous models. Several attempts also have been made by the various authors to capture the dynamics of these processes or quantitative measures of the dynamical processes. A series of displacement experiments were conducted to investigate the impacts of viscous and capillary forces on displacement stability and fluid saturation distributions in pore network micromodel with precisely micro fabricated pore structures.

Experimental observations were done to understand the effects of different parameters such as fluid viscosity and density, interfacial tension, wetting properties and heterogeneity of the porous media, fluid flow rates, and the considered length scales on the fluid flow in porous micromodel systems. Pore-scale multi-phase displacement phenomena were visualized in micromodels, which were two-dimensional (2D) pore network patterns, etched into materials, such as silicon, glass, polydimethylsiloxane (PDMS). Many investigators utilized the micromodel in numerous studies to visualize EOR processes. Steam injection, polymer-assisted dilute surfactant flooding, water alternating gas (WAG) as well as gravity-assisted tertiary gas injection process were performed to increase the sweeping efficiency in oil recovery processes. Some investigators also used real sandstone micromodel to visualize and characterize water injection in low permeable rock. In recent time, many authors have conducted a number of flow visualization experiments to study the effect of bacterial flooding on oil phase distribution at the pore scale. Hence, considerable progress has been done both at the fabrication part in developing methodology to fabricate micromodels of numerous

geometry, topology and developing various experimental setup for carrying out many experiments to investigate the microscale fluid behavior at pore scale.

In this study, our prime objective is to fabricate a cost effective porous micromodel using a noble method that can be used to investigate the fluid flow behaviour at micron scale. Therefore, we have emphasized on the fabrication steps and explained in detail. In the present work, a noble method to fabricate both homogeneous and heterogeneous porous micromodel have been developed. Furthermore, an attempt has been made to reveal the technical practicability of this strategy, typically by using round hole perforated metal sheets as template to fabricate the micromodels. Thereafter, the fabricated micromodels are tested for fluid flow experiments. In addition, micro PIV analysis of fluid flow is performed to map the velocity field and to find the applicability of these micromodels thus fabricated. Using this method, different porosity micromodels on PDMS substrate can be fabricated very easily and also at a very low cost. The fabricated samples of micromodels are placed under the microscope, and the visualization experiments are carried out using particle image velocimetry (PIV) technique. From the flow visualization, experiments the velocity of the flow field is quantified. The present work also reports the application of micro-PIV analysis to study the pore scale flow through the interconnected pore network geometries that characterize porous media. The feasibility of the technique is demonstrated by performing single-phase flow measurements through the pore bodies and adjacent pore throats of a two-dimensional flow cell.

In addition, the fractured porous micromodel in PDMS has been also fabricated using a method similar to that of soft lithography technique where a readymade master pattern is used. Thereafter, an attempt has been made to study the single-phase and two-phase flow phenomena in fractured porous media. The flow visualization experiments are then performed at various locations of the micromodel to get an overview of effect of flow rate on the fluid flow pattern in case of single-phase flow and to get information about fluid saturation and dynamics of fluid movement on a special designed fracture geometry in case of two-phase flow. The micro-Particle Image Velocimetry (μPIV) analysis is carried out to map the flow velocity near the fracture and at other locations of the porous micromodel whereby the effects of fracture on fluid-fluid interaction are evaluated.

Our prime aim was to check the effect of flow rate on the flow pattern (whether regular or chaotic) at any location of the micromodel for single-phase flow at the presence of fractures.

Thereafter, fluid flow observations are performed to check the fluid saturation and instability of fluid phase in case of two-phase flow in a specially designed newly fabricated fractured micromodel, which is fabricated by a novel approach. Previous authors studied the instabilities at pore level in various homogeneous and heterogeneous micromodels (Roman et *al*., 2016). Therefore, in our case, we have also studied the instabilities of two-phase flow in this fractured micromodel with the help of fluorescent microscopy and micro-PIV method is used to quantify the flow field and to observe it in a much clear view compared to the works of previous authors. It is worth noting that the main advantage of this fabrication method lies in its flexibility as this fabrication method can be adopted to fabricate fractured micromodels having different orientation of fractures and geometry at a very low cost. In future, we have planned to study more about two-phase flow mechanism in many aspects by conducting experiments in micromodels having fractures of different dimension, orientation and geometry.

Chapter 3

Flow Visualization in Porous Micromodels

3.1 Introduction

Porous media are found everywhere in nature and almost all of the materials are porous up to some extent. These porous media consist of random structures where the position of solid and liquid phases are random function of space. Flow and transport through porous media is also important in fields like designing drug delivery system and tissue engineering. In some porous media such as oil reservoirs, the pressure gradient force plays an important role to drive the fluid flow. Although in practical scenario, the flow through porous media has applications mostly in multiphase flow. The present study focuses into the single-phase flow without inertia effects.

Porous media can exist in nature in different atmosphere and geographic topology as well as in other engineering fields. It is also important to understand that the flow through porous media are surrounded by another porous medium having different volume fraction. Some typical examples are found in filters and oil reservoirs where the dual porosity exists together. In addition, the fluid flow through fractured porous media has received a great deal of attention in fields like geotechnical and petroleum engineering. In practical situation, these fractures are generated when two different porous matrix section are separated by free space. These conditions are depicted using schematic diagram as shown in Figure 3.1.

As briefly stated at the beginning, understanding the physics of flow in porous media is important in many engineering fields like the recovery of oil from underground reservoirs in the presence of gas and water phases and other chemical engineering applications. Over the years, many experimental investigations have been performed to visualize the insight of flow mechanism in the porous media. However, due to the opacity of these porous media, visualizing and understanding the fluid interaction inside the porous media becomes extremely difficult. Because of this, micromodels are often used.

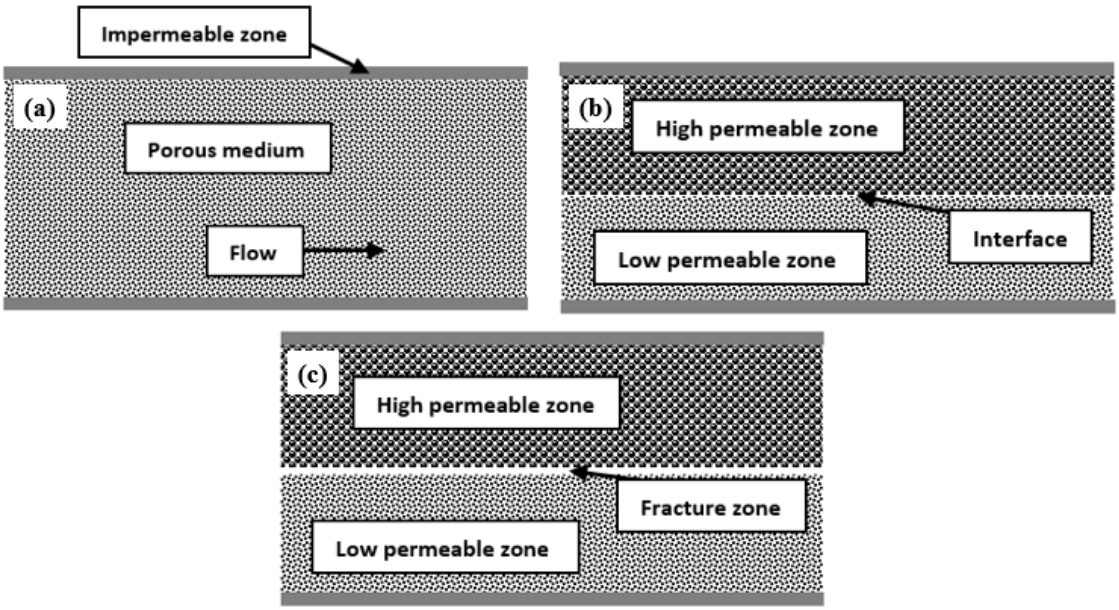

Figure 3.1: Schematic diagram of (a) homogeneous porous medium, (b) dual porosity system where a porous medium is adjacent to another porous medium, and (c) a dual porosity system with a horizontal fracture

An efficient way to study the fluid-fluid interaction in a porous medium is through the development of an artificial transparent porous medium with known properties, commonly referred to as a micromodel. These micromodels are found to be very useful tool to study the pore scale transport processes. Visualizing the fluid flow in soils and geomaterials is a challenging task as these materials are not transparent to visible light. Most of the experimental analysis are therefore based on the visualization of flow phenomena in artificial porous medium, also known as micromodels (Karadimitriou and Hassanizadeh 2012). These micromodels are comprised of a network of connecting pores, an artificial portrayal of real porous medium. Thus, using these micromodels it becomes possible to study and to gain information regarding pore scale flow events up to the considerable extent. In early studies, these micromodels had simple and plain porous network structure. The very first fabricated micromodel that was used to explore the behaviour of fluid flow at microscale in porous media was a single layer of glass spheres sandwiched between two flat glass plate (Chatenever et *al.* 1952). With the passage of time, the use of micromodels as visualization tool in various multidisciplinary studies, has been increasing to understand the fluid flow mechanism in further details. The application of micro-models has increased over the past several decades, especially with regard to visualize the processes relating to enhanced oil recovery (EOR) and other oil recovery processes. Since 1980s, with the development of new computer based application software, it has become possible to fabricate the micromodels containing complex network

patterns (Tsakiroglou and Avraam 2002). At present, the most common method of fabricating micromodels is the lithography technique, which transfers the predesign geometric pattern from a mask to a photoresist layer on the substrate like silicon wafer or glass. The most commonly used lithography technique is the photolithography technique (Chen et *al.* 2003). In this method, a photomask containing pore network design is printed. Thereafter, a photoresist material is spin coated on the micromodel substrate and the pore network design is transferred from the mask to the photoresist material by exposing it to ultraviolet light. Later, with the help of a developer solution, the specific area containing the pore network is washed away. Finally, with the help of etching technique, the network pattern is constructed on the surface of the micromodel substrate. In most of the cases, this micromodel substrate embedded with a pore network (also known as master pattern) is directly bonded with transparent sheet like glass plate to construct the final version of the micromodel. This kind of fabrication process like photolithography and etching is costly and time consuming. The cost of the substrate material like silicon wafer is also very high that creates an obstacle to the researchers while studying the fluid flow behaviour in permeable media.

Glass-etched micromodels also have been intensively used to study numerous characteristics of fluid flow in porous media such as chemically assisted water flooding process in heavy oil recovery (Mohammadzadeh et *al.* 2019), effect of carbonate water injection in both homogeneous and heterogeneous porous media in oil recovery (Mahdavi and James, 2019; Mosavat and Torabi 2016). The first etched-glass micromodel was developed by Mattax and Kyte (1961). The pore network of the micromodel was built up by the straight interconnected flow channels. It was a very good approach to observe and visualize flow behaviour. The main drawbacks of such micromodels was the formation of concave shaped pore walls during the etching process. A further development of the micromodel was achieved by Davis and Jones (1968). They worked on the drawbacks and limitations of the micromodel and came up with a new fabrication technique. A photosensitive fluid, which was resistant to several solvents after being exposed to ultraviolet light, was coated on glass. Hence, they could produce more complex pore structures, which met the requirements for more realistic experiments. The structure of the pore networks embodied into a micromodel are usually created either by analyzing the images of thin sections or by process-based analysis. McKellar and Wardlaw (1982) used a photo-imaging technique of thin sections followed by chemical etching of glass to produce micromodels.

The first silicon substrate micromodel was produced by Hornbrook et *al.* (1991). The pore structure of the micromodel was based on a thin section of a Berea sandstone. With a scanning electron microscope (SEM), a high resolution photograph was taken and digitally processed. The drawback of this technique was that the SEM captured only a very little portion of the thin section. Hence, the edges of the photograph had to be processed to loop this unit cell image together and to produce the definite matrix area. Direct pore scale observation was also done using the novel calcite micromodel chip (Jamshidi et *al.* 2019). At present, the commonly used substrate material to fabricate micromodels are silicon wafers and glass slides. The silicon wafer is more favorable as it gives more precise and controllable etching process and micron scale pore structure also can be represented in these wafers. These features of the silicon wafer makes it the most suitable substrate to mimic and replicate complex pore structures analogous to that of real reservoir rocks structures.

In recent times, the use of thermosetting plastics as substrate material have also been observed to fabricate various porous micromodels. A rigid plastic known as cyclic olefin copolymer (COC) have been used by Hsu et *al.* (2017) to fabricate fractured micromodel by using hot embossing technique and thereafter to carry out two-phase flow experiments. In addition, complex techniques such as stereo lithography (Ikuta et *al.* 1994), laser-chemical three-dimensional writing (Bloomstein 1992) as well as micro- joinery (González et *al.* 1998) are the other techniques developed to form complicated micromodels on the different substrate materials. Furthermore, photolithography technique is used to fabricate 3-D microchannel in elastomer substrate, where the micromodel was fabricated in layer-by-layer configuration (Jo et *al.* 2000).

However, there is an another method where the master mould is used as patterned template to replicate and transfer the pore network into soft materials like polymers to reduce the cost of fabrication in photolithography process. This method is known as soft lithography (Xia and Whitesides 1998). On the other hand, polymers are less expensive and serve as good alternative substrates to fabricate the micromodels. Among them PDMS is the most commonly used polymer to fabricate the microfluidic devices as it can be easily replicated to any desired shape. PDMS micromodels are very useful to perform visualization experiments because of its transparency and its ease of sealing onto substrates like glass. Several investigators have used PDMS micro-moulding technique to fabricate the micro fluidic devices (Folch et *al.* 1999). The micro-moulding method is straightforward and quick as compared to the conventional

etching and bonding approaches. By using soft lithography technique, the cost of fabrication of micromodel can be reduced. However, it requires a master pattern (produced by photolithography process) embedded with the pore network. Interestingly, photolithography itself is a costly and time consuming process due to which many researchers are deprived of using these facilities. However, unlike in photolithography, where the master mould is directly used to get the final version of the micromodel, here (in soft lithography) the same master mould is used as patterned template and the pore network features is replicated to low cost soft materials. In order to tackle these situations and to fulfill the shortage of low cost micromodels, numerous strategies have been continuously explored to reduce the high expenses that arises from the use of conventional photolithography method.

In the present work, a noble method has been developed to fabricate both homogeneous as well as heterogeneous porous micromodels at a very low cost. Using this method, different porosity micromodels on PDMS substrate can be fabricated. In addition, the technical applicability of this noble strategy that uses thin perforated metal sheet as patterned template to fabricate the porous micromodels are also checked. The fabricated samples of micromodels are placed under the microscope, and the visualization experiments are carried out using micro-PIV technique. From the flow visualization, the velocity of the flow field is quantified. The present work also reports the application of micro-PIV analysis to study the pore scale flow through the interconnected pore network geometries that characterize porous media. The feasibility of the technique is demonstrated by performing single-phase flow measurements through the pore bodies and adjacent pore throats of a two-dimensional flow cell.

3.2 Materials and Methods

Unlike photolithography, a mask that contains the pore network is not used as master to fabricate these channels. However, in this work, a readymade pattern is used. Thin round hole perforated sheets (readymade pattern) are used as master pattern to fabricate these channels. Apart from this material, polydimethylsiloxane (Sylgard 184, Dow Corning) along with curing agent, silicone connecting tubes, and silicone adhesive sealant are used. Thin glass slides coated with tiny layer of cured PDMS is used to cover the open side of the micromodel. The sample image of the porous plate that is used as master template is shown in Figure 3.2. The porous matrix area of the micromodel covers a rectangular area (50 mm × 25 mm) of the porous plate and the convergent areas on the both side are covered with adhesive tape (as shown in Fig. 3.3a) for the purpose of providing the inlet and outlet ports, and the inlet and outlet flow areas.

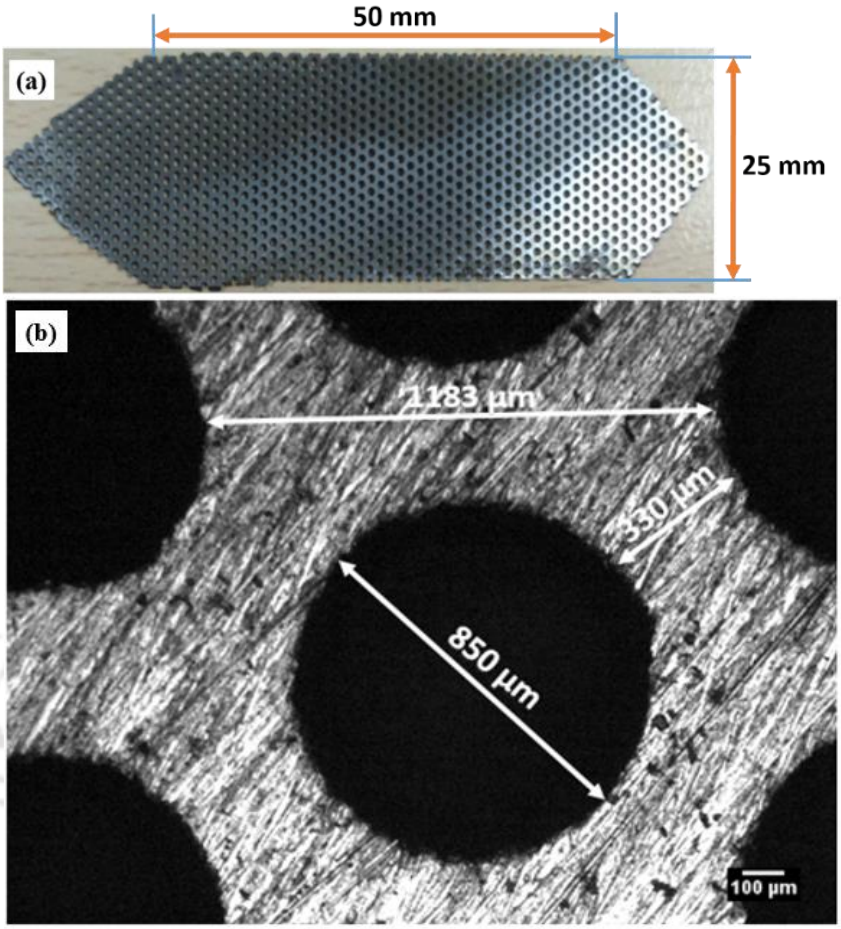

Figure 3.2: Image of the (a) master pattern, (b) enlarged view of the pattern

3.2.1 Creation of homogeneous micromodel

The master is kept on a petri dish in such way that the bottom side is fixed firmly with the petri dish and the mould is thus prepared. The liquid silicon elastomer sylgard 184 is then mixed with its curing agent in 10:1 mass ratio (Karadimitriou *et al.* 2013). The liquid mixture is mixed thoroughly for several minutes in a container. In this work, the physical amount used to fabricate one unit of micromodel is 50 g of silicone elastomer and 5 g of curing agent respectively. The volume of liquid mixture taken in each case should be judged carefully, so that it provides a considerable thickness to the final version of PDMS micromodel. On the other hand, it should be sufficiently thin so that it can be drilled easily to make holes for inlet and outlet purposes. However, in this fabrication process, inlet and outlet ports having smooth edges are created by placing screws vertically at the required positions. During the mixing process, plenty of bubbles are entrapped in the mixture. These bubbles are necessary to be removed before curing the mixture, otherwise it may cause faulty porous sections within the micromodel. Therefore, to expel these air pockets, the container containing the mixture is

placed into a vacuum chamber. After degassing the liquid mixture, it is poured over the master pattern in a Petri dish. The liquid mixture must be poured very slowly over the master pattern to avoid any further entrapment of air bubbles. The necessary precautions that should be kept in mind while pouring the liquid PDMS are well explained in the work of Karadimitriou et *al.* (2013). The container can be kept for couple of minutes in an open environment so that the remaining trapped bubbles can come up to the surface. The Petri dish is then placed in a hot air oven at around 80^0C for almost 2 hours for the purpose of setting the liquid PDMS.

In general, many combination sets of curing temperature and time are available and can be employed easily. The extreme two sets that can be used for curing the PDMS are 200^0C for 10 minutes and keeping the mixture in ambient temperature for 48 hours (Karadimitriou et *al.* 2013). However, both these sets have their own demerits as the use of very high temperature can establish residual stress inside the material, and on the other hand, allowing the liquid mixer to set in an open environment can attract dust particles resulting the formation of a faulty micromodel. Hence, a suitable combination is used to cure the mixture. After curing the mixture, it is permitted to reach the ambient temperature and the PDMS slab is separated from the template pattern very carefully. It is also important to notice that the process of separation of the slab from the pattern should be very slow; else, it can leave some pore network features in the template that results in the formation of faulty micromodel. After peeling it off, the open side of the micromodel containing the pore network grooves is covered with a thin glass slide. Use of glass slide is beneficial in giving a rigid base to the micromodel and at the same time, it provides the optical transparency for visualization experiments. Thus, in order to seal the micromodel, a glass slide is used to give a firm base. There are a number of PDMS bonding strategies that have been reported till now and these strategies are also compared with each other in accordance with their bonding strength and their suitability during application (Eddings et *al.*, 2008; Samel et *al.*, 2007). In the present case, the inner side of the glass slide is also coated with a tiny layer of liquid PDMS to provide a uniform wettability throughout the micromodel. Finally, the PDMS replica with the pore network grooves facing down is placed on the glass slide, where pressure is applied gently on the slab for its conformal adhesion and it is again put inside the oven for another two hours at 80^0C. This final temperature treatment allows the PDMS slab to crosslink with the tiny layer of the liquid PDMS that is coated on the glass slide. Once the PDMS slab is bonded to the glass plate, the edges of all lateral sides are sealed with silicone adhesive sealant to get the final applicable version of the micromodel. Figure 3.3 depicts the pictorial demonstration of steps involved in the fabrication process.

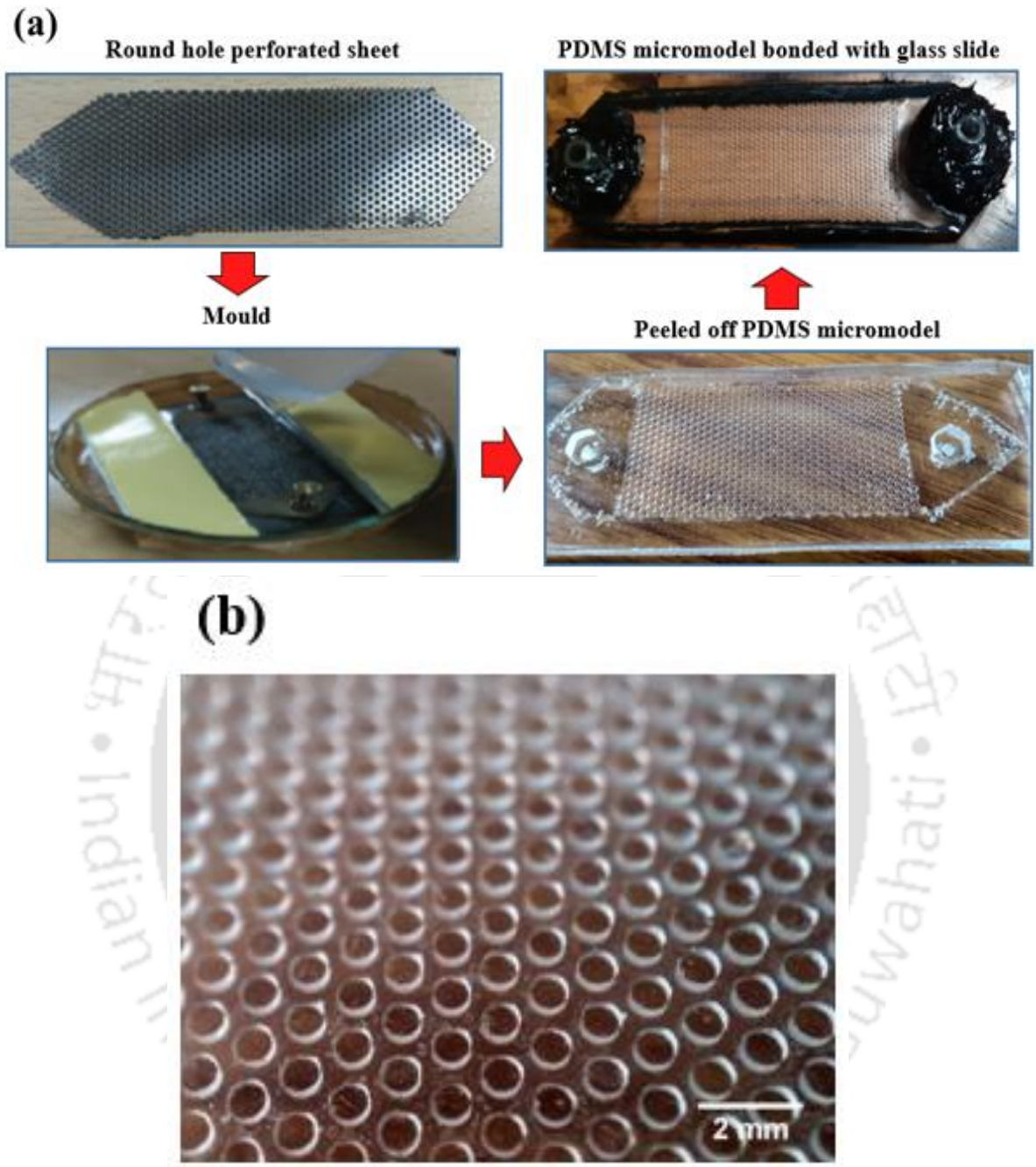

Figure 3.3: (a) Schematic description of steps for fabricating the micromodel, (b) enlarged view of the cylindrical pillars of the micromodel

3.3 Experimental setup

Upon completion of the fabrication of these micromodels, the samples are used as a tool to perform the pore scale visualization experiments. Figure 3.4a depicts the experimental setup, while Figure 3.4b shows the fabricated porous micromodel. The micromodel consists of an inlet port, an outlet port and the homogeneous porous matrix area of dimension 50 mm × 25 mm × 0.15 mm ($L \times W \times H$).

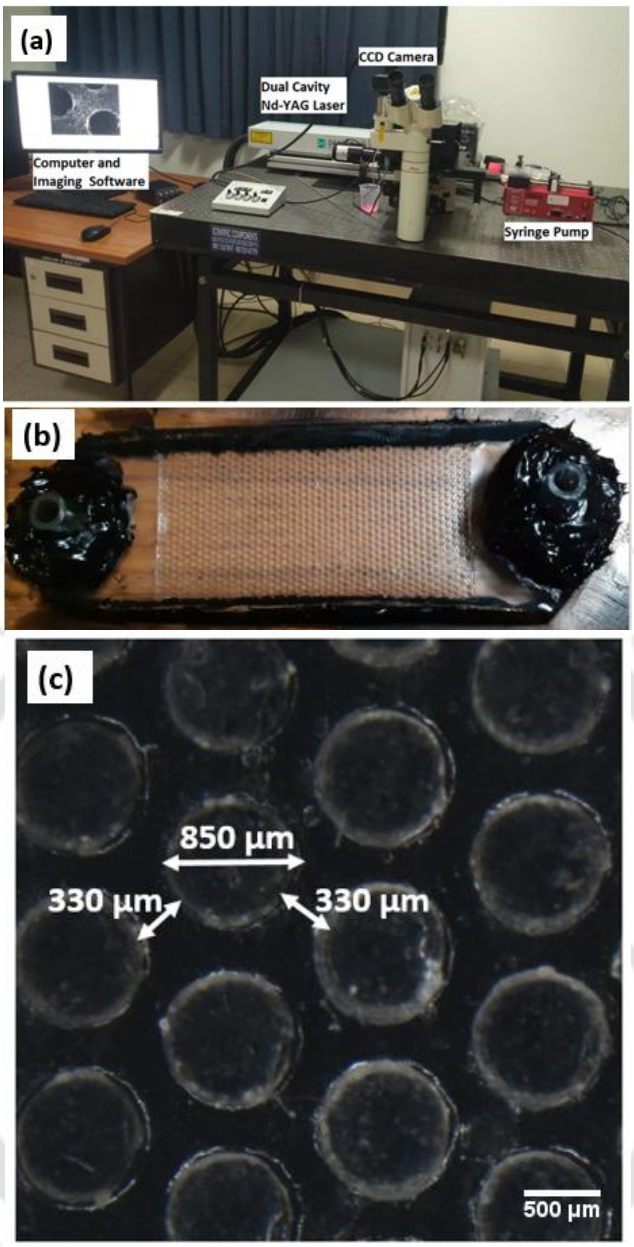

Figure 3.4: Details of (a) Experimental setup, (b) image of the micromodel and (c) enlarged view of a part of the homogeneous porous micromodel

The porous region containing uniformly distributed cylindrical pillars of diameter (*D*), 850 micron are arranged in a pattern similar to two-dimensional hexagonal structure (Figure. 3.4b). The depth of the micromodel (*H*) is same as that of the thickness of porous plate, which is 150 micron. The inlet and outlet dimensions of the micromodel are of 3 mm, whereas the maximum distance (pore size, *s*) and the minimum distance between the pillars (throat, *t*) are 1183 µm and 330 µm, respectively that yields approximately a porosity of 0.61 (Figure 3.4c). A syringe pump (NE 1000 single syringe pump, New Era Pumps, USA) is used to deliver the working fluid to the micromodel at steady pressure. A Leica DM IL inverted microscope having 10x magnification lens (numerical aperture = 0.25) is used for imaging the flow process. While an

Nd:YAG double-pulsed (532 nm) laser is used for illumination and a double-shutter PIV CCD camera (FlowSense EO 4M camera, 2048×2048 pixels at 16 fps) is used to capture the sequence of images. The entire experiments are performed at normal room temperature and at the atmospheric pressure. The single-phase flow experiments are conducted and visualization of fluid flow is performed at three different locations. At each location, three different flow rates viz. 100 µl/min, 300 µl/min and 500 µl/min are used (Reynolds number, Re << 1). The fluid is seeded with FluoSpheres carboxylate-modified microsphere1.0-micron size particles (from Fisher Scientific). The seeding concentration is set at 0.03% (roughly) by volume.

3.4 Results and Discussion

3.4.1 Micro-PIV measurements

During the last decade, the particle image velocimetry (PIV) technique has been used in numerous applications as a non-invasive measurement tool to study the complicated flow fields (*Grant, 1997*). It is a technique used to measure macroscopic velocity of fluid by adding seeding particles to the fluid (Raffel et *al.* 2007). These seeded particles are illuminated with the help of a light source. The successive images are then taken at certain interval of time. These images are sub-grouped to small areas known as interrogation windows. These interrogation windows from successive frames are correlated and the displacement of particles over a certain time interval are estimated statistically to give the flow velocity. The prime advantage of this technique is its non-intrusive nature. Further, this technique is capable of measuring both two-dimensional and three-dimensional fluid flows. Unlike the laser Doppler velocimetry (LDV) (Durst et *al.* 1995) which is a single point measurement technique, the PIV has the ability to map the velocity at multiple points simultaneously. The micro-PIV is the modified version of PIV specially designed to map the fluid velocities at micron scale analogous to microfluidic devices (Devasenathipathy et *al.* 2003; Meinhart et *al.* 1999; Santiago et *al.* 1998).

The PIV is an optical technique to map the fluid flow velocity field on macroscopic level and it becomes micro-PIV when it is applied to microscale. The fundamentals of micro-PIV technique is similar to that of PIV where it is used to get the velocity field at micron scale (Adrian, 2005). Another difference lies with the use of volume illumination in place of light sheet illumination. The simplest form of a micro-PIV setup can be achieved with a microscope connected to a continuous light source such as lamp and a digital camera to capture the images. However, this kind of setup can perform well only for very low flow rate. In case of fast flows,

a longer time interval between two successive images can cause blurred images of the particles giving erroneous results. In that case, the micro-PIV setup composed of a pulsed light source such as laser that is synchronized with a digital camera by a timing unit should be used. The synchronization is done in such a way that the first light pulse is set at the end of first camera frame and the second pulse position is adjusted within the second frame according to the flow velocity. In this way, the time gap between the two frames becomes independent of the camera frame rate. Usually, the frequency double pulsed dual cavity Nd:YAG lasers at 532 nm wavelength is a standard source of light in micro-PIV experiments. These lasers are robust and the light can be coupled easily into the standard beam path of a microscope. Double cavity lasers are composed of two lasers and a beam-combining optics. These two cavities can be triggered independently and can be adjusted for the overlap with the help of beam-combining optics. For capturing the image frames, the double shutter CCD cameras can be used. These cameras are used for high velocities with high magnification, whereby the time interval between two successive images can be reduced to 1 microsecond. The use of florescent particles as tracers can significantly improve the raw image quality in micro-PIV experiments. When these tracers are illuminated by monochromatic laser light source, it gets excited and emits light of longer wavelength, while other obstacles like solid region and boundary of the channel emits light at its original wavelength. A dichroic mirror is placed between the light collecting objective and the CCD camera. It acts as an optical filter that allows the excited florescence light to fall on the camera sensor and blocks the unwanted wavelength generated from the walls and other solid objects. This process significantly enhances the image quality. Figure 3.5 shows the schematic setup of the micro-PIV.

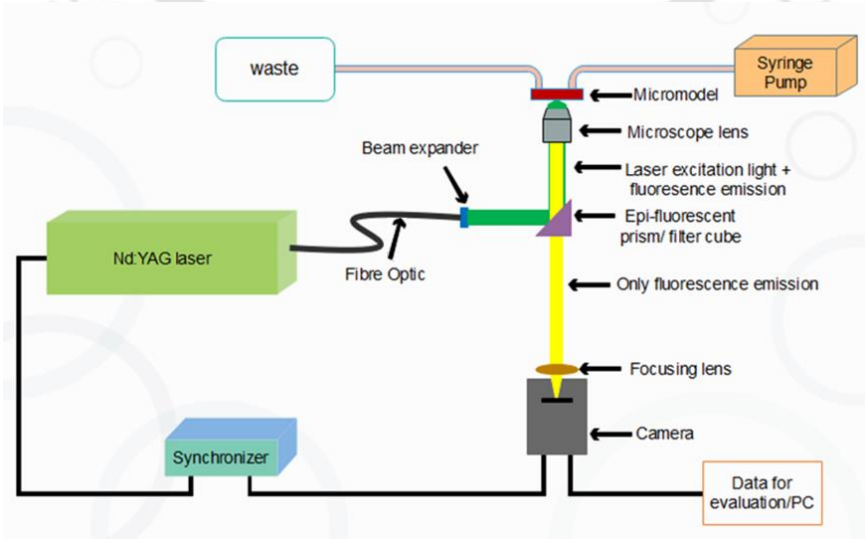

Figure 3.5: Schematic diagram of a micro-PIV setup

During the experiments, a set of paired image frames having tracer particles are recorded at three definite locations of the fabricated micromodel as marked in Fig. 3.6. The masked raw images at three different locations of the micromodel is shown in Fig. 3.7. The black circular regions represent the solid cylindrical pillars, whereas the fluid flow region is seen due to the presence of bright tracer particles. The acquired images are not suitable for direct PIV measurement due to the presence of background noise. These raw images then require pre-processing to remove the unwanted background noise. The velocity vector field is obtained by MATLAB based PIV lab software that uses two frame cross-correlation method to interrogate consecutive image pairs (Thielicke and Stamhuis 2014).

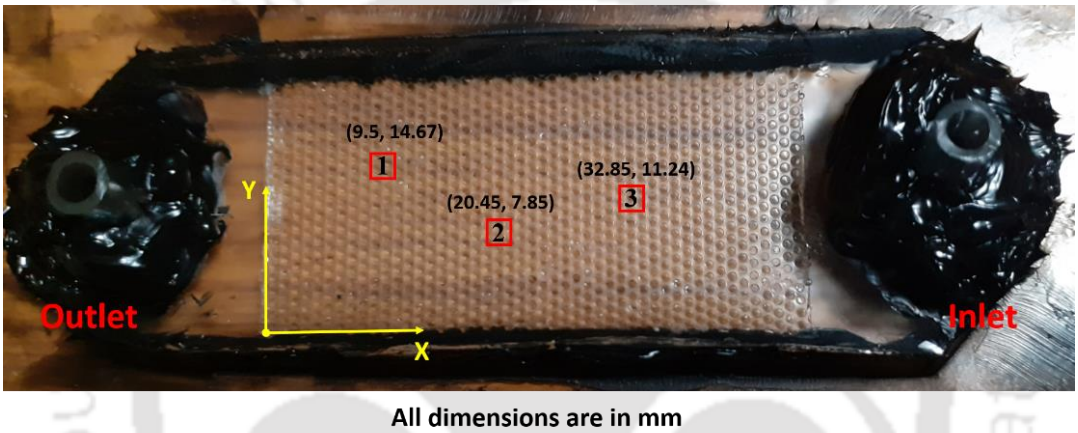

Figure 3.6: Image of the fabricated micromodel with highlighted locations where velocity fields are obtained

The PIV lab software is also used for the image pre-treatment before being processed for cross-correlation. After the pre-processing of the images, it contains only the bright particles that hold the details of movement of the bright particles. The sole purpose of image pre-processing is to enhance the image quality that consequently provide better measurement accuracy. In the cross-correlation methodology, firstly, each image frame is divided into many identical small areas, known as interrogation windows. Later these subdivided areas are correlated spatially with the respective areas of another consecutive frame to obtain the information regarding the displacement of the tracer particles during a definite interval of time. Therefore, to perform this analysis, a fast Fourier transform (FFT) method with multiple passes is used. The first pass contains larger interrogation area as compared to the subsequent passes. Larger interrogation area gives greater signal to noise ratio, but at the same time, it shows poor vector resolution. This is the reason to use smaller interrogation areas for further iterations, which enhances the resolution of vectors.

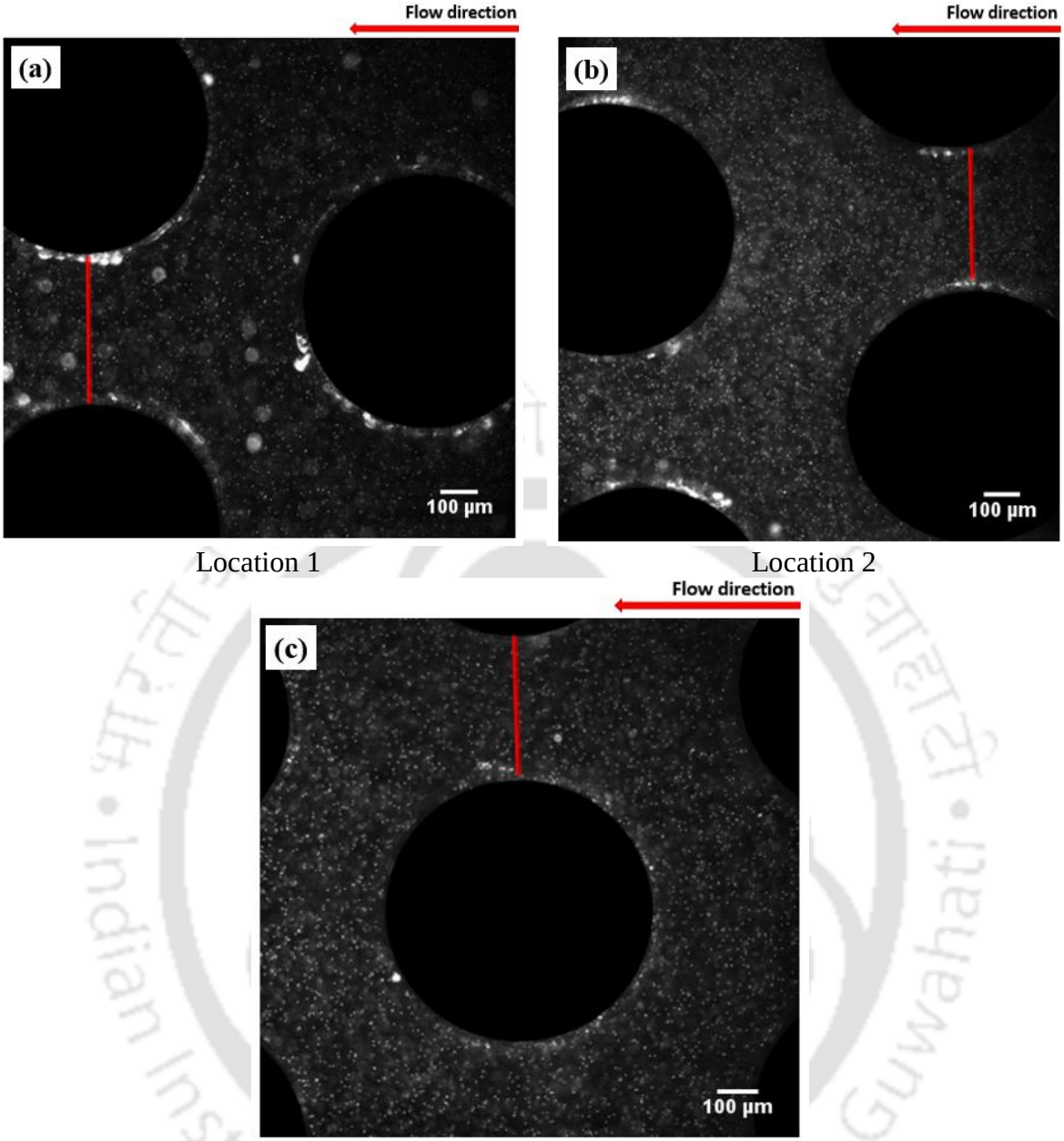

Figure 3.7: Image of the fluorescent particles at different sections of the micromodel

This type of iterative method delivers a wide range of dynamic velocity that provides a larger vector resolutions and better signal-to-noise ratio. In present case, the first pass uses an interrogation area of size 64 × 64 pixels, whereas the second or the final pass uses an interrogation area size of 32 × 32 pixels. To get the satisfactory results in PIV analysis, each interrogation window in the final pass should hold at least 5-10 particles.

The size of the interrogation window must be chosen wisely to allow uniform displacement of the particles within the area and simultaneously it should be of considerable size to hold sufficient data for the calculation (Lindken et *al.* 2009). Finally, the interrogation windows are

arranged at 50% overlapping position and the post processing is carried out to get the instantaneous velocity vector field.

3.4.2. Velocity field

A total of fifty consecutive pairs of image frames are captured at each marked location and their resultant vector field is obtained by taking average values of these frames. Figure 3.8 shows the velocity vector fields at three definite locations as shown in Figure 3.7.

The uniform flow patterns are observed at all the three locations of micromodel. In addition, the magnitude of the velocity vectors are nearly zero in the vicinity of solid boundaries and maximum at the center of throat. At each location, the velocity profile is also obtained for three definite flow rates at various locations along the red line (Figure 3.6). The magnitude of maximum (throat) velocity is found to increase proportionally with the increase in flow rates.

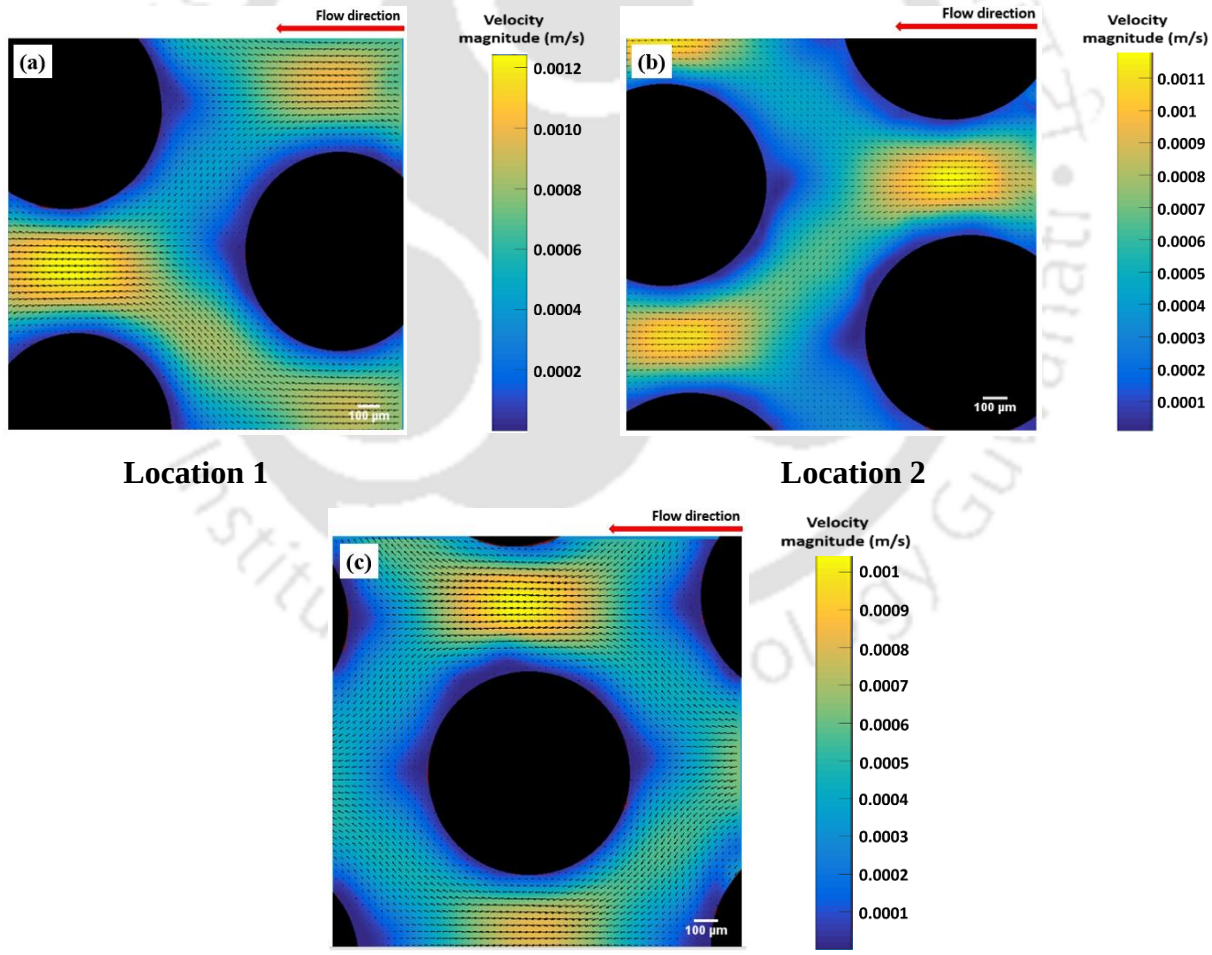

Figure 3.8: Velocity vector map of the micromodel at the three locations (along the red line) corresponding to the images shown in Figure 3.6

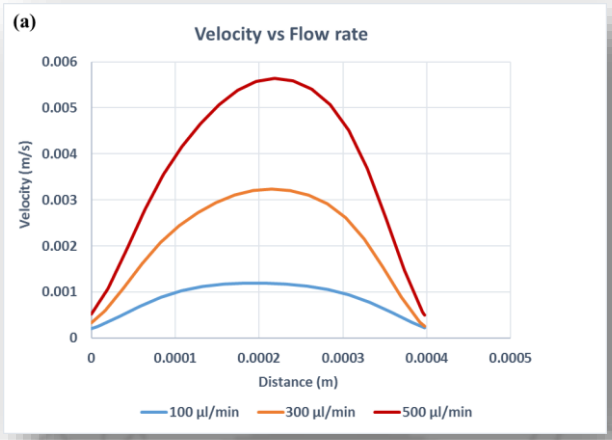

Location 1

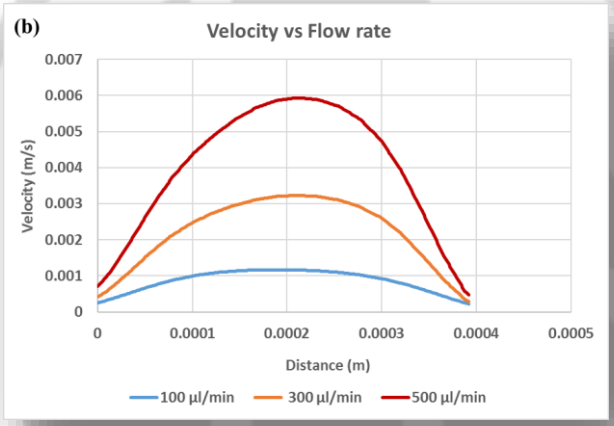

Location 2

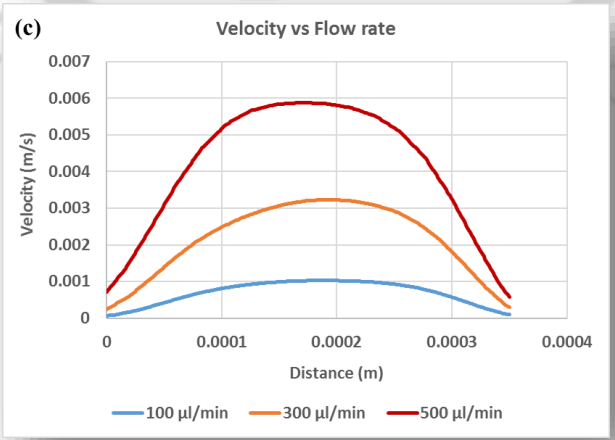

Location 3

Figure 3.9: Velocity profile for the three flow rates at each three section of the micromodel along the red line shown in Figure 3.7

The velocity profile obtained at the throat is observed to be different from its parabolic nature (Figure 3.9). This may happen as the flowing fluid continuously experiences bifurcation and confluence of flow throughout the various locations in the micromodel. Bifurcations tend to distribute the flow over a larger area while confluences tend to concentrate the flow into fewer flow paths characterized by a higher flow rate. In addition, the size and optical properties of the tracer particles must be compatible with the experimental system so that micro-PIV experiments can be carried out smoothly to obtain the velocity of the flow field accurately. Moreover, the camera properties along with the objective lens of the microscope must be selected in such a way that the particles size in the image frame should be resolved up to a minimum of 2–3 pixels (Sen et *al*. 2012). The time gap between two successive images frames must be opted in such a way that the movement of the particles within two consecutive image frames should not be more than the three times the image size of the particles diameter from its initial position.

3.4.3. Effect of orientation

The perforated plate that is used as master pattern in the present fabrication process consists of round holes in two different orientations. Experiments have been carried out at a flow rate of 100 µl/min to investigate the effect of orientation of the fluid flow by changing the orientation in the direction of fluid flow for the same porosity. The flow velocities in two different orientations are quantified and a comparison of the flow velocity in these two orientations are performed. Figure 3.10 shows the schematic of the two orientations of the porous micromodel.

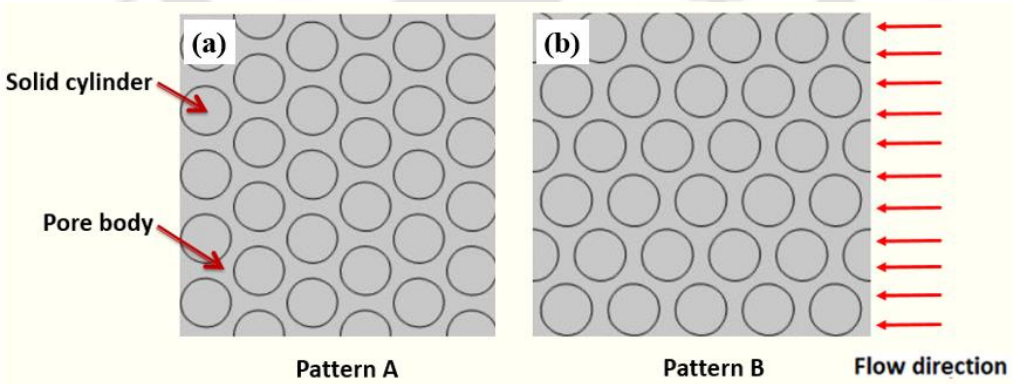

Figure 3.10: Schematic of two different orientations (a) pattern A and (b) pattern B in porous section of the micromodel

The micromodels having porosity 54% and 61% are used to perform the experiments. In each case, the two different orientations of the micromodel having 61% porosity (Patterns A and B) and 54% porosity (Patterns C and D) are shown in Figure 3.11. The impact of orientation on velocity field is seen for both 61% and 54% porosity micromodels. Though the porosity is same

for the two orientations, interestingly, different magnitudes of velocity is observed. Even for the same porosity micromodels, different magnitudes of velocity is observed at different orientations. This is probably due to the formation of preferential path during the fluid flow. In pattern A, both bifurcation and confluence of flow path are seen.

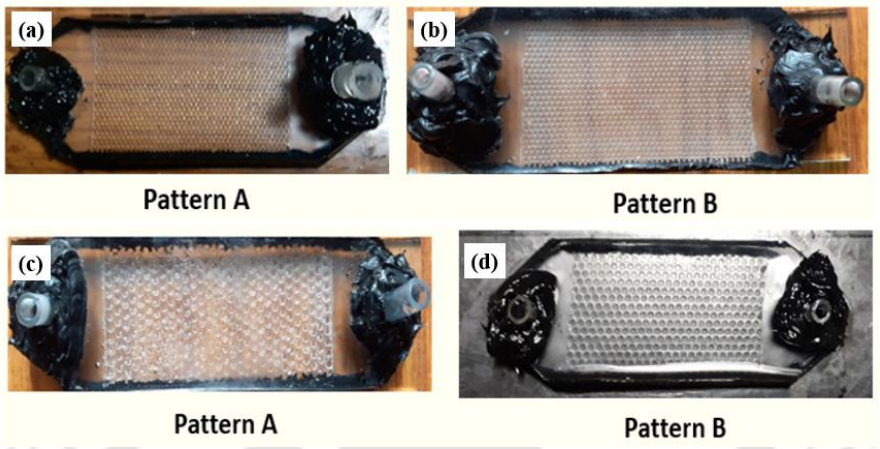

Figure 3.11: Images of micromodels at the two different orientations for (a, b) 61 % and (c, d) 54% porosity

The pressure drop at different flow rates are also studied. To measure the pressure drop across the inlet and outlet of micromodel, the inlet and outlet port are connected to a digital differential pressure manometer (from RS Components and Controls Ltd., India). The range of the manometer is 13.79 kPa with a resolution of 0.01 kPa. The steady flow rates are provided by a syringe pump (NE 1000 single syringe pump, New Era Pumps, USA) as shown in Figure 3.12.

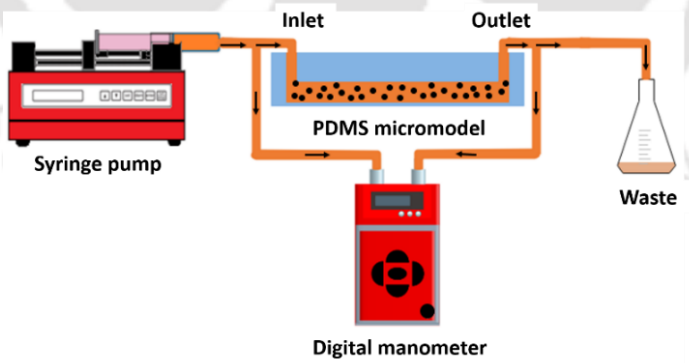

Figure 3.12: Schematic diagram of experimental setup used for pressure difference measurement between inlet and outlet

Figure 3.13 shows the comparison of pressure drop against the flow rates for both the patterns. A higher pressure drop is observed in pattern A than in pattern B of the micromodel for the same flow rate. It happens due to the existence of larger flow area for pattern A as compared to pattern B. While pattern B contains many stagnant region of fluid, the wavy flow paths are seen in pattern B and these flow paths do not merge to other flow paths.

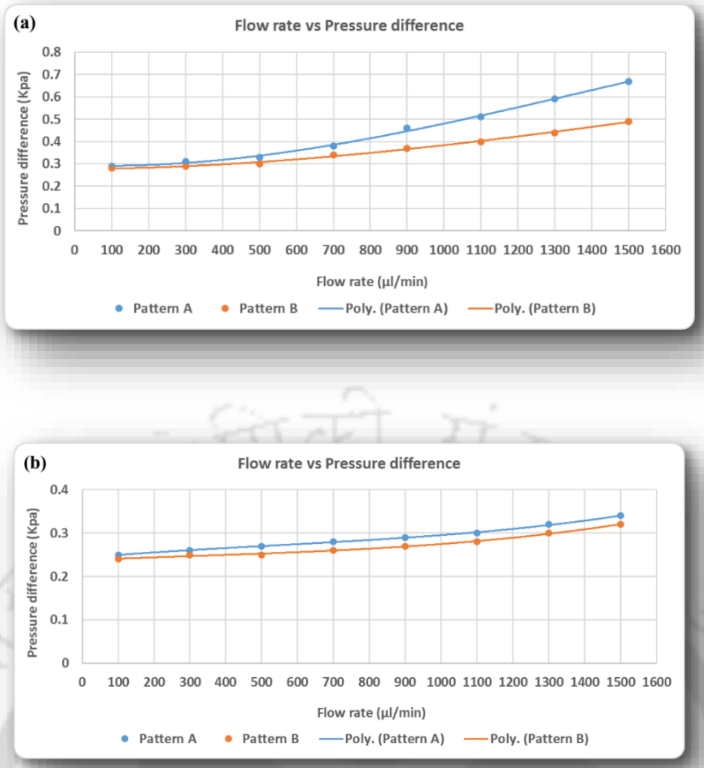

Figure 3.13: Variation of flow rate with pressure drop for (a) 61% and (b) 54% porosity micromodel

Figures 3.14 and 3.15 show the streamlines of two orientations of the micromodels. It is worth noting that even the pressure drop is more in pattern A, the maximum throat velocity is found to be more in pattern A because of the merging of flow paths. It is therefore observed that the orientation creates the different preferential paths that affects the flow velocities. Figures 3.16 and 3.17 show the velocity vector fields at a chosen locations in the two different orientations for 61% and 54% micromodels, respectively.

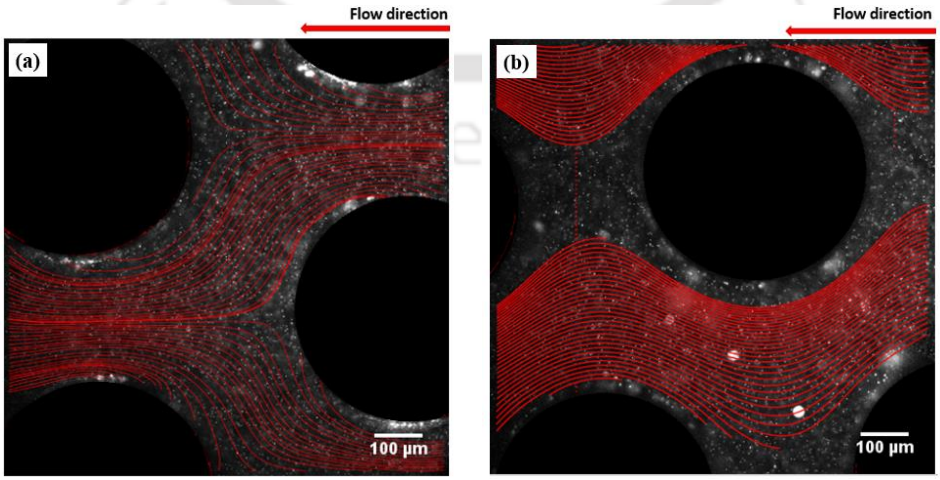

Pattern A **Pattern B**

Figure 3.14: Streamlines at two arbitrary locations of (a) pattern A, and (b) pattern B for 61% porosity micromodel

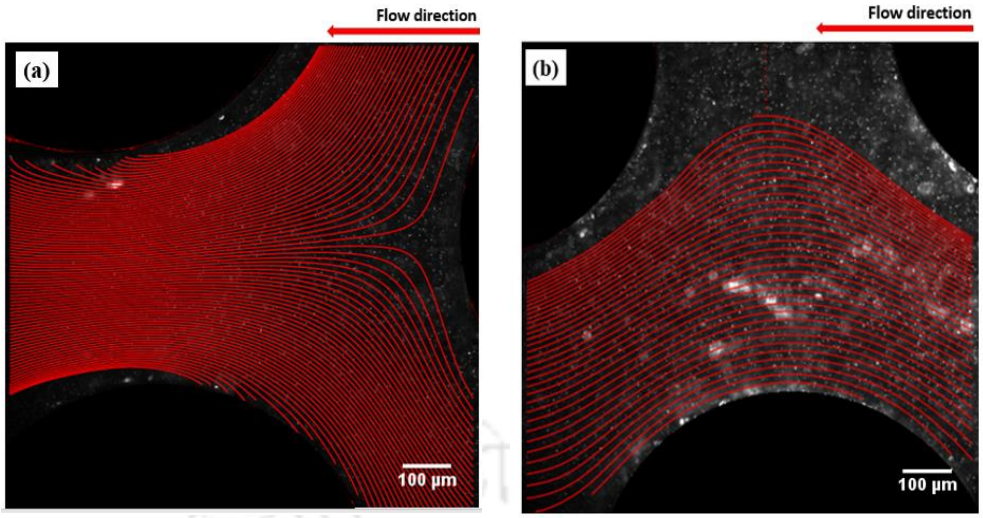

Pattern A **Pattern B**

Figure 3.15: Streamlines at two arbitrary locations of (a) pattern A and (b) pattern B for 54% porosity micromodel

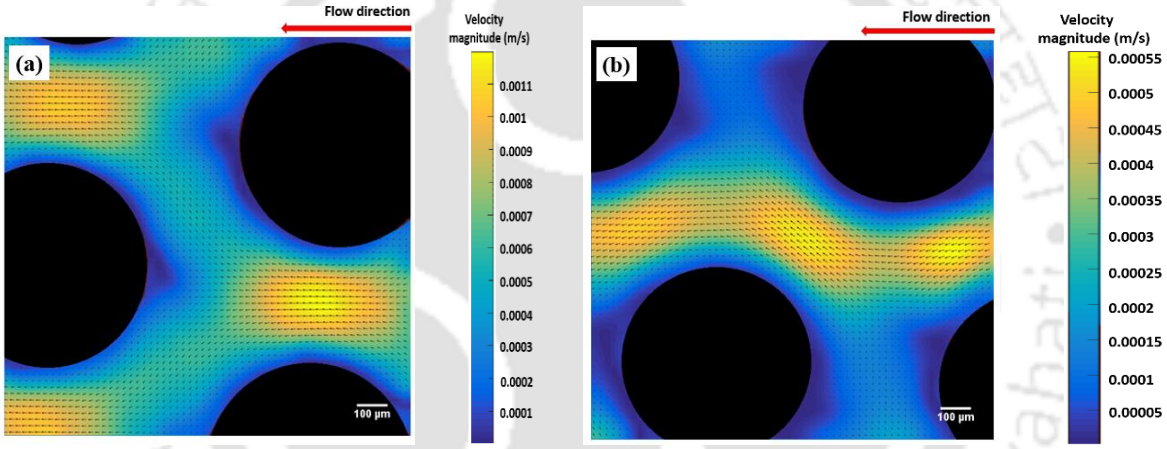

Pattern A **Pattern B**

Figure 3.16: Velocity contours at two arbitrary locations of (a) pattern A And (b) pattern B for 61 % porosity micromodel

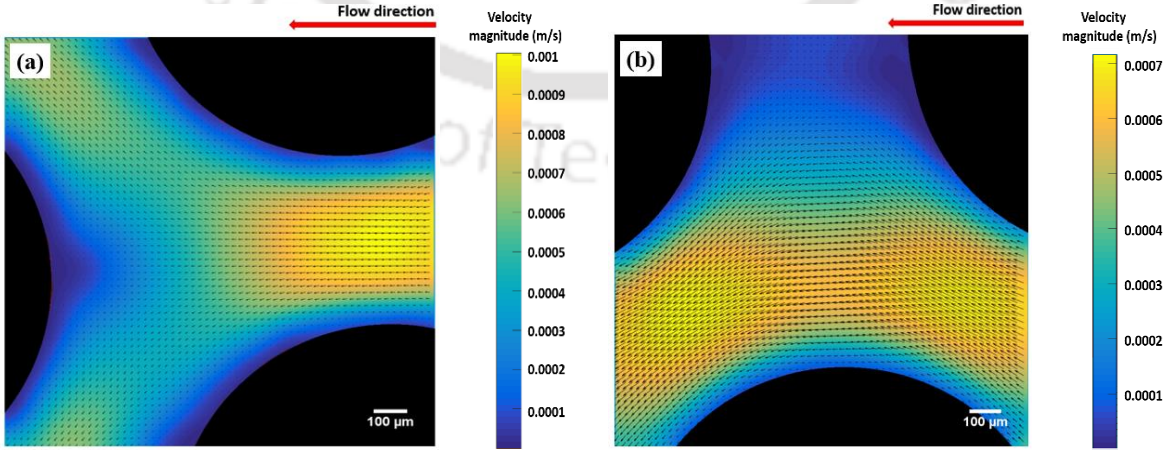

Pattern A **Pattern B**

Figure 3.17: Velocity contours at two arbitrary locations of (a) pattern A and (b) pattern B for 54 % porosity micromodel

3.4.4 Creation of heterogeneous porous micromodel

Natural porous media are composed of many heterogeneities like fractures, cracks, and fissures. These discontinuities often affect the movement of fluid flow by establishing a non- uniform flow with wide range of velocities. This kind of flow phenomena is often regarded as the preferential flow (Germann and Dipietro 1996). Preferential flow takes the flow regime to a non-equilibrium position with respect to the pressure head or the solute concentration or both (Wang 1991; Brusseau and Rao 1990), and finally it restricts the ability to predict the fluid flow and other transport processes in an undisturbed region.

Dual porosity models often describe transport and flow processes in heterogeneous porous media. In such cases, the porous media is assumed to be composed of normally two regions. One region is associated with higher permeability or fractures, while the other region with a comparatively low permeability and low porosity. The fabrication of these dual porosity micromodels is not only a challenging task but also a costly affair. The convenient method where optical lithography is combined with soft lithography is very costly and time-consuming as the creation of master pattern is difficult.

Buchgraber et *al.* (2012) used photolithography technique to fabricate dual porosity micromodel of uniform depth in a silicon wafer substrate and performed pore level visualization experiments for multiphase flows. The pore network pattern of the mask was derived from a carbonate reservoir rock sample. Zhang et *al.* (2011) used similar dual permeability micromodel to visualize the liquid CO_2-water displacement process. A slight modification was seen in the works of Yun et *al.* (2017), where they fabricated a dual depth dual porosity silicon-based micromodel using a two-step photolithography technique and performed multiphase flow displacement experiments. Xu et *al.* (2017) developed a novel 2.5-D porous micromodel on glass substrate in order to mimic real 3-D porous media and performed various multiphase flow experiments. They used a standard lithography process followed by hydrofluoric (HF) acid etching to fabricate the glass microfluidic chip. Though these methods of fabricating complex micromodel are very successful to replicate pore network in micron scale, yet these techniques are found to be very costly, time consuming and beyond the reach of many researchers among the developing and underdeveloped nations.

The carbonate reservoirs hold substantial petroleum resources. It is very difficult to characterize these fields due to multiscale variation in its porosity and other physical properties. The heterogeneity having different permeable zones affect the sweeping efficiency significantly during the recovery of oil. Hence, heterogeneous micromodels are necessary to perform these experiments. While the method of fabrication of homogeneous porous

micromodel is presented here, it will be shown how this methodology can be easily adopted to fabricate micromodels of a variety of other matrix topology by using suitable templates. In fact, the strength of this technique mainly lies with its flexibility and ability to fabricate a variety of homogeneous and heterogeneous porous micromodels.

3.4.5 Creation of dual porosity micromodel

Oil sweep in the enhanced oil recovery processes always arises through reservoir heterogeneities. The displacing fluid always tries to follow less resistive path and hence it flows through high permeable zones leaving behind trapped oil in the low permeable zone. To understand these effects, it is necessary to perform visualization experiments in dual porosity micromodels. Therefore, creation of dual porosity micromodels is necessary to understand these effects. However, the design and fabrication of these micromodels via soft lithography process are costly and time consuming. A simple method to fabricate these micromodels is described here. The overall fabrication method is the same as mentioned earlier in section ***3.2.1***. Here, the two perforated sheets having different size holes are joined very carefully and the mould is then prepared in a petri dish. Thereafter, the silicone elastomer along with curing agent in exact proportion is poured onto the mould and it is cured.

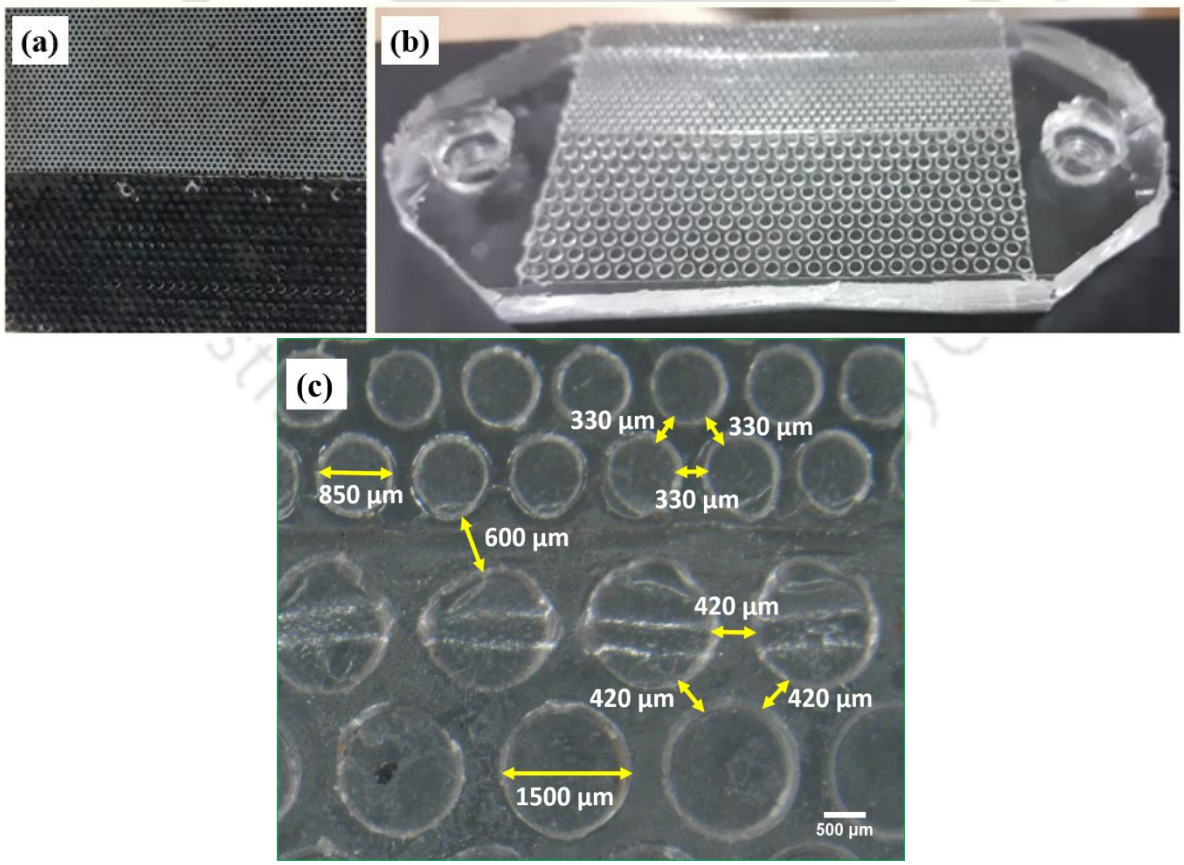

Figure 3.18: Image of the (a) dual porosity pattern, (b) dual porosity micromodel and (c) enlarged view at the interface of the micromodel

Figure 3.18a shows the master pattern used for the creation of dual porosity pattern, while Figure 3.18b shows the fabricated dual porosity micromodel. This micromodel contains two porous regions having porosity of 61% and 54 %. The overall size of the matrix section is 50 mm × 30 mm ($L \times W$) that constitute the overall porosity of 57.5%. The minimum distance between the pillars are 0.42 mm and 0.33 mm for 51 % and 61 % porous regions, respectively (Figure 3.4c). The Micro-PIV experiments are done to check its applicability. The velocity flow fields are obtained at two different sections near the inlet and the outlet of micromodel at the flow rate of 100 µl/min. Figure 3.19 shows the various locations where pore level observation is performed.

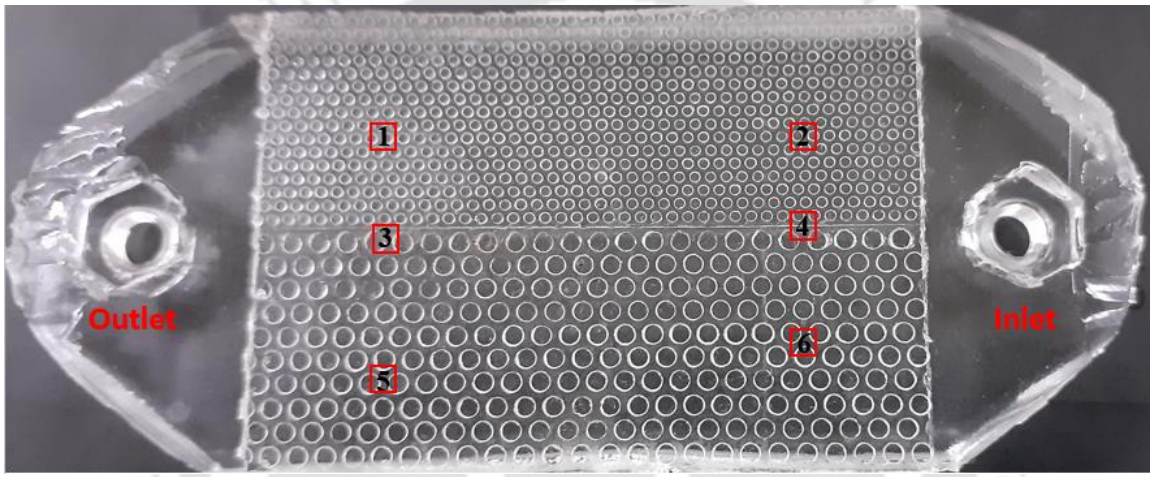

Figure 3.19: Dual porosity micromodel with highlighted locations where velocity fields are obtained

The velocity flow field are obtained at two different porous regions as well as at the interface. Figure 3.20 shows the velocity vector field at various locations of the micromodel. The velocity of flow along a section is found to be slightly higher in 51 % porosity region than the 61% porosity region. Interestingly, the maximum velocity (throat velocity) is found to be more in the low permeable region. It happens due to the presence of larger throat length in 51% porosity region, that consequently gives lesser resistive path to flow compared to 61% porosity area. Conn et *al.* (2014) created dual porosity with central fracture micromodel and visualized multiphase displacement experiments at pore level. In the fabrication process, the master pattern was created in a silicon wafer using photolithography, while the PDMS microfluidic device was prepared using soft lithography technique. In addition, using the same method, dual porosity with fracture micromodel can also be fabricated easily by simply covering the holes of perforated plate using adhesive tape. In this process, the well-defined fractures can be

generated very easily. Figure 3.21 shows the fabricated dual porosity fractured micromodel. The dual porosity fractured micromodel consists of two permeable regions along with a central fracture in between the two regions. The low permeable region has cylindrical pillars of approximate diameter 1.5 mm constituting 54 % porosity, whereas the high permeable region has 61 % porosity having cylindrical pillars of 0.85 mm diameter. The micromodel has a 42 mm × 42 mm flow area that constitutes an overall porosity of 57.5%.

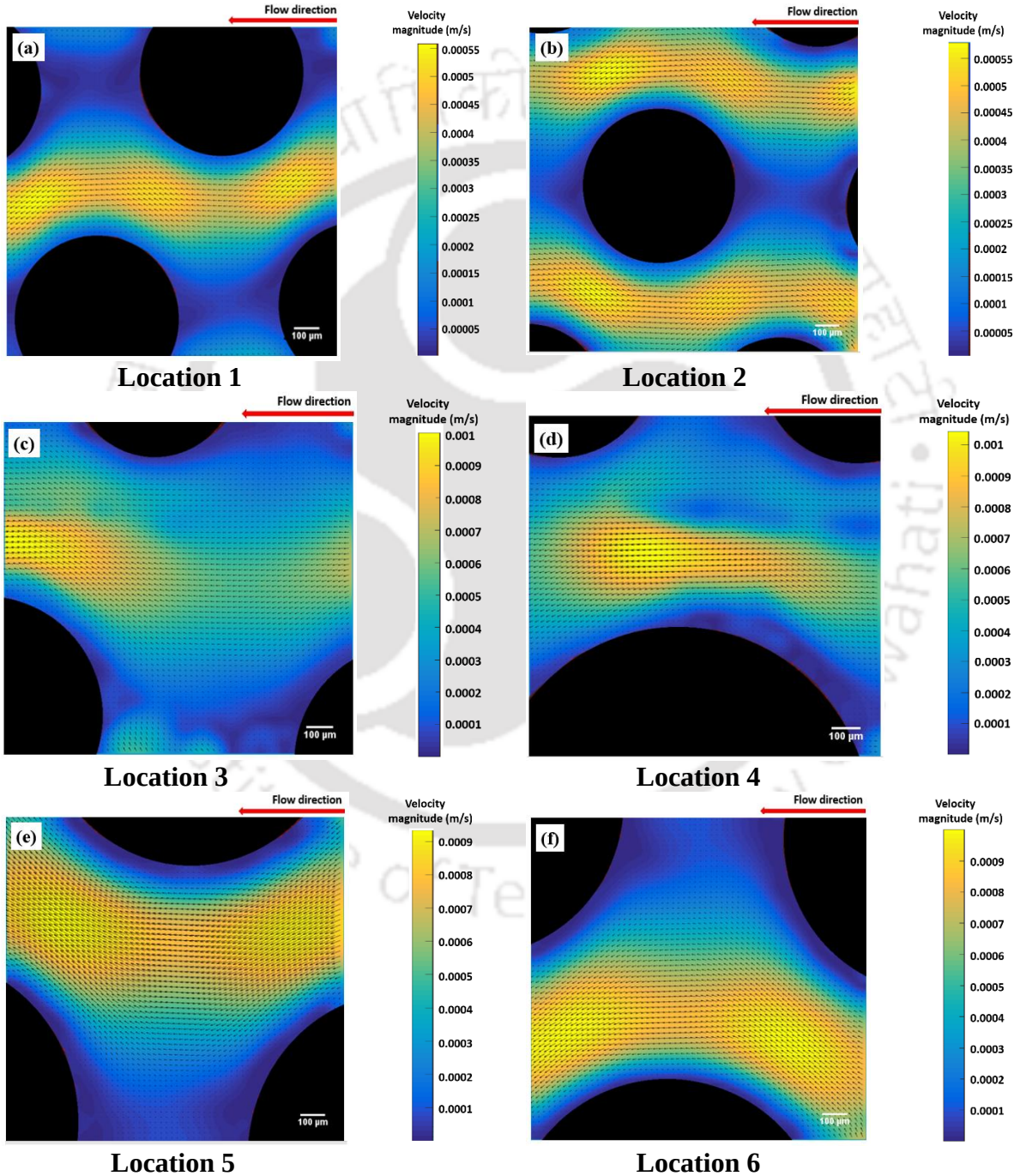

Figure 3.20: Velocity vector map at locations corresponding to the image shown in Fig. 3.17

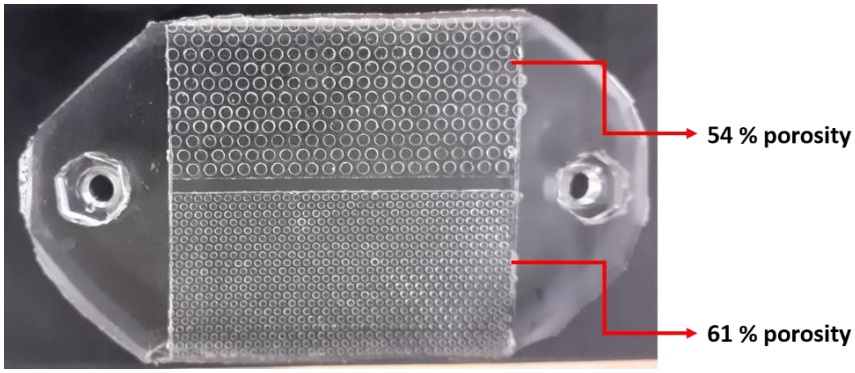

Figure 3.21: Dual porosity micromodel with fracture along the fluid flow

3.4.6 Effect of discontinuity on fluid flow

The discontinuity in the porous micromodel in the form of dual porosity can affect the fluid flow behavior. The present study aims at the pore level investigation of fluid flow inside the micromodel. The pore size and their distribution can significantly affect the flow field. To investigate the impact of dual porosity and the presence of fracture, the single-phase flow visualization experiments at 100 µl/min are performed, and micro PIV analysis is done to quantify the velocity field. Figure 3.22 depicts the regions where the velocity flow fields are obtained, while Figure 3.23 shows the velocity field at the highlighted region. It is found that along a section, the flow velocity is maximum in the fracture. It happens due to the low resistance offered by the fracture along the flow. In addition, the flow velocity in the porous region is very low in the fractured micromodel compared to the dual porosity model without any fracture. Though the single-phase flow experiments cannot give more information, yet these models can serve as very useful tool to perform multiphase flows and to gain insight of flow dynamics in heterogeneous regions.

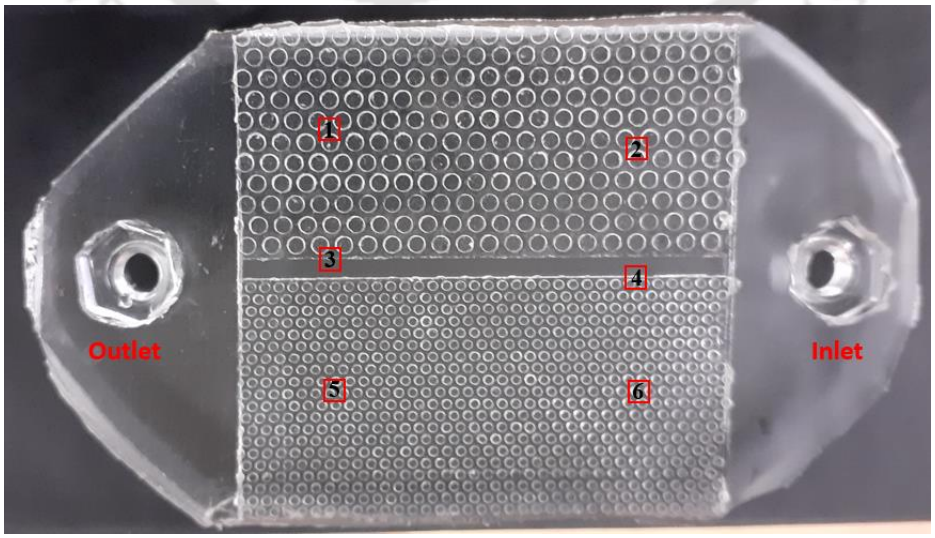

Figure 3.22: Dual porosity fractured micromodel with highlighted locations where measurements are performed

3.5 Investigation of velocity field in porous micromodels

The pore distribution, throat area between the cylindrical pillars in micromodels can affect the flow field significantly. To investigate these phenomena, three homogenous porous micromodel (with same porous matrix region but of different pore size and porosity) have been taken. Figure 3.24 shows three different micromodels viz. A, B and C. These micromodels comprise of a homogeneous porous section of 50 mm × 25 mm ($L \times W$) having different pore size distribution.

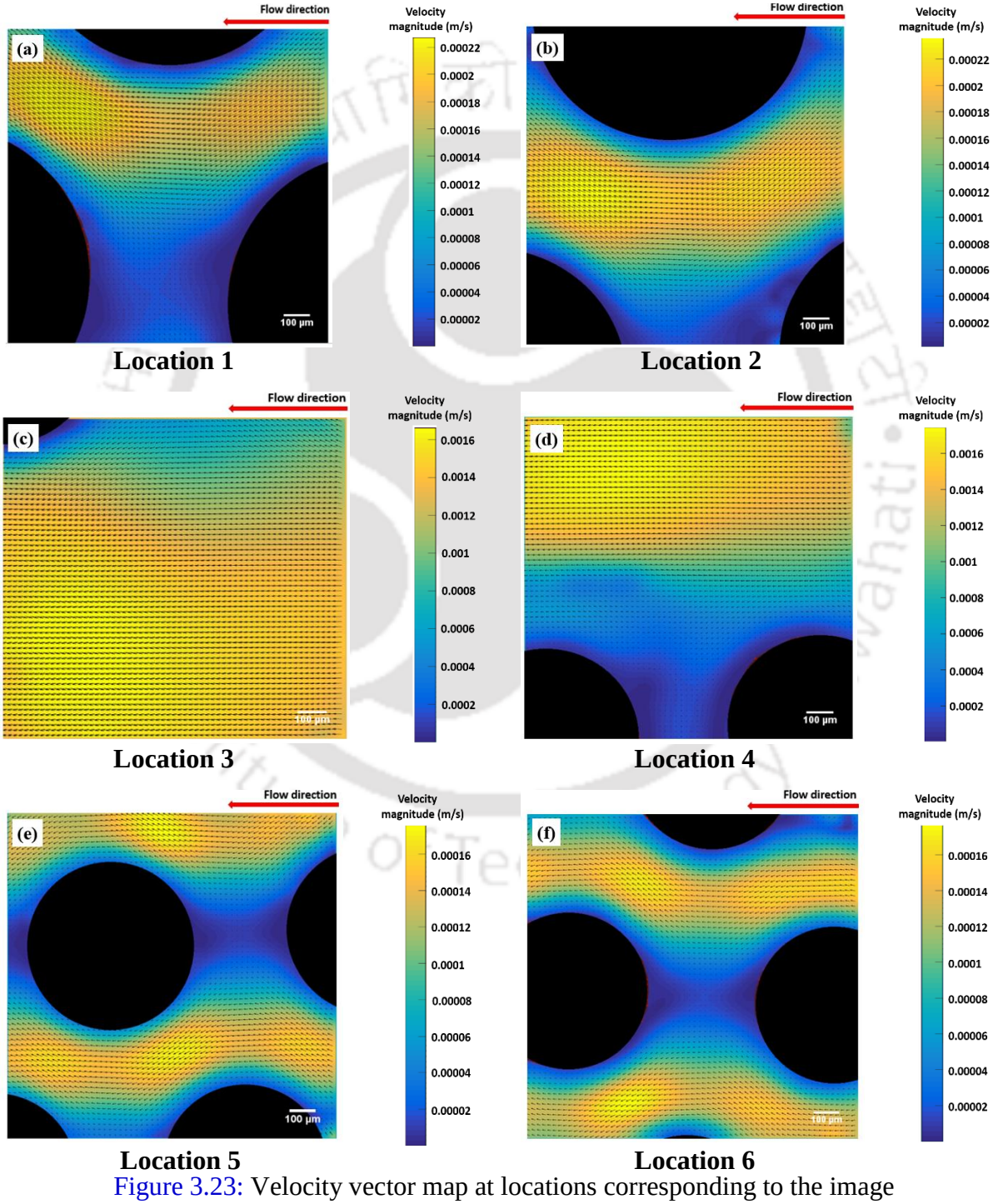

Figure 3.23: Velocity vector map at locations corresponding to the image shown in Figure 3.22

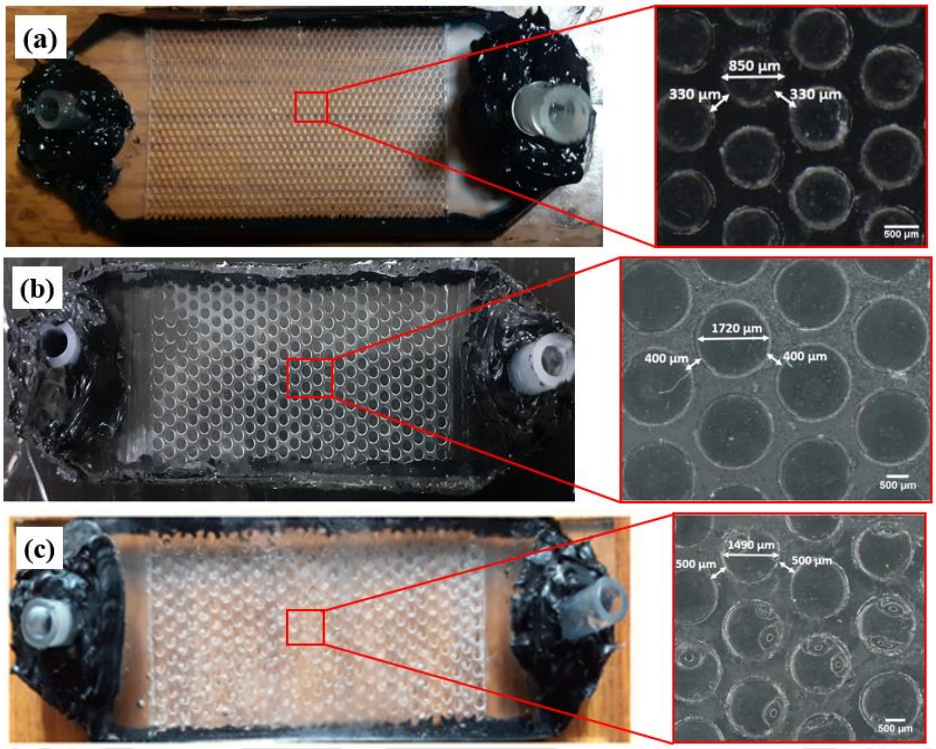

Figure 3.24: Micromodel images having different porosity (a) micromodel A (61%), (b) micromodel B (45%) and (c) micromodel C (54%)

The micromodel A contains uniform-sized cylindrical pillars. These pillars have diameter of 850 micron arranged in a pattern similar to two dimensional hexagonal closed packed structure and constitute a porosity of 61 %. The other micromodels B (having pillar diameter of 1490 µm) and C (having pillar diameter of 1720 µm) have the same pore matrix pattern and porosity of around 45% and 54%, respectively. The single-phase fluid flow experiments are performed at selected locations of the micromodels at a flow rate of 200 µl/min and their respective velocity at those locations are compared. These locations are not taken very near to the outlet or inlet of the micromodel.

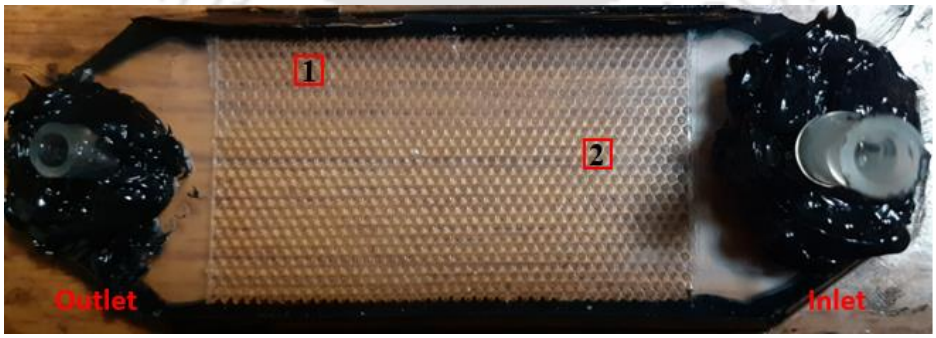

Figure 3.25: Sample image of the micromodel with highlighted locations where velocity field is obtained

Figure 3.25 shows the locations of a micromodel where observations are performed. The location 1 is 10 mm away from the outlet porous region, whereas the location 2 is at a distance

of 10 mm from the inlet porous region. The locations to be examined visually are same for all the micromodels. At these locations, the pore scale velocity is quantified and comparison is made for all the fabricated micromodels.

The velocity along a section normal to the fluid flow is found to be almost same both at the center and near the two sides of the micromodel. However, a reduction in the flow velocity is observed along the length of the micromodel. Micromodel B has a porosity of 45 %, which contains the uniform sized cylindrical pillars, and these pillars are uniformly distributed. Figure 3.26 shows the velocity contours at the two different highlighted sections for the micromodel A. While Figures 3.27 and 3.28 show the velocity contours for the micromodels B and C at the highlighted locations respectively. The maximum velocity is seen in the 45 % porosity micromodel as it has the least area for the fluid flow.

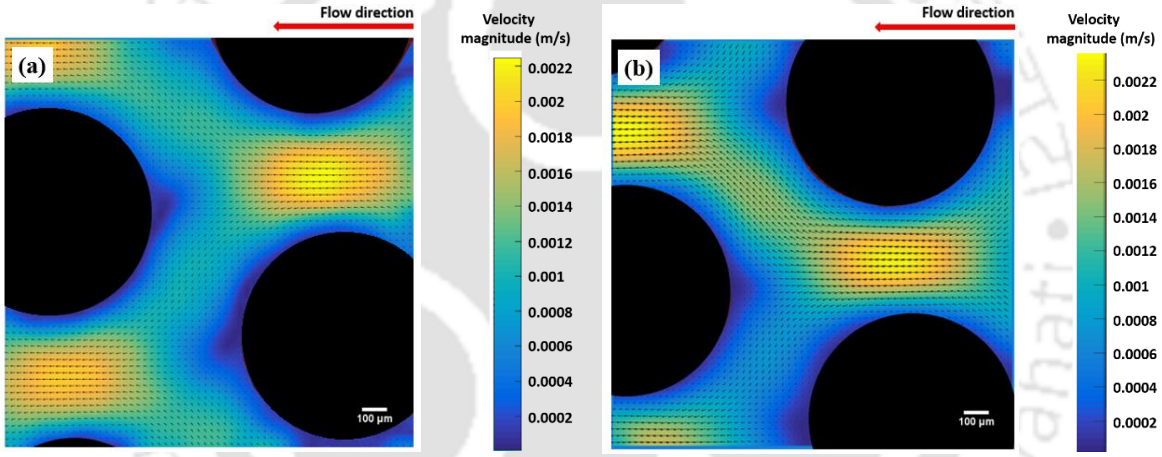

Location 1 **Location 2**

Figure 3.26: Velocity vector map at the two locations corresponding to the image shown in Fig. 3.24 for micromodel A

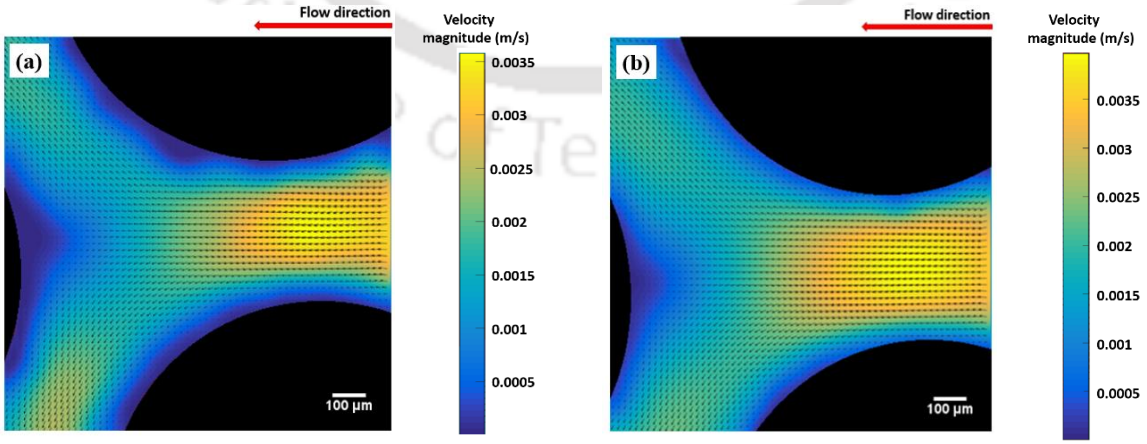

Location 1 **Location 2**

Figure 3.27: Velocity vector map at the two locations corresponding to the image shown in Fig. 3.25 for micromodel B

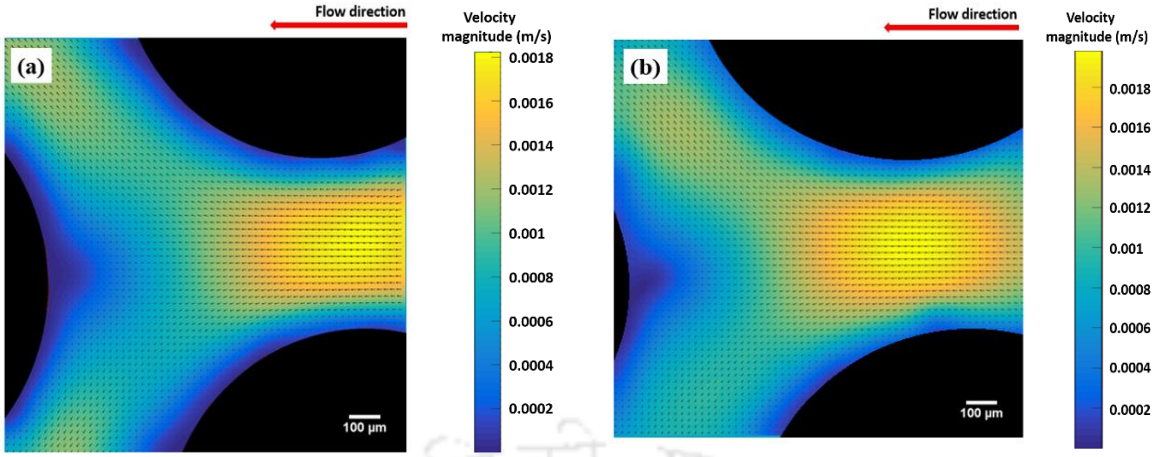

Location 1 **Location 2**

Figure 3.28: Velocity vector map at locations corresponding to the image shown at the highlighted locations shown in Fig. 3.25 for micromodel C

It is also observed that the velocity at a particular distance from the inlet is same along a section normal to the flow direction. Hence, it is understood that flow is predominantly flowing in one direction only and no crossflow is seen. In addition, along the length, the velocity is found to decrease, however, this reduction is very small as the overall length of the micromodel is very short. It is expected that the difference in velocity between the inlet and outlet will be significant for large region in the case of real porous medium. Figure 3.29 shows the pressure drop in the three micromodel patterns. In spite of being 61% porosity in pattern A micromodel, a high pressure drop is observed. This happens due to the presence of large number of pillars, as compared to other two models, which continuously increases the resistance to the fluid flow.

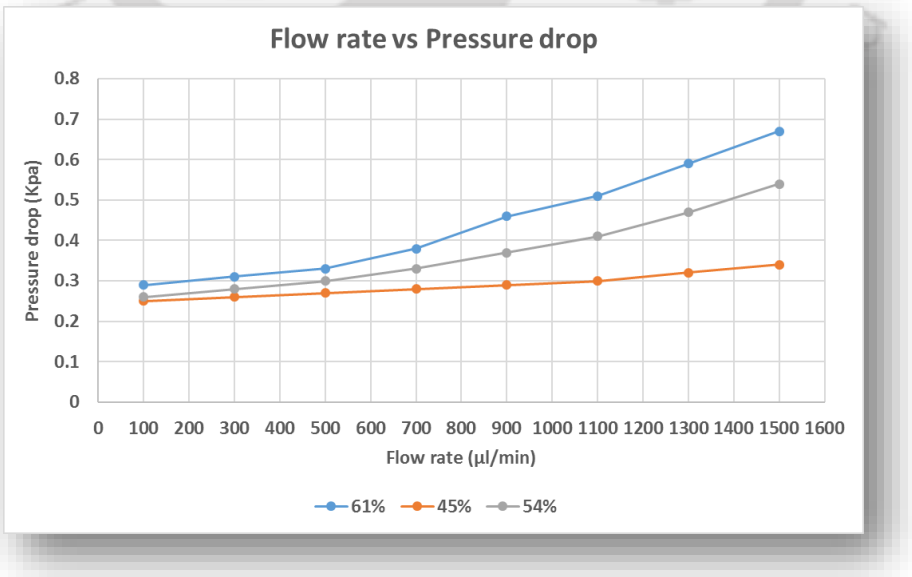

Figure 3.29: Flow rate vs pressure drop for different porosity micromodels

3.6 Summary

In the present work, an economical and efficient method to fabricate both homogenous and heterogeneous porous micromodel has been reported. The methodology involved to fabricate these micromodels using thin and round hole perforated plate as template pattern is demonstrated briefly. Utilizing this methodology of fabrication and using PDMS as a substrate, porous micromodels having different pore size have been fabricated easily within a time span of 7 to 8 hours. This method of fabricating porous micromodel in PDMS is economic, less time consuming as compared to the traditional photolithography and soft lithography techniques. However, it is necessary to mention that in the present method, the complexity of the pore network solely depends on the pattern template, and porous plate containing complicated geometry is difficult to find in the market. However, by adopting this methodology, one can not only fabricate the low cost porous micromodels very easily, but also can perform visualization experiments to gain the fundamental understanding of complex flow processes at micron scale.

The experimental setup used to capture the image frames containing tracer particles has been explained briefly. Furthermore, the reliability and experimental applicability of these micromodels are tested by carrying out micro-PIV analysis. The captured images are processed using MATLAB based PIV lab software and the velocity contour of the flow field is obtained with the help of two-frame cross correlation method. The results produced from the experimental analysis provide satisfactory results that enhances the reliability of this noble method. It can be concluded from the present investigation that this methodology can be adopted to fabricate the porous micromodels which can be used in an efficient way to investigate the fluid flow at pore scale in enhanced oil recovery (EOR) applications. The visualization experiments are performed in the micromodels having different porosity and their flow velocities are compared. In addition, a unique low cost method has been also discussed to fabricate dual porosity micromodel and the reliability of these models are also tested by performing visualization experiments.

Chapter 4

Flow Visualization and Measurements in Fractured Micromodels

4.1 Introduction

Flow through porous media has received much attention over the last few decades because of its applications in various fields of science and engineering (Wei and Zheng 2014; Kececioglu and Jiang 1994; Fand et *al.* 1987), such as in oil and gas recovery (Mohammadzadeh et *al.* 2019; Lu 2018; Zampieri and Moreno 2017), ground water hydrology, filtration technology, waste water treatment (Cahn and Li 1974) and medical and biological applications (Häfeli et *al.* 2014; Patil and Liburdy 2012). Apart from industrial processes, the application of flow through fractured porous media are also encountered in nature such as in oil and gas reserves, and in other fractured natural resources (Wu 2015). Because of these, fluid flow through fractured porous media has received extensive consideration due to its importance in understanding the physics of transport processes in fields like geotechnical and petroleum engineering (Duguid and Lee 1977).

Many studies have been performed to understand the effects of fracture on fluid flow by experimental measurements (Fathollahi et *al.* 2019; Jamshidi et *al.* 2019; Hasham et *al.* 2018), analytical studies (Dutra et *al.* 1992) and numerical analysis (Khoei et *al.* 2016; Kwlcklis and Healy 1993). Existence of damage or cracks inside a porous media can significantly affect the flow behaviour and mechanism of fluid flow within the fracture. The flow behaviour within these regions can thus be very different from the rest of the porous matrix section. In porous section, the macroscopic flow behaviour deviates from the pore scale flow (Jia et *al.* 2008). To understand the flow behavior in such situations, the velocity field needs to be investigated in the presence of fracture. Such analysis always provides valuable data for understanding and modelling of imbibition/displacement processes occurring inside porous media.

The flow process in oil recovery (Mosavat and Torabi 2016; Conn et *al.* 2014; Kianinejad et *al.* 2014), ground water hydrology (Berkowitz 2002) and other industrial applications are driven by the infiltration of a particular fluid into the porous medium to displace another resident fluid. The co-existence of different immiscible phases in the same porous region leads to the formation of fluid-fluid interface. The migration of fluid-fluid interface (known as front) appears due to the mobilization of one phase that is usually driven by the force induced due to pressure gradient, gravity and other external agencies.

The dynamics associated with these pore scale phenomena can induce irregular front and can trap immovable pockets of resident fluid surrounded by the displacing fluid, also known as blobs and ganglia (Mahdavi and James 2019; Sedaghat et *al.* 2016). These trapped pockets can block the regular flow movements in certain areas and have the ability to alter the flow pathways owing to the formation of preferential paths, known as channeling. These complex multi-phase flow processes are still not well understood and experimental methods are considered as the most appropriate analysis for understanding the physics behind the complex mechanism that drives these fluid-fluid interactions. Moreover, the experimental data collected to understand the physics of the fluid-fluid displacement are necessary to validate and develop robust numerical models (Suga 2013; Worner 2012; Meakin and Tartakovsky 2009).

Visualizing the fluid flow in soils and geomaterials is a challenging task as these real materials are not transparent to visible light. Most of the experimental analysis are thus based on the flow visualization phenomena in artificial porous medium (known as micromodels) with an aim to characterize the dynamics of flow mechanism at pore scale. As a result, the micromodels can be used as an artificial representation of porous medium because of their transparency and ease of conducting the flow visualization experiments (Rangel-German and Kovscek 2006). The micromodels are considered to be the most useful tool in recent times, and they allow the optical visualization of fluid flow and transport at minute scale that are relevant to chemical (Mejia et *al.* 2019; Yu et *al.* 2019; Lyu et *al.* 2018), biological (Du et *al.* 2017; Folch et *al.* 1999), and physical (Wan et *al.* 1996) fields of engineering. These micromodels are comprised of a network of connecting pores, an artificial portrayal of real porous medium. Thus, using these micromodels it becomes possible to study and to gain scientific data of the pore scale flow events to a greater extent. In the past, these micromodels had simple and plain porous network structure. The very first fabricated micromodel that was used to explore the behaviour of fluid flow at microscale in porous media was a single layer of glass spheres sandwiched between two flat glass plate (Chatenever et al. 1952). Lenormand et al. (1983) investigated the pore scale flow process in a simple geometry micromodel, and captured images of two immiscible phase interaction. They opined the basic mechanism of pore scale phenomena to

be like a piston type movement or snap off. Fourar et *al.* (1993) studied the flow structures by performing the two-phase flow experiments in horizontal artificial fractures that were made by maintaining a gap between two glass plates.

With the development of computer generated digital design tools, it has now become possible to fabricate a wide variety of complex 2D and 3D micromodels (Tsakiroglou and Avraam 2002). At present, the common method of fabricating micromodels is the lithography technique that transfers the predesign geometric pattern from a mask to a photoresist layer on the substrate like silicon wafer or glass. The most frequently used lithography technique is the photolithography technique (Chen et *al.* 2003). In this method, a photomask containing pore network design is printed. A photoresist material is then spin coated on the micromodel substrate, and the pore network design is transferred from the mask to the photoresist material by exposing it to ultraviolet light. Later, with the help of a developer solution, the specific area containing the pore network is washed away. Finally, with the help of etching technique, the network pattern is constructed on the surface of the micromodel substrate. In most cases, this micromodel substrate embedded with a pore network (known as master pattern) is directly bonded with transparent sheet like glass plate to construct the final applicable version. This kind of fabrication process like photolithography and etching are costly and time consuming. Furthermore, being expensive, the substrate material like silicon wafer creates an obstacle to the researchers while studying the fluid flow behaviour in permeable media. In order to reduce the cost of fabrication, the master mould is currently used as a patterned template to replicate and transfer the pore network into soft materials like polymers. This method is known as soft lithography (Xia and Whitesides 1998). On the other hand, polymers being less expensive can serve as a good alternative to fabricate the micromodels. Among them, the PDMS is widely used polymer to fabricate the microfluidic devices due to its ability to replicate any desired shape easily. PDMS micromodels are very useful to perform visualization experiments as they are transparent and can easily be sealed onto substrates like glass.

The other complex techniques include stereo lithography (Ikuta et *al.* 2002), laser-chemical 3D writing (Bloomstein 1992) as well as micro- joinery (González et *al.* 1998) to form complicated micromodels on different substrate materials. Additionally, the photolithography technique is used to fabricate 3-D microchannel in elastomer substrate, where the micromodel is fabricated in layer-by-layer configuration (Jo et *al.* 2000). A rigid plastic known as cyclic olefin copolymer (COC) have been used by Hsu et *al.* (2017), who fabricated the fractured micromodel by using hot embossing technique. However, the visualizations experiments to study the effects of fracture on these instabilities by using fractured micromodel have been very limited.

In the present investigation, the fractured porous micromodel in PDMS has been fabricated using a method similar to that of soft lithography technique where a readymade master pattern is used. Thereafter, an attempt has been made to study the single-phase and two-phase flow phenomena in fractured porous media. The flow visualization experiments are then performed at various locations of the micromodel. The micro-Particle Image Velocimetry (μPIV) analysis is carried out to map the flow velocity near the fracture and at other locations of the porous micromodel whereby the effects of fracture on fluid-fluid interaction are evaluated.

4.2 Materials and Methods

Polydimethylsiloxane (Sylgard 184, Dow Corning) is the substrate material used in the fabrication process. Other supplementary materials are thin perforated metal sheets of identical sized circular holes, silicone connecting tubes and silicone adhesive sealant and glass slides. One side of these glass slides are coated with thin layer of cured PDMS and later these slides are used to cover the open side of the micromodel. The perforated sheet of 150 micron thickness is used as the master pattern during the fabrication process. The sample image of the perforated plate is shown in Figure 4.1. The array of holes along the two orthogonal thin lines are covered with adhesive tape to create the desired fracture. The porous matrix area along with the two fractures of the micromodel covers a rectangular area (40 mm × 20 mm) of the porous plate and the convergent areas on the both side are covered with adhesive tape (as shown in Fig. 4.1) for the purpose of providing inlet port, outlet port, inlet flow area and outlet flow area.

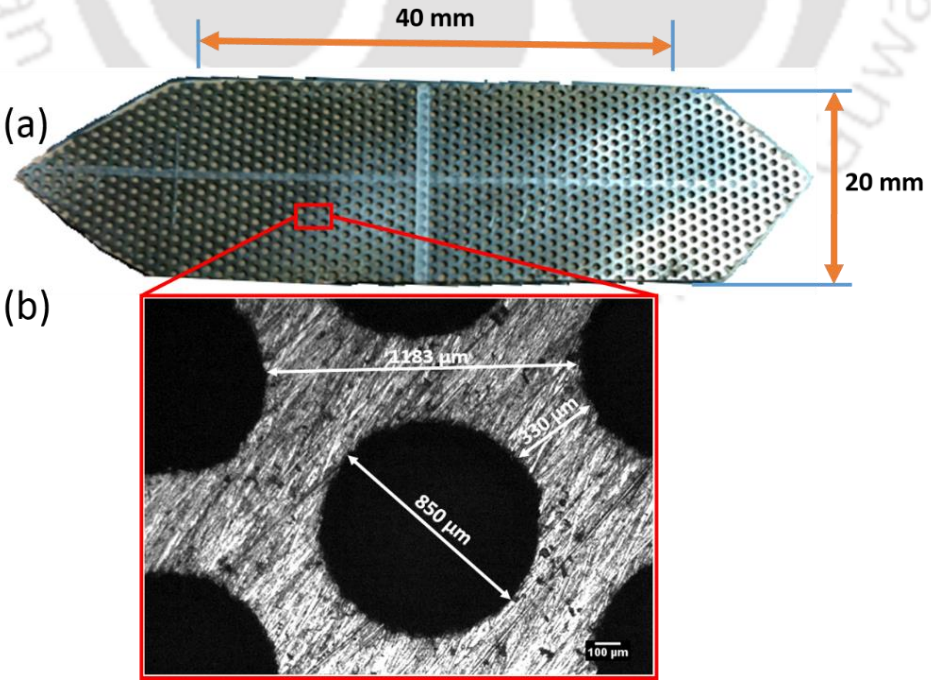

Figure 4.1: (a) Image of the porous plate having circular holes (holes along the marked cross strips are covered to get the desired fracture), (b) enlarged view of circular hole

4.2.1 Method of fabrication

Polydimethylsiloxane (PDMS) is the most widely used substrate among all soft materials for the fabrication of micromodels since it can replicate any coveted shape easily. It allows visualization of the sample and is easy to seal onto substrates like glass (Jia et *al.* 2008; Verma et *al.* 2006). During the fabrication process, a silicone elastomer base (Sylgard 184 from Dow Corning) along with a corresponding curing agent is used as the raw materials. The silicone elastomer base and the curing agent primarily available in the liquid state is mixed thoroughly at 10:1 mass ratio (Karadimitriou et *al.* 2013). For fabricating one unit of micromodel, the physical amount of silicone elastomer and its curing agent is taken as 40 g and 4 g, respectively.

During the mixing process, the air bubbles enter into the mixture and are trapped. In order to expel these air pockets, the container containing the mixture is placed into a vacuum chamber. After degassing the liquid mixture, it is poured over the work design in a Petri dish. The liquid mixture has to be poured very slowly over the master pattern to avoid any further entrapment of air bubbles. After pouring the liquid PDMS over the pattern, the Petri dish is placed inside a hot air oven at a temperature of around 80^0C for 2 hours for curing and setting the liquid mixture. The necessary precautions that should be kept in mind while pouring the liquid PDMS are well explained in the work of Karadimitriou et *al.* (2013). The liquid mixture being taken out of the oven is allowed to reach the ambient temperature. The replica is then peeled off very carefully without destroying the pore network features. Finally, the PDMS slab is bonded to the glass plate and the edges of all lateral sides are sealed with silicone adhesive sealant. The relevant description of the fabrication method is reported by Haque et *al.* (2019).

The pore sizes used in our micromodels are large and comparable to natural fracture dimension. This is due to large size of the holes of the perforated plate used in our study compared to the typical grain size in the geological porous media. This was purposefully done since larger throat dimensions provides better flow visualization using microscopic techniques. A number of literature shows applications of micromodels with larger sized pore throats to investigate the pore-scale velocity field measurement in the porous medium (Sen et *al.* 2012; Lu et *al.* 2018, Huang et *al.* 2008; Dutta et *al.* 2014; Sabbage et *al.* 2020). Figure 4.2 depicts the pictorial demonstration of steps involved in the fabrication process.

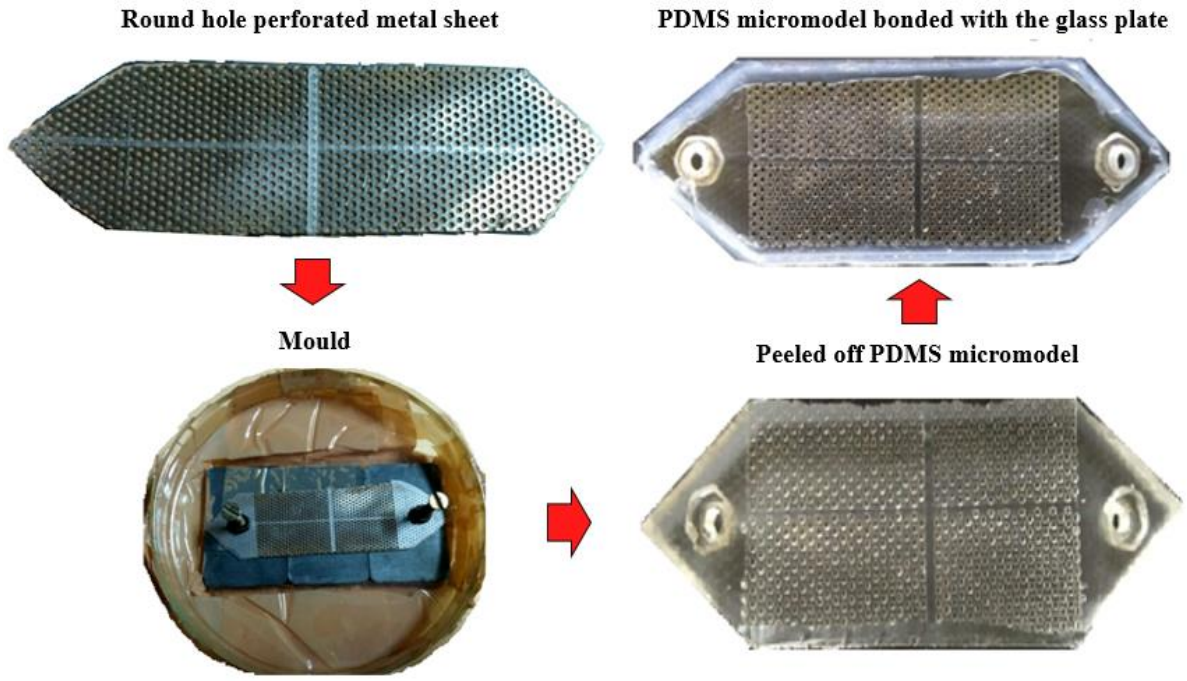

Figure 4.2: Steps of the fabrication of the fractured micromodel

4.2.2 Experimental setup

The fabricated fractured porous micromodel is shown in Figure 4.3. The micromodel consists of two fractures and they intersect approximately at the centre of the matrix pattern of dimensions 40 mm × 20 mm ($L \times W$) that contains the uniform-sized cylindrical pillars. The fractures have dimensions of 20 mm × 1.23 mm ($l \times b$) and 40 mm × 0.85 mm ($l \times b$). These cylindrical pillars having diameter (D) of 850 micron are arranged in a pattern similar to that of a two-dimensional hexagonal structure as shown in Figure 4.3(b). The depth of the micromodel (d) is identical to that of the porous plate thickness (d = 150 micron). The inlet and outlet dimensions of the micromodel are of 3 mm diameter. The maximum distance (pore size, s) and the minimum distance between the pillars (throat, t) are 1183 μm and 330 μm, respectively that yields a porosity of 0.62 approximately.

A syringe pump (NE 1000 single syringe pump, New Era Pumps, USA) is used to deliver the working fluid to the micromodel at a steady pressure. A Leica DM IL inverted microscope having 10x magnification lens (numerical aperture = 0.25) is used for imaging the flow process. While an Nd:YAG double-pulsed (532 nm) laser is used for illumination and a double-shutter PIV CCD camera (FlowSense EO 4M camera, 2048×2048 pixels at 16 fps) is used to capture the sequence of images.

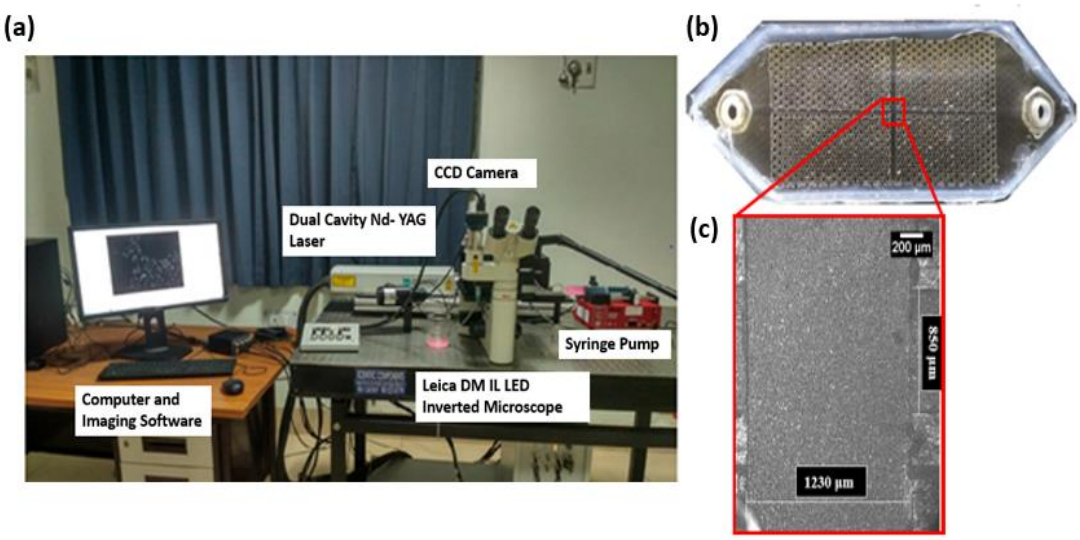

Figure 4.3: (a) Experimental setup, (b) image of the fractured micromodel and (c) enlarged view at the junction of the two fractures

4.3 Results and Discussion

Among the two sets of experiments performed, the first one consists of the single-phase flow experiments, while second one explains the two-phase imbibition process. The single-phase flow experiments are done at two different flow rates viz. 100 µl/min and 1000 µl/min. These two flow rates are chosen to study the effect of different flow rates on flow pattern in presence of fracture within the micromodel. The working fluid that is used to perform the single-phase flow is a mixture of glycerol and water in a ratio of 57:43 (by volume). The fluid is seeded with FluoSpheres carboxylate-modified microsphere of 1.0-micron size (from Fisher Scientific, USA) and the seeding concentration of these particles is kept around 0.03% by volume. The density of the tracer particles is almost similar to that of aqueous glycerol mixture, which minimizes the sedimentation.

The two-phase imbibition experiments are then performed to trace the fluid-fluid interaction. A mixture of glycerol and water (fluid A, $\mu_A \approx 7.8$ m Pa s at 25 ^{0}C) in a ratio of 57:43 (by volume) is used as wetting phase, while silicone oil is used as non-wetting phase (fluid B, $\mu_B \approx$ 96 mPa s at 25 ^{0}C). The interfacial tension (σ) was 11.7 mN/m, the viscosity ratio ($M = \mu_A/\mu_B$) was 0.08, and the density ratio (ρ_A/ρ_B) was 1.2 (Blois et *al*. 2016).

4.3.1 Flow visualization and micro-PIV measurements

The flow visualization techniques are found to be very useful as the insight of a physical process can be better understood by a visual inspection. It is evident that most of the fluids are

transparent media and their transient movement remains indistinguishable to the human eye at the time of direct observation. Hence, in order to visualize the flow, certain techniques need to be adopted to make it visible. These techniques are called flow visualization techniques. One of the first such method applied to map the fluid velocity was Laser Doppler velocimetry (LDV) (Durst et *al.* 1995; Nishihara et *al.* 1982). The LDV is a non-invasive single point measurement technique that probes into every single measurement point of flow field to get the velocity flow map of the entire field of view. Hitherto, many different techniques have been adopted for the visualization purpose (Breugem et *al.* 2013; Huang et *al.* 2008; Dijk and Berkowitz 1999) and these methods are very popular due to their individual contribution towards the understanding of different fluid flow phenomena. With the application of these techniques in the porous micromodels, it has become possible to gather a substantial amount of information regarding flow field inside the porous materials. On the other hand, one can derive quantitative data from the images obtained. In addition, these techniques give information about the complete flow field under the study without disturbing the fluid flow physically.

The most commonly applied method to retrieve the velocity field is Particle Image Velocimetry (PIV) technique (Raffel et *al.* 2007; Adrian 2005). Unlike Laser Doppler velocimetry (LDV), a single point measurement technique, the PIV permits the quantification of flow velocity at multiple points simultaneously within a span of single plane in the porous medium. Moreover, with the help of the sequential PIV system, one can gather information from more than one plane that is comparable to the 3-D flow system. The PIV is an optical technique to map the fluid flow velocity field on macroscopic level. This technique becomes a micro-PIV when it is applied to microscale. The basic experimental setup of micro-PIV is shown in Figure 4.4.

A typical micro-PIV setup consists of a light source, mostly a pulsed light source, which is synchronized with a digital camera. The synchronization is done in such a way that the first pulse is set at the end of the first camera frame and the second pulse can be set at any random position of the second frame. In this way, the time interval between the two subsequent exposures can be varied very easily that is necessary for high-speed flow experiments. The time interval between two images thus become independent of camera frame rate. The dual cavity Nd: YAG lasers at 532 nm wavelength are mostly used as pulsed light source for micro-PIV experiments. The two lasers can be triggered independently, and it has the ability to freeze

the particles movement within microseconds. The images of flowing fluid seeded with fluorescent tracer particles are recorded with the help of a digital camera like charged coupled device (CCD) camera. The role of dichroic mirror is to act like a filter that allows only the fluorescence emission to camera for data evaluation. At a later stage, these data are evaluated with the help of imaging software to get the velocity of flow field.

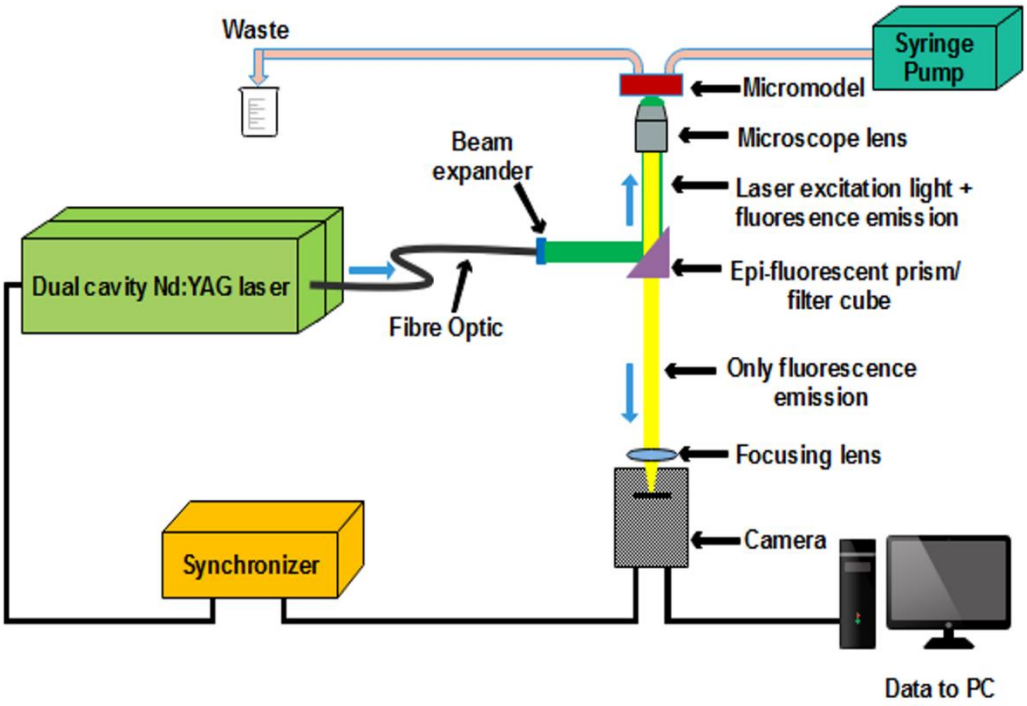

Figure 4.4: Experimental setup used for micro-PIV experiment

The fundamentals of micro-PIV technique (Wereley and Meinhart 2010; Lindken et *al.* 2009) is similar to that of PIV, but it is used to get the velocity field at a micron scale. Another difference is that the volume illumination is used in place of light sheet illumination. The working fluid is seeded with tracer particles that has nearly the same density to that of the fluid. It is then illuminated by a light source and pairs of images are recorded after a definite time interval. The image frames are then sub grouped into many small areas, known as interrogation windows. Thereafter, two frame cross correlation method is applied to these consecutive image pairs to get the displacement of the seeded particles. The velocity of fluid is thus determined by dividing the displacement of seeded particles by the time gap between two consecutive images. Figure 4.5 shows the basic steps involved to get the velocity vector of the flow field.

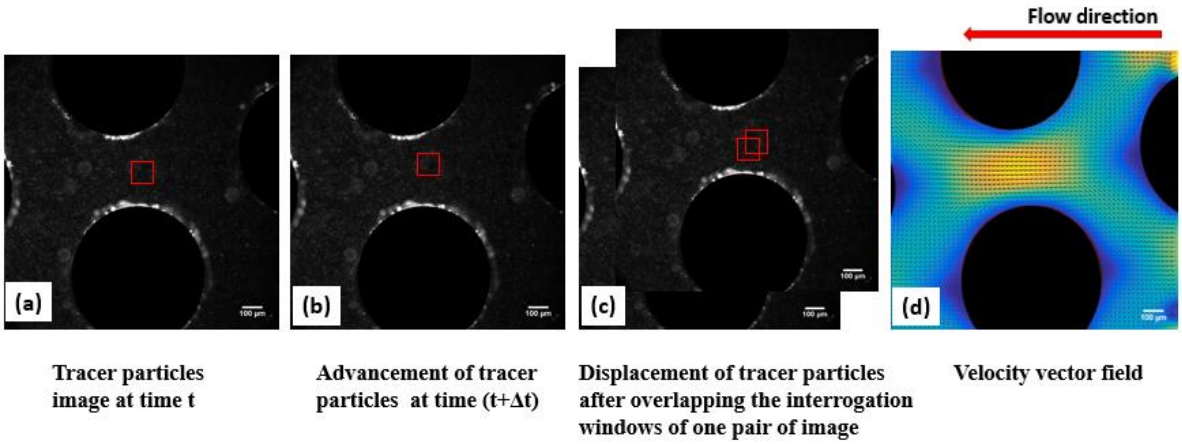

Figure 4.5: Basic steps of PIV analysis to get the velocity flow field

4.3.2 Single-phase flow observation

The fabricated micromodels are checked for its applicability by performing single-phase flow experiments. The single-phase flow experiments are performed at 100 µl/min and 1000 µl/min. The two flow rates are chosen deliberately to investigate the effect of flow rate in the flow pattern in presence of the fractures in the micromodel. During the experiments, a series of paired images containing tracer particles are recorded at the junction of two fractures and at other locations near the fracture of the micromodel.

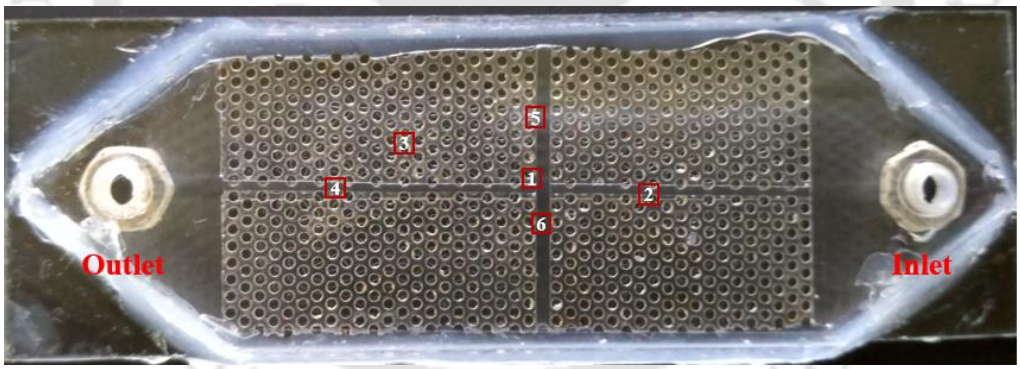

Figure 4.6: Image of the micromodel with highlighted locations where velocity field was obtained for flow rate 100 µl/min

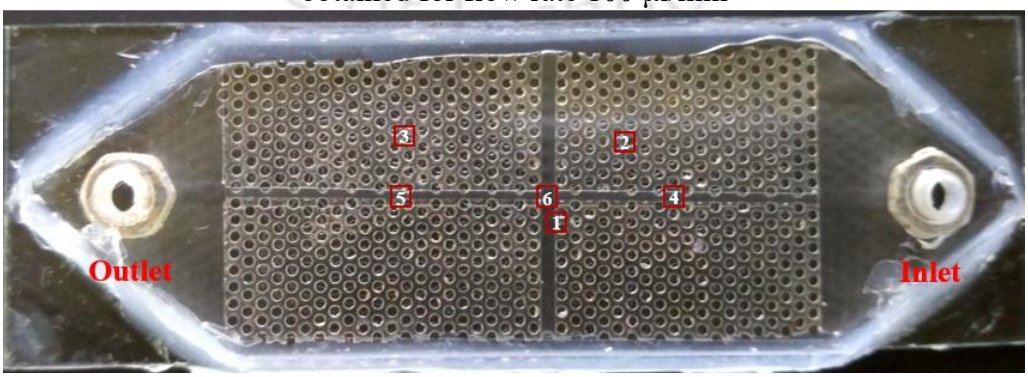

Figure 4.7: Image of the micromodel with highlighted locations where velocity field was obtained for flow rate 1000 µl/min

Figure 4.6 depicts the various locations in the micromodel where images are captured for flow rate of 100 µl/min and Figure 4.7 shows highlighted locations where images are captured for 1000 µl/min flow rate. The raw images are captured both at the junction of the two fractures and at the pore throat of the micromodel. A total of fifty consecutive pairs of image frames are captured at each marked location and their resultant vector field is obtained by taking average values of these frames. Figure 4.8 shows the sample raw images taken at various highlighted locations as shown in Figure 4.6. The acquired images are not suitable for the direct PIV measurement due to the presence of background noise. Hence, these raw images require pre-processing to remove the unwanted background noise. The velocity vector field is obtained by a MATLAB based PIV lab software that uses two-frame cross-correlation method to interrogate consecutive image pairs (Thielicke and Stamhuis 2014).

The PIV lab is used for the image pre-treatment before being processed for cross-correlation. After the pre-processing of the images, it contains only the bright particles that hold the details of movement of the bright particles. The sole purpose of image pre-processing is to enhance the image quality that consequently provide better measurement accuracy. In the cross-correlation methodology, firstly, each image frame is divided into many identical small areas, known as interrogation windows. Later, these subdivided areas are correlated spatially with the respective areas of another consecutive frame to obtain the information regarding the displacement of the tracer particles during a definite time interval. Hence, to perform this analysis, a fast Fourier transform (FFT) method with multiple passes is used. The first pass contains larger interrogation area as compared to the subsequent passes. Larger interrogation area gives greater signal to noise ratio, but at the same time, it shows poor vector resolution. This is the reason behind the use of smaller interrogation areas in the further iterations, which enhances the resolution of vectors. This type of iterative method delivers a wide range of dynamic velocity that provides a larger vector resolutions and better signal-to-noise ratio. In present case, the first pass uses an interrogation area of 64 × 64 pixels, whereas the second pass uses an interrogation area of 32 × 32 pixels. To get satisfactory results from the PIV analysis, each interrogation window in the final pass should hold at least 5-10 particles. The size of the interrogation window must be chosen wisely to allow uniform displacement of theparticles within the area, and simultaneously it should be of considerable size to hold sufficient data for the calculation. Finally, the interrogation windows are arranged at 50% overlapping position and the post processing is carried out to get the instantaneous velocity vector field.

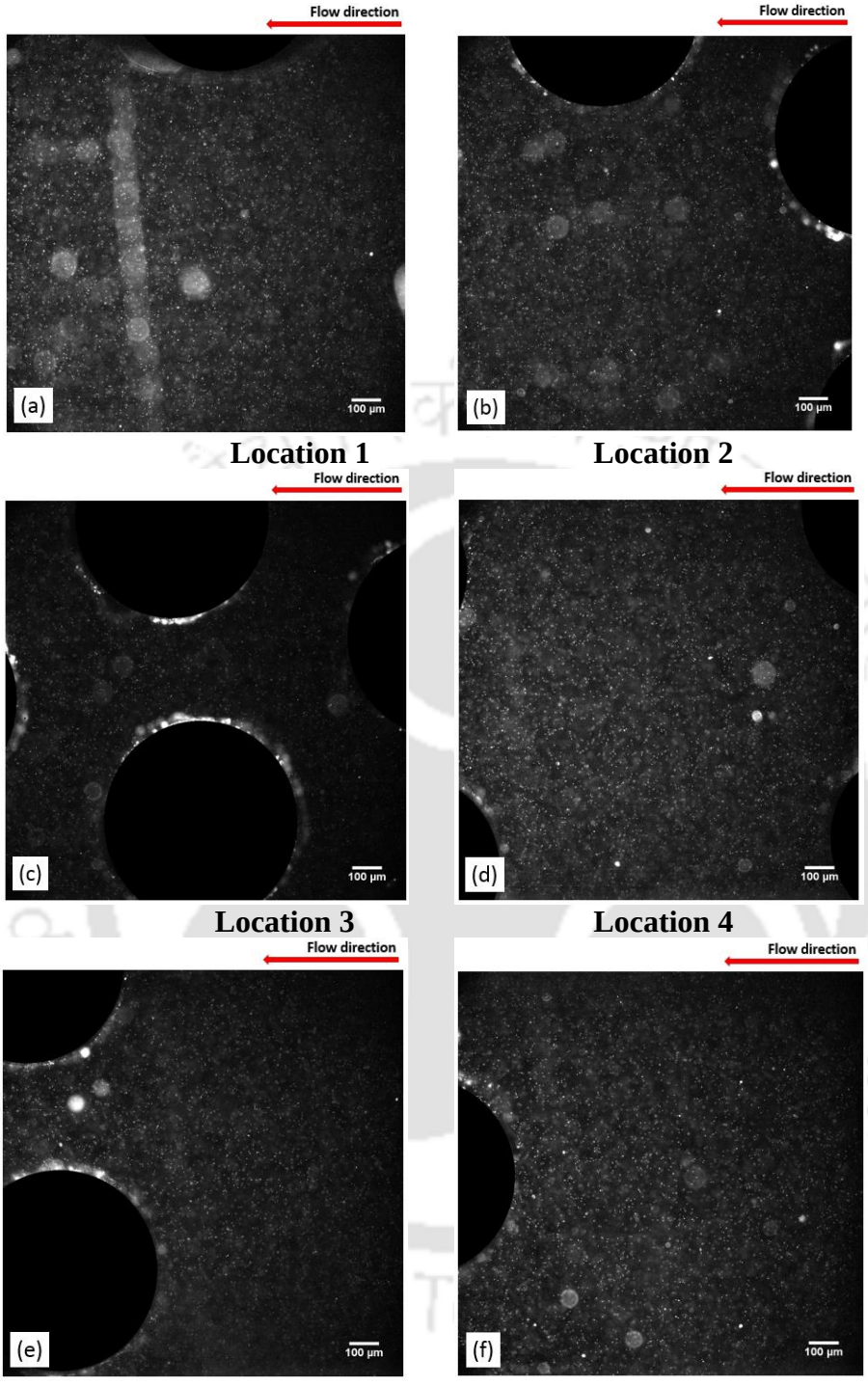

Figure 4.8: Image of the fluorescent particles at various locations of the micromodel as highlighted in Fig. 4.6

In addition, the size and optical properties of the tracer particles must be compatible with the experimental system so that the micro-PIV experiments can be carried out smoothly to obtain accurate velocity of the flow field. Moreover, the camera properties along with the objective lens of the microscope must be selected in such a way that the particle size in the image frame

should be resolved up to a minimum of 2–3 pixels (Sen et *al.* 2012). The time gap between two successive images frames must be chosen in such a way that the movement of the particles within two consecutive image frames should not be more than three times the image size (diameter) of the particles from its initial position.

Due to microscope magnification limitation, the full view of both the fractures could not have been obtained. To overcome this limitation and to gain more information about the pore scale flow, some additional experiments are performed and images are taken at various regions near the two fractures and the velocity flow field is quantified. Experiments are also performed to understand how the presence of fracture can affect the flow field. The test sections show a steady single-phase flow of pressurized aqueous glycerol mixture, which is predominantly flowing in the horizontal direction (*x* direction) owing to the driving pressure gradient. These flow fields can be characterized by flow features like confluences and bifurcations regions. Though random flow is seen along the pillars, no significant cross flow (normal to bulk pressure gradient) is seen and it has been observed that the flow is maintaining a regular flow pattern. Bifurcations tend to distribute the flow over a larger area while confluences tend to concentrate the flow into fewer flow paths characterized by a higher flow rate. These two competing mechanisms govern the distribution of flow in the porous network. Despite the presence of lateral fracture (along *y* direction), no significant effect is seen as the fluid flow pattern is regular and the flow is along the bulk pressure gradient (*x* direction) for the both flow rates. Further, no vortices are seen in the flow field due to the presence of discontinuity along the flow, while small randomness in the flow field is observed.

Figure 4.9 shows the velocity vectors superimposed over the velocity contour at the highlighted locations of Figure 4.6 for flow rate of 100 µl/min (Re ≈ 0.12). While Figure 4.10 shows the velocity field at the marked locations of Figure 4.7 for flow rate of 1000 µl/min (*Re* ≈1.2).

In the present study, the fracture dimensions are predetermined and have smooth edges and the overall matrix region is very small compared to real porous media found naturally. In addition, cylindrical pillars have smooth edges that help the fluid flow to remain stable. Blois et *al.* (2013) and Roman et *al.* (2016) performed both single phase and two phase immiscible fluid displacement experiments in both homogeneous and heterogeneous porous micromodels and obtained pore scale flow fields using micro-PIV technique. To perform visualization experiments, they fabricated the porous micromodels using photolithography technique and observed regular flow fields for single-phase flow in the homogeneous porous region.

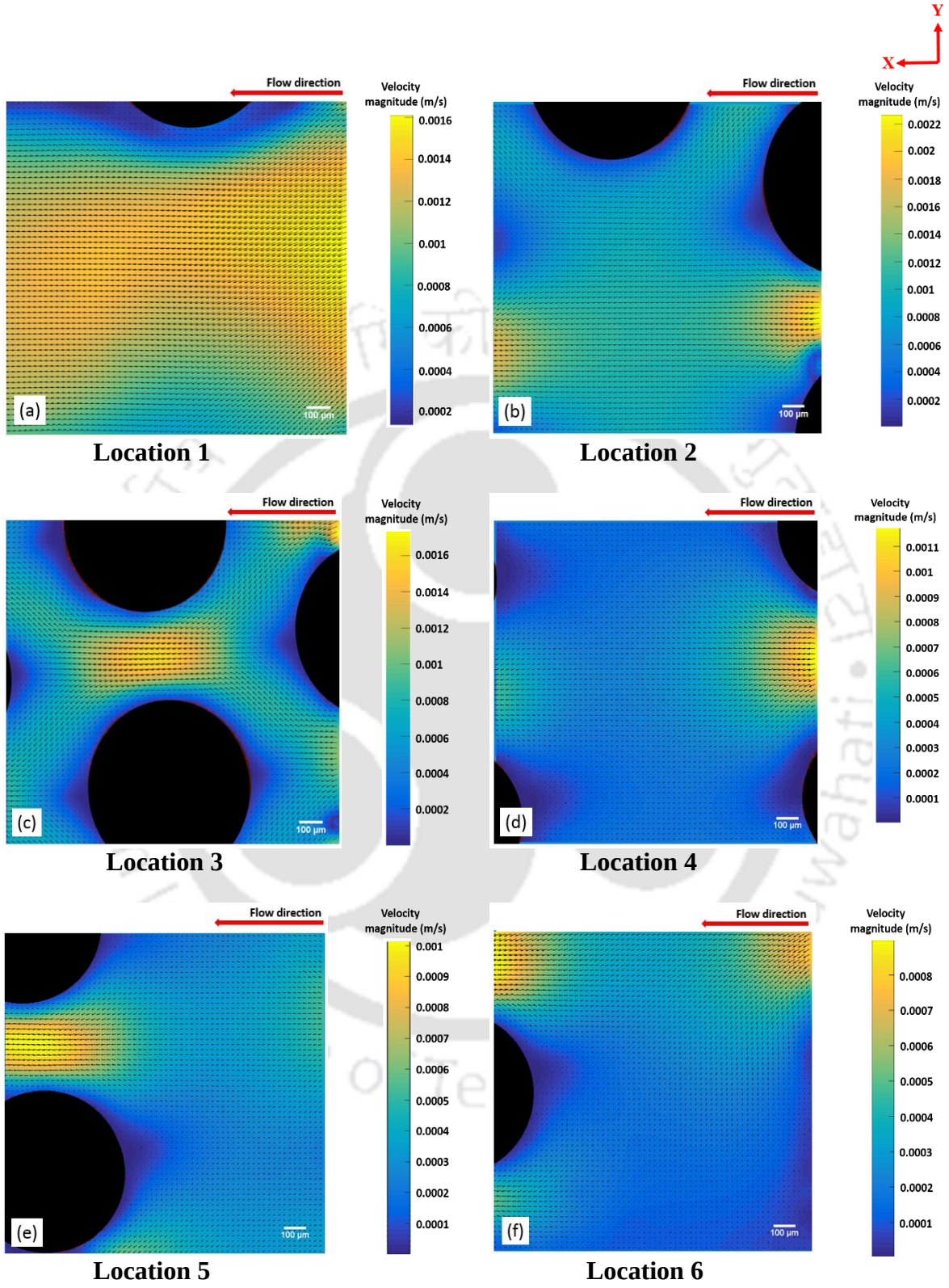

Figure 4.9: Velocity contour map of the micromodel at various locations as highlighted in Fig. 4.6 for flow rate 100 µl/min

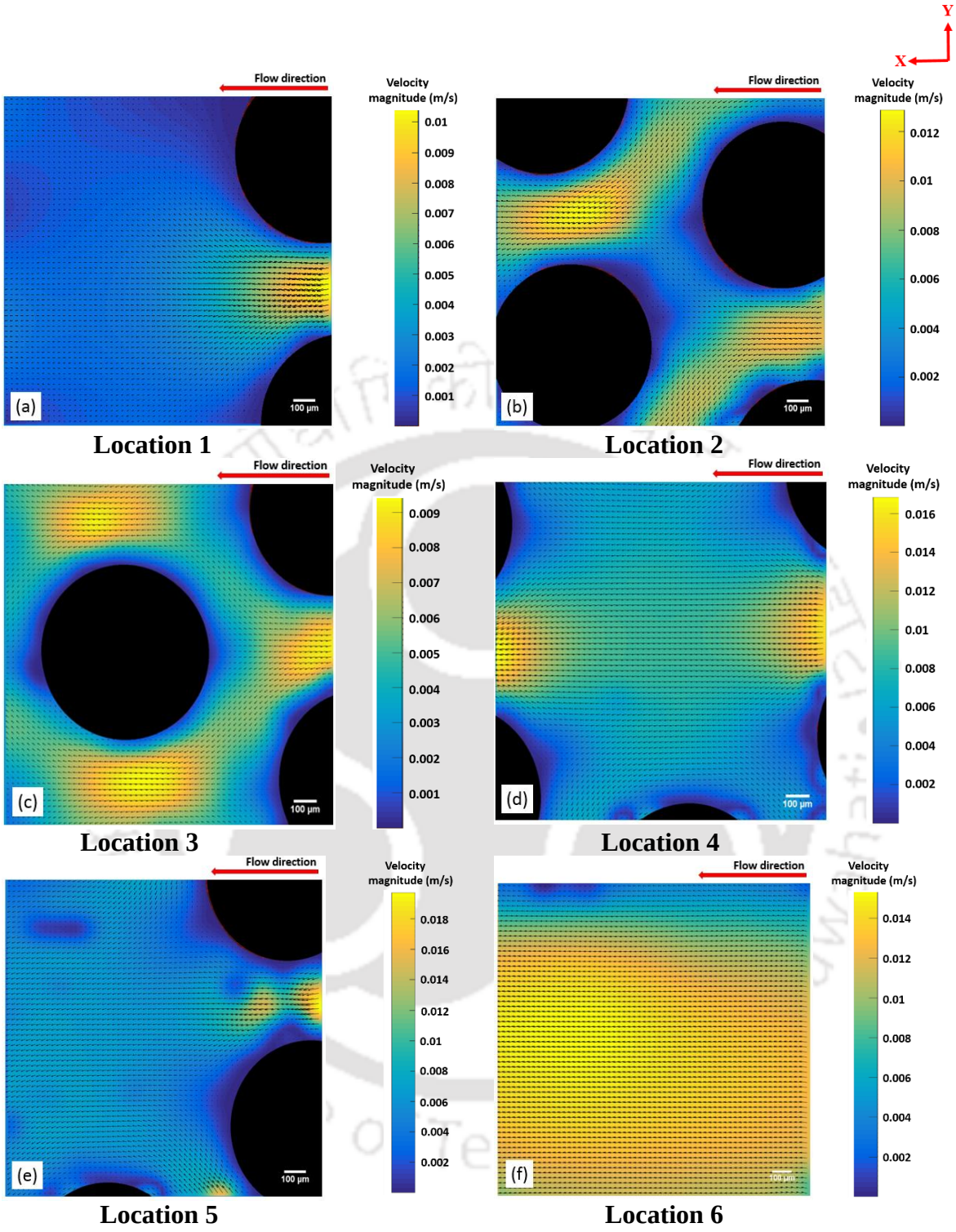

Figure 4.10: Velocity contour map of the micromodel at various locations as highlighted in Fig. 4.7 for flow rate 1000 µl/min

4.3.3 Two-phase flow mechanisms using micro-PIV technique

The fluid-fluid interaction is investigated in two-phase imbibition experiment using micro-PIV technique and most significant observations are reported. The wetting phase (aqueous glycerol) is a mixture of glycerol and water in 57:43 ratio (by volume), while the non-wetting phase is

silicone oil. The wetting phase is seeded with FluoSpheres carboxylate-modified microspheres 1.0 micron size particles (from Fisher Scientific, USA). The seeding concentration is set at roughly 0.03% by volume. The micromodel is first saturated with the silicone oil (non-wetting phase). The injection of the single phase is ceased after fully saturating the micromodel. The second stage imbibition experiments start with the beginning of wetting phase injection (aqueous glycerol). The wetting phase is injected at a flow rate of 1000 µl/min. The maximum capillary number for the wetting phase is found to be in the order of 10^{-2} to 10^{-3}.

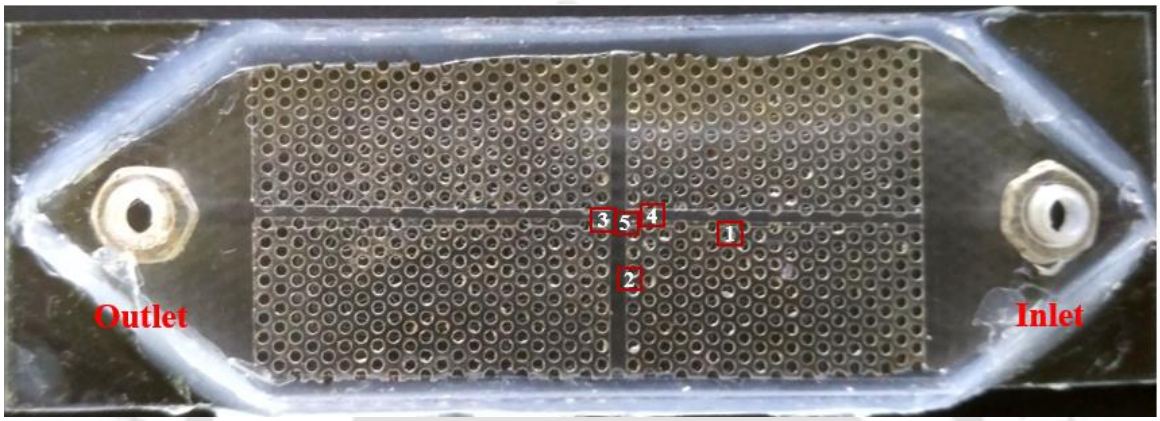

Figure 4.11: Image of the micromodel with highlighted locations where velocity field was obtained for two-phase immiscible flow (flow rate =1000 µl/min)

4.3.4 Instabilities in the imbibition process

The pore scale flow dynamics of aqueous glycerol infiltration into fractured porous micromodel saturated with silicone oil is observed. The micromodel is first saturated with silicone oil and the imbibition process is performed using aqueous glycerol until the residual saturation of silicone oil is reached. The images are thereby captured to track the fluid-fluid interaction. Figure 4.11 highlights the various locations in the micromodel where images are captured.

Figure 4.12 shows the sample raw images of the imbibition process of the highlighted locations shown in Figure 4.11 where the porous medium saturated with silicone oil (non-wetting phase) is invaded by injection of aqueous glycerol (wetting phase). The menisci formed at the interface is clearly observed as the aqueous glycerol is visible due to the light emitted by the seeded tracer particles. While the non-wetting phase as well as the solid cylindrical pillars are not visible and remain dark in the image frame. Hence, the velocity field is obtained for the wetting phase only.

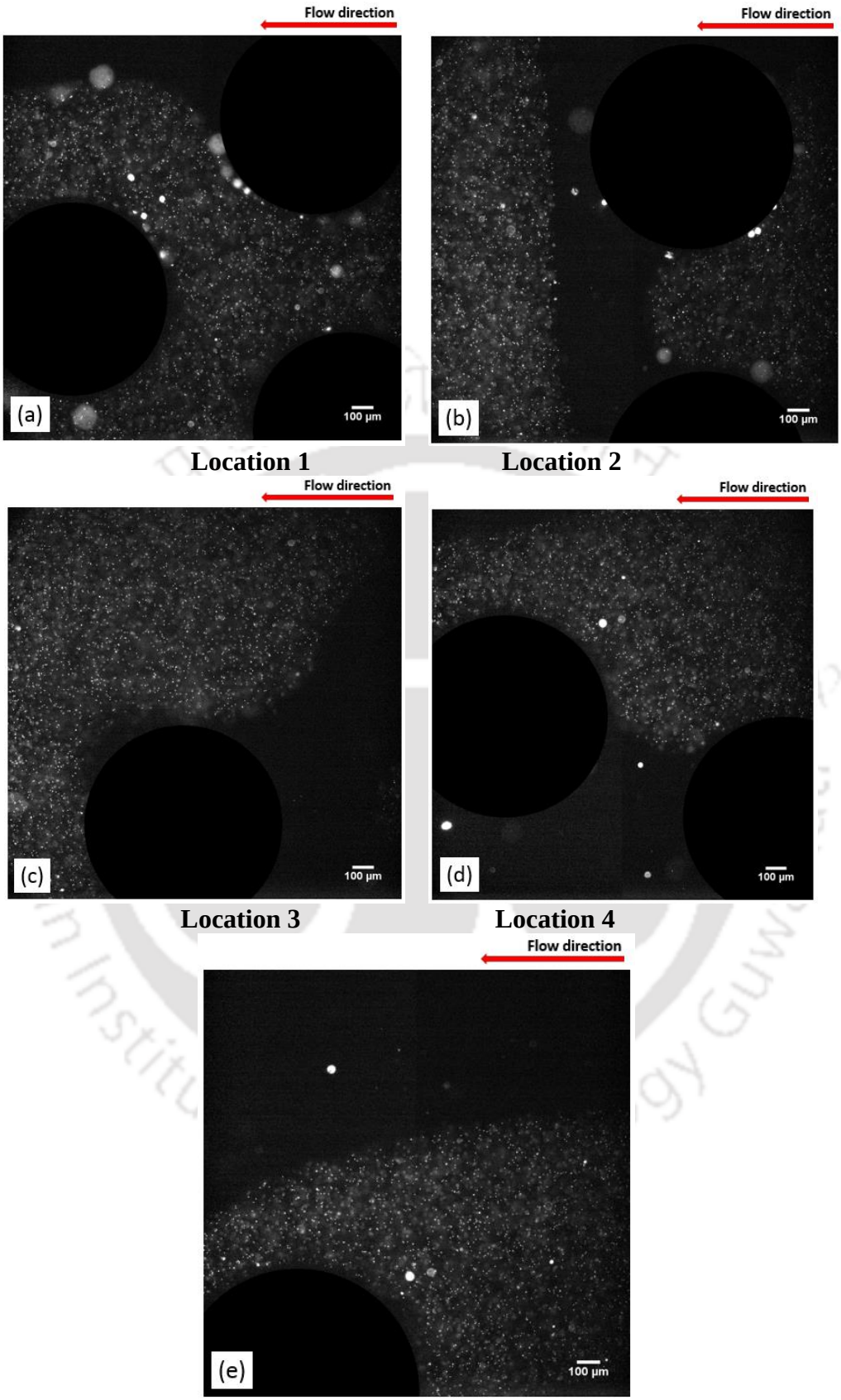

Figure 4.12: Image of the fluorescent particles at various locations of the micromodel as highlighted in Fig. 4.11

Figure 4.13 shows the infiltration of aqueous glycerol into the fractured micromodel saturated with silicone oil using velocity vector field. The dark circular bodies represent the cylindrical pillars, while the silicone oil (non-wetting phase) is shown in grey colour. The velocity vector field is obtained for the wetting phase only at corresponding locations shown in Figure 4.11. It is worth noting that the flow patterns in the two-phase imbibition process is not the same as in single-phase flow even in the homogeneous porous section. Perhaps, it is dramatically different from the single-phase case both in terms of velocity magnitudes and flow direction. Interestingly, the displacement of the front does not follow any regular path and chaotic movements are seen. In certain regions, the flow path becomes straight over multiple pore throats and moves along the diagonal orientations of the staggered pore network (Figure 4.13a). It can therefore be assumed that the fluid-fluid interaction is mostly controlled by the local pressure gradient rather than the bulk (macroscopic) pressure gradient.

Most of the irreducible resident phase is observed in the fracture zone only. This may happen due to the movement of the immiscible phase along a direction normal to the bulk pressure gradient (along *y*-direction). Figure 4.13b depicts the case where the wetting phase moves along a direction perpendicular to the bulk flow direction. However, in the homogeneous porous region, the sweeping is found to be more compared to the fracture region (Figure 4.13a).

Figure 4.14 shows two velocity contours at the same location for oscillating flow. It can be seen that even for the same direction of bulk flow, the direction of the velocity vector magnitude is opposite to each other. This proves the back and fro movement of the front, which can be regarded as the oscillating movement. The development of oscillating movement may be due to the presence of unstable interface configuration that causes the oscillation in the pressure (Morrow 1970). This phenomenon implies that the perturbation of two-phase flow is mostly controlled by local pressure gradient that changes the direction and magnitude of the fluid flow (Blois et *al.* 2013). It is obvious that these movements not only occur for the wetting phase but also for the non-wetting phase. However, the velocity field could not be mapped for the silicone oil (non-wetting phase) due to the absence of tracer particles in it.

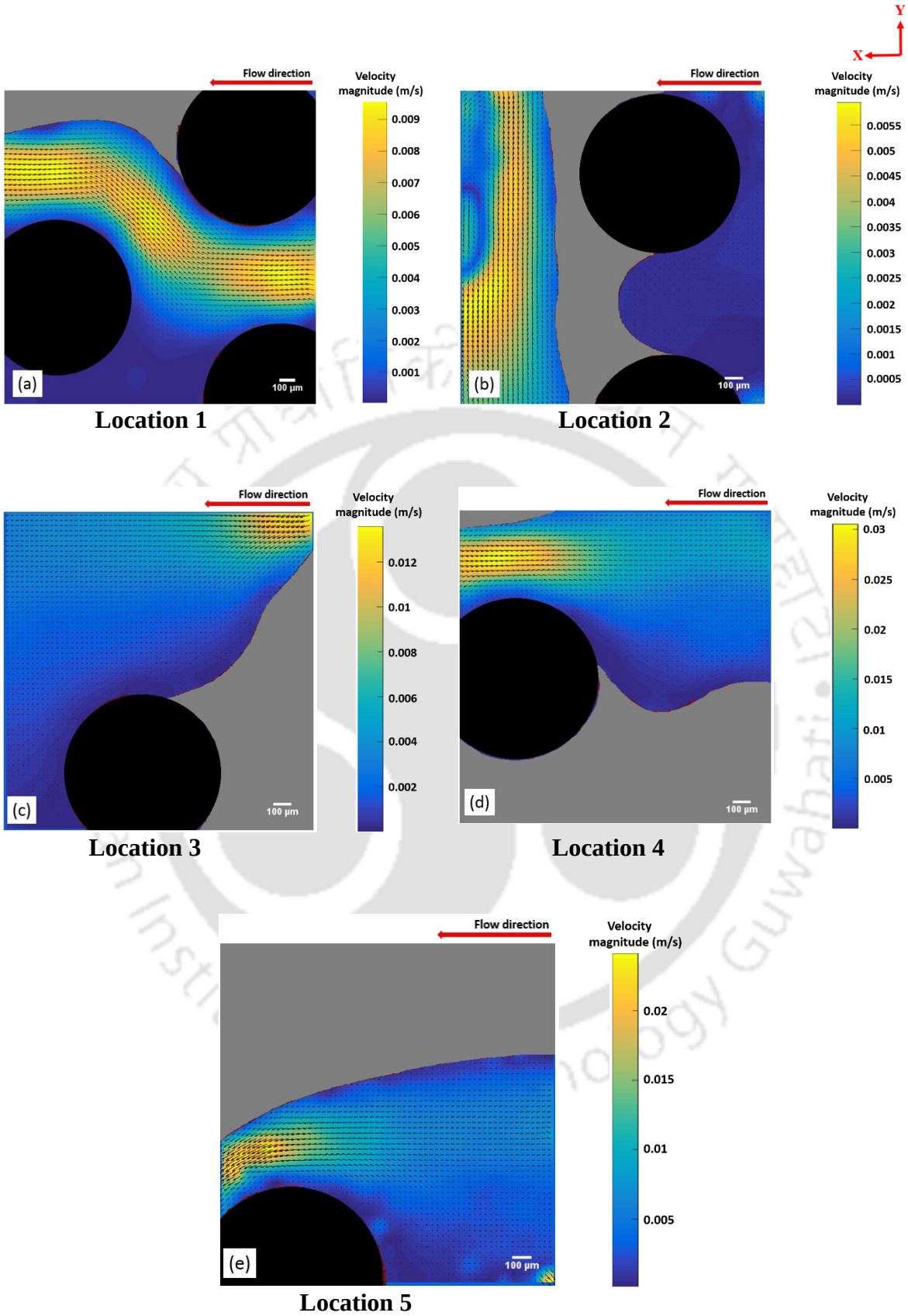

Figure 4.13: Velocity contour map of the micromodel at various locations as highlighted in Fig. 4.11 for two-phase immiscible flow (flow rate =1000 µl/min)

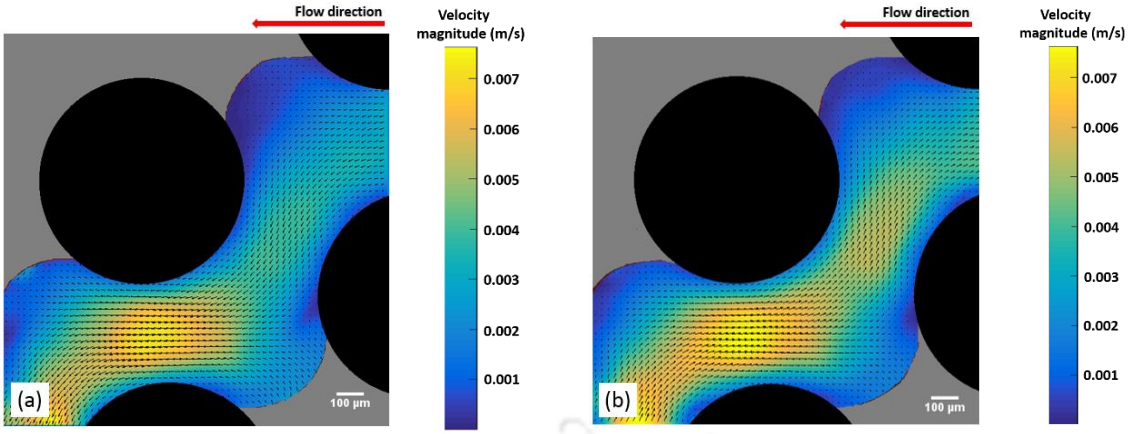

Figure 4.14: Velocity vector contours showing oscillating movement

4.3.5 Recirculation

During the imbibition process, the stagnant pockets of wetting phase remain trapped and are surrounded by the silicone oil phase. Figure 4.15 shows a sample raw images of the static pockets of aqueous glycerol. Here, the wetting phase is surrounded by the non-wetting phase and by the cylindrical pillars. The non-wetting phase and the solid cylinders remain dark, while the trapped areas are visible due to the presence of bright seeded particles. The velocity vector field of these regions cannot be obtained using micro-PIV technique as the seeded particles are immovable along with the wetting phase fluid. These trapped blobs appears at random regions and affects the other neighboring pore bodies that modify the flow structures and finally lead to the formation of preferential paths.

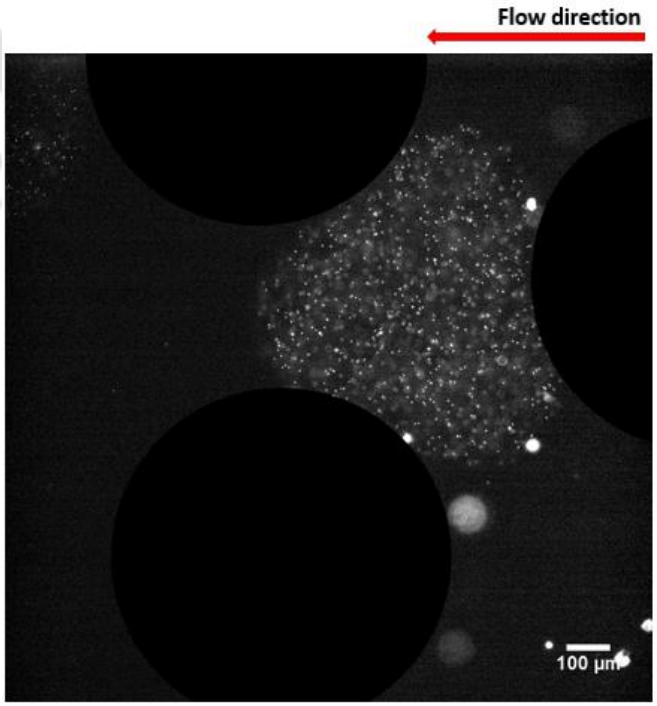

Figure 4.15: Image of tracer particles for the trapped wetting phase

However, these pockets of wetting phase in some regions near the fracture are found to be not immobile; instead the circulating motions are seen until the end of capturing the image frames. Figure 4.16a shows the velocity vector field and Figure 4.16b shows the circulation of the phase with the help of streamlines superimposed over the tracer particles at a certain location near the fracture. The circulating motion of immobile residual fluid (displaced phase) had been reported by Roman et *al.* (2016). In the present case, since the displacing phase (aqueous glycerol) is only seeded with the particles, the velocity vector field is mapped only for the displacing phase. Hence, the velocity vector field of the displaced phase could not be obtained. In addition, at the interface, high velocity magnitude is observed and this circulation may be seen due to the shear force that is induced from the transfer of the momentum of flow at the interface (Kazemifar et *al.* 2015).

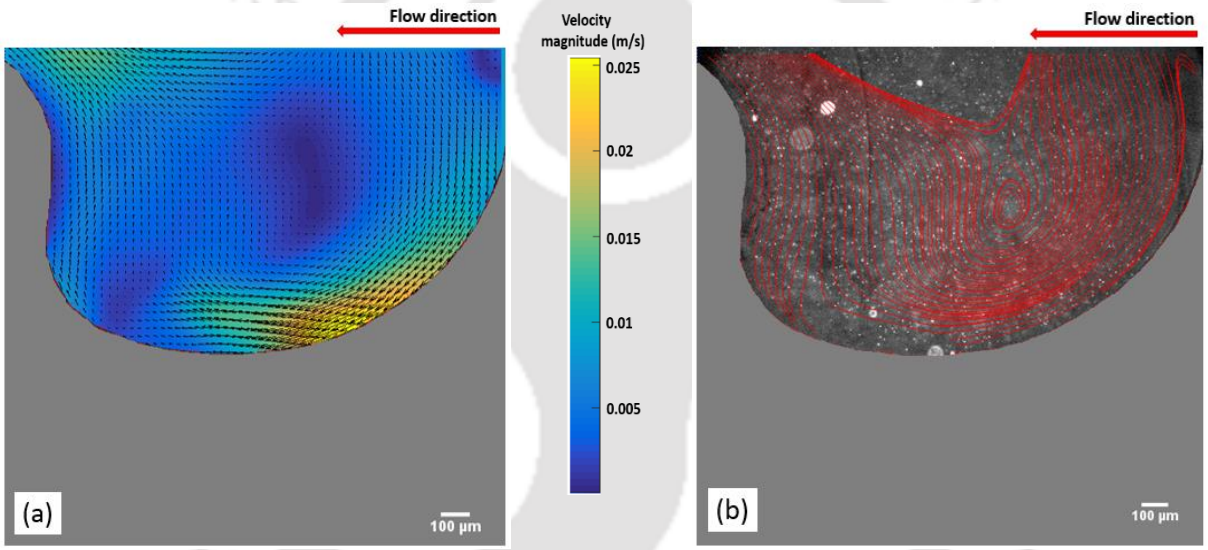

Figure 4.16: (a) Velocity vector field for circulating motion and (b) streamline image at the corresponding location

4.4 Summary

The present investigation reports the fabrication of fractured porous micromodel in PDMS and the experiments associated with both single-phase flow and two-phase flow. Utilizing the present method of fabrication and using PDMS as a substrate, the fractured porous micromodels having different fracture dimension and different pore size have been fabricated. This method of fabricating fractured porous micromodel in PDMS is economic, less time consuming as compared to the traditional photolithography and soft lithography techniques. Flow distribution phenomena have been reported for both single-phase and two-phase flow and the flow velocity is quantified using the micro-PIV technique. For the single-phase flow, no significant effects are observed on the fluid flow due the presence of fracture and regular flow

patterns are seen in the porous region. However, the flow structures for the two-phase flow are found to be completely different from the single phase pattern. In case of two-phase imbibition process, many peculiarities such as preferential flow, oscillating flow of the front, trapped fluid phase and recirculation have been reported in detail. More residual pockets of silicone oil has been observed near the junction of fractures as compared to the regular porous region. Further, with the help of micro-PIV technique, the dynamics of flow distribution has been quantified that can be helpful to gain more insight of these complex processes.

Chapter 5

Conclusions and Future Scope

5.1 Conclusions

This thesis presents a suite of noble fabrication methodology, micro-fluidic experiments, investigating fundamental single-phase and multiphase flow at the pore scale. Throughout, fluid flow in specifically designed unique micro-models has been imaged using optical microscopy. The methodology adopted for designing and fabricating micromodels is very cost effective, simple and time efficient. Most of the experiments are conducted at ambient temperatures and pressures.

5.1.1 Findings of Porous Micromodel Experiments

- ✓ A straightforward and highly economical method has been developed to construct numerous porous micromodels in PDMS substrate. In addition, a unique low cost method has been also discussed to fabricate dual porosity micromodels and the reliability of these models are also tested by performing visualization experiments.
- ✓ Through a series of steps, it has been demonstrated that the round hole perforated metal sheets can be used as a master for the rapid construction of porous micromodels. This method usually takes only 7-8 hours. However, it is necessary to mention that in the present method, the complexity of the pore network solely depends on the pattern template and porous plate containing complicated geometry is difficult to find in the market.
- ✓ This method is cost-effective, flexible and convenient as compared to traditional techniques like photolithography or soft lithography. With the help of this technique, it is also possible to construct porous micromodels having different pore geometry and pore sizes very easily. This method will increase the adaptability of fabrication and utilization of microfluidic devices.
- ✓ Visualization setup that provides images of the distribution of fluid seeded with tracer particles at different porous sections of the micromodel is also explained in detail. The

results produced from the experimental analysis provide satisfactory results that enhances the reliability of this noble method.

- ✓ Furthermore, the captured images are processed using PIV lab (MATLAB tool) and the velocity contour as well as velocity profile of the flow field is obtained with the help of two-frame cross correlation method. The analysed velocity profiles indicate the reliability and applicability of the fabricated micromodel.
- ✓ This type of micromodel can be used in an efficient way to investigate the fluid flow at pore scale, which is crucial to the processes like enhanced oil recovery, hydrology, wastewater management and other engineering and natural applications.

5.1.2 Findings of Fractured Micromodel Experiments

- ✓ In this work, we have also reported the fabrication of fractured porous micromodel in PDMS and performed both single-phase and two phase flow experiments. Using this method, the fractured porous micromodel having different fracture dimension and different pore size can be fabricated very easily. This method of fabricating fractured porous micromodel in PDMS is economic, easy and less time consuming as compared to the traditional photolithography and soft lithography technique.
- ✓ Flow distribution phenomena have been reported for both single-phase and two-phase flow and the flow velocity is quantified using the micro-PIV technique.
- ✓ For the single-phase flow, no significant effects are observed on the fluid flow due the presence of fracture and regular flow patterns are seen in the porous region. However, the flow structures for the two-phase flow are found to be completely different from the single-phase pattern.
- ✓ In case of two-phase imbibition process, many peculiarities such as preferential flow, oscillating flow of the front, trapped fluid phase and recirculation have been reported in detail. More residual pockets of silicone oil has been observed near the junction of fractures as compared to the regular porous region during the imbibition process, when mixture of glycerol-water infiltrates through the porous region and displaces silicone oil.
- ✓ Further, with the help of micro-PIV technique, the dynamics of flow distribution has been quantified that can be helpful to gain more insight of these complex fundamental processes.

5.2 Future Work

Conventional methods involved during fabrication of porous micromodel like optical lithography, soft lithography and etching are very costly and time consuming. In addition, utilization of these methods require special clean and high cost lab setup, which is difficult to establish by most of the researchers. In that case, this noble method of fabrication provides an economic platform to fabricate micromodels having different topology and geometry very easily with low cost and easily found materials. Our primary work was to establish this unique methodology to fabricate micromodels having considerable flexibility in regards of porosity, geometry and distribution of pore space. In addition, fractured micromodels having numerous geometry can be fabricated.

The literature and experimental work related to the flow visualization study whether it is single-phase or two-phase flow, in porous media is limited. It is mainly due to the need of costly optical equipment and the high cost of fabrication of micromodels. In the present work, we have tried to reduce the cost of fabrication of micromodels by using a low cost noble method. The biggest advantage of using this method lies in its flexibility in fabricating micromodels having different geometry and topology. Therefore, in future, both homogeneous and heterogeneous micromodels can be fabricated easily using these method and experiments can be performed to study the fundamental flow processes inside porous media.

In addition, multiphase flow experiments can also be performed in these micromodels, which has vital applications in many fields like oil recovery, hydrology, waste management and other engineering and natural systems.

References

Adrian, R. J., 2005, "Twenty years of particle image velocimetry," *Experiments in Fluids*, **39**(2), pp. 159–169.

Ahmed, T. H., 2019, Reservoir Engineering Handbook, fifth edition, *Gulf Professional Publishing*.

Arnold, J., Dasbach, U., Ehrfeld, W., Hesch, K., and Löwe, H., 1995, "Combination of excimer laser micromachining and replication processes suited for large scale production," *Applied Surface Science*, **86**(1-4), pp. 251–258.

Almajid, M., M., Kovscek, A., R., 2016, "Pore-level mechanics of foam generation and coalescence in the presence of oil," *Advance Colloid Interface Science*, **233**, pp. 65–82.

Askarinezhad, R., Hatzignatiou, D. G., Stavland A. 2018 "Core-based evaluation of associative polymers as enhanced oil recovery agents in oil-wet formations," *Journal of Energy Resource Technology*, **140**, pp. 032915.

Auset, M., and Keller, A. A., 2004, "Pore-scale processes that control dispersion of colloids in saturated porous media," *Water Resources Research*, **40**(3).

Avraam, D. G., Kolonis, G. B., Roumeliotis, T. C., Constantinides, G. N., and Payatakes, A. C., 1994, "Steady-state two-phase flow through planar and nonplanar model porous media," *Transport in Porous Media*, **16**(1), pp. 75–101.

Baouab, Z., Najjari, M., Ouerfelli, H., and Nasrallah, S. B., 2007, "Experimental study of the effects of hydraulic gradient and injected-gas flow rate on fragmentation in porous media," *Journal of Petroleum Science and Engineering*, **59**(3-4), pp. 250–256.

Basov, N. G., Danilychev, V.A., Popov, Y. M., and Khodkevich, D. D., 1970, "Laser operating in the vacuum region of the spectrum by excitation of liquid xenon with an electron beam," *Journal of Experimental and Theoretical Physics*, **12**, pp. 329.

Baumann, T., 2007, Colloid transport processes: experimental evidence from the pore scale to the field scale, colloidal transport in porous media. *Springer-Verlag, Berlin*. pp. 55–86.

Baumann, T., and Werth, C. J., 2004, "Visualization and modeling of polystyrol colloid transport in a Silicon micromodel," *Vadose Zone Journal*, **3**(2), pp. 434–443.

Berkowitz, B., 2002, "Characterizing flow and transport in fractured geological media: A review," *Advances in Water Resources*, **25**(8-12), pp. 861–884.

Blois, G., Barros, J. M., and Christensen, K. T., 2015, "A microscopic particle image velocimetry method for studying the dynamics of immiscible liquid–liquid interactions in a porous micromodel," *Microfluidics and Nanofluidics*, **18**(5-6), pp. 1391–1406.

Bloomstein, T. M., 1992, "Laser-chemical three-dimensional writing for microelectromechanics and application to standard-cell microfluidics," *Journal of Vacuum Science & Technology B: Microelectronics and Nanometer Structures*, **10**(6), pp. 2671.

Blunt, M., and King, P., 1991, "Relative permeabilities from two and three-dimensional pore-scale network modelling," *Transport in Porous Media*, **6**(4).

Bowden, S. A., Cooper, J. M., Greub, F., Tambo, D., Hurst, A., 2010, "Benchmarking methods of enhanced heavy oil recovery using a micro scaled bead-pack," *Lab on a Chip*, **10**, pp. 819–823.

Breugem, W.-P., Dijk, V. V., and Delfos, R., 2014, "Flows through real porous media: x-ray computed tomography, experiments, and numerical simulations," *ASME Journal of Fluids Engineering*, **136**(4).

Brusseau, M., and Rao, P., 1990, "Modeling solute transport in structured soils: a review," *Geoderma*, **46**(1-3), pp. 169–192.

Buchgraber, M., Al-Dossary, M., Ross, C., and Kovscek, A., 2012, "Creation of a dual-porosity micromodel for pore-level visualization of multiphase flow," *Journal of Petroleum Science and Engineering*, **86-87**, pp. 27–38.

Budwig, R., 1994, "Refractive index matching methods for liquid flow investigations," *Experiments in Fluids*, **17**(5), pp. 350–355.

Cahn, R. P., and Li, N. N., 1974, "Separation of phenol from waste water by the liquid membrane technique," *Separation Science*, **9**(6), pp. 505–519.

Chang, L.-C., Tsai, J.-P., Shan, H.-Y., and Chen, H.-H., 2009, "Experimental study on imbibition displacement mechanisms of two-phase fluid using micro model," *Environmental Earth Sciences*, **59**(4), pp. 901–911.

Chatenever, A., and Calhoun, J. C., 1952, "Visual examinations of fluid behavior in porous media - Part I," *Journal of Petroleum Technology*, **4**(06), pp. 149–156.

Chen, C., Hirdes, D., and Folch, A., 2003, "Gray-scale photolithography using microfluidic photomasks," *Proceedings of the National Academy of Sciences*, **100**(4), pp. 1499–1504.

Chen, D., Pyrak-Nolte, L. J., Griffin, J., and Giordano, N. J., 2007, "Measurement of interfacial area per volume for drainage and imbibition," *Water Resources Research*, **43**(12).

Cheng, J.-T., 2004, "Linking pressure and saturation through interfacial areas in porous media," *Geophysical Research Letters*, **31**(8).

Chuoke, R., Meurs, P. V., and Poel, C. V. D., 1959, "The instability of slow, immiscible, viscous liquid-liquid displacements in permeable media," *Transactions of the AIME*, **216**(01), pp. 188–194.

Conn, C. A., Ma, K., Hirasaki, G. J., and Biswal, S. L., 2014, "Visualizing oil displacement with foam in a microfluidic device with permeability contrast," *Lab on a Chip*, **14** (20), pp. 3968–3977.

Corapcioglu, M.Y., and Fedirchuk P., 1999, "Glass bead micro-model study of solute transport," *Journal of Contaminant Hydrology*, **36**, pp. 209-230.

Corapcioglu, M. Y., Yoon, S., and Chowdhury, S., 2009, "Pore-scale analysis of NAPL blob dissolution and mobilization in porous media," *Transport in Porous Media*, **79**(3), pp. 419–442.

Corapcioglu, Y. M., Chowdhury, S., and Roosevelt, S. E., 1997, "Micromodel visualization and quantification of solute transport in porous media," *Water Resources Research*, **33**(11), pp. 2547–2558.

Cottin, C., Bodiguel, H., and Colin, A., 2011, "Influence of wetting conditions on drainage in porous media: A microfluidic study," *Physical Review* E, **84**(2).

Crandall, D., Ahmadi, G., Ferer, M., and Smith, D. H., 2009, "Distribution and occurrence of localized-bursts in two-phase flow through porous media," *Physica A: Statistical Mechanics and its Applications*, **388**(5), pp. 574–584.

Crandall, D., Ahmadi, G., Leonard, D., Ferer, M., and Smith, D. H., 2008, "A new stereolithography experimental porous flow device," *Review of Scientific Instruments*, **79**(4), pp. 044501.

Datta, S. S., Ramakrishnan, T., and Weitz, D. A., 2014, "Mobilization of a trapped non-wetting fluid from a three-dimensional porous medium," *Physics of Fluids*, **26** (2), pp. 022002.

Davis, J., and Jones, S., 1968, "Displacement mechanisms of micellar solutions," *Journal of Petroleum Technology*, **20**(12), pp. 1415–1428.

Dawe, R. A., Caruana, A., and Grattoni, C. A., 2010, "Immiscible displacement in cross-bedded heterogeneous porous media," *Transport in Porous Media*, **87**(1), pp. 335–353.

Devasenathipathy, S., Santiago, J. G., and Takehara, K., 2002, "Particle tracking techniques for electrokinetic microchannel flows," *Analytical Chemistry*, **74**(15), pp. 3704–3713.

Devasenathipathy, S., Santiago, J. G., Wereley, S. T., Meinhart, C. D., and Takehara, K., 2003, "Particle imaging techniques for microfabricated fluidic systems," *Experiments in Fluids*, **34**(4), pp. 504–514.

Dijk, P., Berkowitz, B., and Bendel, P., 1999, "Investigation of flow in water-saturated rock fractures using nuclear magnetic resonance imaging (NMRI)," *Water Resources Research*, **35**(2), pp. 347–360.

Du, Y., Li, N., Yang, H., Luo, C., Gong, Y., Tong, C., Gao, Y., Lü, S., and Long, M., 2017, "Mimicking liver sinusoidal structures and functions using a 3D-configured microfluidic chip," *Lab on a Chip*, **17**(5), pp. 782–794.

Duguid, J. O., and Lee, P. C. Y., 1977, "Flow in fractured porous media," *Water Resources Research*, **13**(3), pp. 558–566.

Durandet, A., Joubert, O., Pelletier, J., and Pichot, M., 1990, "Effects of ion bombardment and chemical reaction on wafer temperature during plasma etching," *Journal of Applied Physics*, **67**(8), pp. 3862–3866.

Durst, F., Jovanovic, J., and Sender, J., 1995, "LDA measurements in the near-wall region of a turbulent pipe flow," *Journal of Fluid Mechanics*, **295**(-1), pp. 305.

Dutra, T., and Aziz, K., 1992, "A new double-porosity reservoir model for oil/water flow problems," *SPE Reservoir Engineering*, **7**(04), pp. 419–425.

Eddings, M. A., Johnson, M. A., and Gale, B. K., 2008, "Determining the optimal PDMS–PDMS bonding technique for microfluidic devices," *Journal of Micromechanics and Microengineering*, **18**(6), pp. 067001.

Ehrfeld W., Lehr H., Michel F. Wolf A., 1996, Micro electro discharge machining as a technology on micromachining, in *SPIE Proceedings Series*, **2879**, pp. 332-337.

Ehrfeld, W., Abraham, M., Ehrfeld, U., Lacher, M., and Lehr, H., 1994 "Materials for LIGA products," Proceedings IEEE Micro Electro Mechanical Systems An Investigation of Micro Structures, *Sensors and Actuators*, Machines and Robotic Systems.

Fand, R. M., Kim, B. Y. K., Lam, A. C. C., and Phan, R. T., 1987, "Resistance to the flow of fluids through simple and complex porous media whose matrices are composed of randomly packed spheres," *ASME Journal of Fluids Engineering*, **109**(3), pp. 268–273.

Fathollahi, A., Rostami, B., and Khosravi, M., 2019, "Fluid displacement mechanisms by foam injection within a microfluidic matrix-fracture system," *Journal of Petroleum Science and Engineering*, **176**, pp. 612–620.

Fatt, I., 1956, "The network model of porous media, I. Capillary pressure characteristics," *Transaction of American Institute of Mining, Metallurgical, and Petroleum Engineers*, **207**, pp. 144-159.

Ferer, M., Ji, C., Bromhal, G. S., Cook, J., Ahmadi, G., and Smith, D. H., 2004, "Crossover from capillary fingering to viscous fingering for immiscible unstable flow: Experiment and modeling," *Physical Review E*, **70**(1).

Folch, A., Ayon, A., Hurtado, O., Schmidt, M. A., and Toner, M., 1999, "Molding of deep polydimethylsiloxane microstructures for microfluidics and biological applications," *Journal of Biomechanical Engineering*, **121**(1), pp. 28–34.

Fourar, M., Bories, S., Lenormand, R., and Persoff, P., 1993, "Two-phase flow in smooth and rough fractures: Measurement and correlation by porous-medium and pipe flow models," *Water Resources Research*, **29**(11), pp. 3699–3708.

Frette, O. I., Måløy Knut Jørgen, Schmittbuhl, J., and Hansen, A., 1997, "Immiscible displacement of viscosity-matched fluids in two-dimensional porous media," *Physical Review E*, **55**(3), pp. 2969–2975.

Fritz, J. L., and Owen, M. J., 1995, "Hydrophobic recovery of plasma-treated polydimethylsiloxane," *The Journal of Adhesion*, **54**(1-4), pp. 33–45.

Geistlinger, H., Ataei-Dadavi, I., Vogel, H-J., 2016, "Impact of surface roughness on capillary trapping using 2d-micromodel visualization experiments," *Transport in Porous Media*, **112**, pp. 207–227.

Germann, P., and Dipietro, L., 1996, "When is porous-media flow preferential? A hydromechanical perspective," *Geoderma*, **74**(1-2), pp. 1–21.

Gervais, T., El-Ali, J., Günther, A., and Jensen, K. F., 2006, "Flow-induced deformation of shallow microfluidic channels," *Lab on a Chip*, **6**(4), pp. 500.

Giordano, N., and Cheng, J.-T., 2001, "Microfluid mechanics: progress and opportunities," *Journal of Physics: Condensed Matter*, **13**(15).

González, C., Smith, R., Howitt, D., and Collins, S., 1998, "MicroJoinery: concept, definition, and application to microsystem development," *Sensors and Actuators A: Physical*, **66**(1-3), pp. 315–332.

Grant, I., 1997, "Particle image velocimetry: A review," *Proceedings of the Institution of Mechanical Engineers, Part C: Journal of Mechanical Engineering Science*, **211**(1), pp. 55–76.

Gutiérrez, B., Juarez, F., Ornelas, L., Zeppieri, S., and Ramos, A. L. D., 2008, "Experimental study of gas–liquid two-phase flow in glass micromodels," *International Journal of Thermophysics*, **29**(6), pp. 2126–2135.

Häfeli, R., Altheimer, M., Butscher, D., and Rohr, P. R. V., 2014, "PIV study of flow through porous structure using refractive index matching," *Experiments in Fluids*, **55**(5).

Haque, N., Singh, A., and Saha, U. K., 2019, "A noble method for rapid prototyping of porous micromodels applicable to enhanced oil recovery," *Journal of Physics: Conference Series*, **1276**, pp. 012022.

Hasham, A. A., Abedini, A., Jatukaran, A., Persad, A., and Sinton, D., 2018, "Visualization of fracturing fluid dynamics in a nanofluidic chip," *Journal of Petroleum Science and Engineering*, **165**, pp. 181–186.

Helba, A., Sahimi, M., Scriven, L., and Davis, H., 1992, "Percolation theory of two-phase relative permeability," *SPE Reservoir Engineering*, **7**(01), pp. 123–132.

Hell, S. W., Lindek, S., Cremer, C., and Stelzer, E. H. K., 1994, "Confocal microscopy with an increased detection aperture: type-B 4Pi confocal microscopy," *Optics Letters*, **19**(3), pp. 222.

Hematpour, H., Mardi, M., Edalatkhah, S., and Arabjamaloei, R., 2011, "Experimental study of polymer flooding in low-viscosity oil using one-quarter five-spot glass micromodel," *Petroleum Science and Technology*, **29**(11), pp. 1163–1175.

Hornbrook, J., Castanier, L., and Pettit, P., 1991, "Observation of foam/oil interactions in a new, high-resolution micromodel," *SPE Annual Technical Conference and Exhibition*. Dallas, Texas.

Hsu, S.-Y., Zhang, Z.-Y., and Tsao, C.-W., 2017, "Thermoplastic micromodel investigation of two-phase flows in a fractured porous medium," *Micromachines*, **8**(2), pp. 38.

Huang, A. Y. L., Huang, M. Y. F., Capart, H., and Chen, R.-H., 2008, "Optical measurements of pore geometry and fluid velocity in a bed of irregularly packed spheres," *Experiments in Fluids*, **45**(2), pp. 309–321.

Huh, D., Mills, K. L., Zhu, X., Burns, M. A., Thouless, M. D., and Takayama, S., 2007, "Tuneable elastomeric nanochannels for nanofluidic manipulation," *Nature Materials*, **6**(6), pp. 424–428.

Hull, C.W., A. C. A., 1986. US Patent No. US 4575330.

Ikuta, K., Hirowatari, K., and Ogata, T., 1994, "Three dimensional micro integrated fluid systems (MIFS) fabricated by stereo lithography," Proceedings IEEE Micro Electro Mechanical Systems An Investigation of Micro Structures, Sensors, Actuators, Machines and Robotic Systems, 25-28 January, Oiso, Japan.

Iqbal, G. M., and Satter, A., 2016, Reservoir engineering: The fundamentals, simulation, and management of conventional and unconventional recoveries, *Gulf Professional Publishing.*

Jamshidi, T., Zeng, F., Tontiwachwuthikul, P., and Torabi, F., 2019, "Viability of carbonated water injection (CWI) as a means of secondary oil recovery in heavy oil systems in presence and absence of wormholes: Microfluidic experiments," *Fuel*, **249**, pp. 286–293.

Jeong, S.-W., and Corapcioglu, M. Y., 2005, "Force analysis and visualization of NAPL removal during surfactant-related floods in a porous medium," *Journal of Hazardous Materials*, **126**(1-3), pp. 8–13.

Jia, Y., Jiang, J., Ma, X., Li, Y., Huang, H., Cai, K., Cai, S., and Wu, Y., 2008, "PDMS microchannel fabrication technique based on microwire-molding," *Science Bulletin*, **53**(24), pp. 3928–3936.

Jo, B.-H., Lerberghe, L. V., Motsegood, K., and Beebe, D., 2000, "Three-dimensional micro-channel fabrication in polydimethylsiloxane (PDMS) elastomer," *Journal of Microelectromechanical Systems*, **9**(1), pp. 76–81.

Karadimitriou, N. K., and Hassanizadeh, S. M., 2012, "A review of micromodels and their use in two-phase flow studies," *Vadose Zone Journal*, **11**(3).

Karadimitriou, N. K., Musterd, M., Kleingeld, P. J., Kreutzer, M. T., Hassanizadeh, S. M., and Joekar-Niasar, V., 2013, "On the fabrication of PDMS micromodels by rapid prototyping, and their use in two-phase flow studies," *Water Resources Research*, **49**(4), pp. 2056–2067.

Kazemifar, F., Blois, G., Kyritsis, D. C., and Christensen, K. T., 2016, "Quantifying the flow dynamics of supercritical CO_2–water displacement in a 2D porous micromodel using fluorescent microscopy and microscopic PIV," *Advances in Water Resources*, **95**, pp. 352–368.

Keane, R. D., and Adrian, R. J., 1992, "Theory of cross-correlation analysis of PIV images," *Applied Scientific Research*, **49**(3), pp. 191–215.

Kececioglu, I., and Jiang, Y., 1994, "Flow through porous media of packed spheres saturated with water," *ASME Journal of Fluids Engineering*, **116**(1), pp. 164–170.

Khoei, A., Hosseini, N., and Mohammadnejad, T., 2016, "Numerical modeling of two-phase fluid flow in deformable fractured porous media using the extended finite element method and an equivalent continuum model," *Advances in Water Resources*, **94**, pp. 510–528.

Kianinejad, A., Rashtchian, D., Ghazanfari, M. H., and Kharrat, R., 2014, "A pore-level investigation of surfactant-crude oil displacements behavior in fractured porous media using one-quarter five spot micromodels," *Energy Sources, Part A: Recovery, Utilization, and Environmental Effects*, **36**(7), pp. 727–737.

Kim, E., Xia, Y., and Whitesides, G. M., 1996, "Micromolding in capillaries: applications in materials science," *Journal of the American Chemical Society*, **118**(24), pp. 5722–5731.

Kolari, K., Saarela, V., and Franssila, S., 2008, "Deep plasma etching of glass for fluidic devices with different mask materials," *Journal of Micromechanics and Microengineering*, **18**(6), pp. 064010.

Kumar, Gunda, N. S., Bera, B, Karadimitriou, N. K., Mitra, S, K., Hassanizadeh, S. M., 2011, "Reservoir-on-a-Chip (ROC): A new paradigm in reservoir engineering," *Lab Chip*, **11**, pp. 3785.

Kwicklis, E. M., and Healy, R. W., 1993, "Numerical investigation of steady liquid water flow in a variably saturated fracture network," *Water Resources Research*, **29**(12), pp. 4091–4102.

Lanning, L. M., and Ford, R. M., 2002, "Glass micromodel study of bacterial dispersion in spatially periodic porous networks," *Biotechnology and Bioengineering*, **78**(5), pp. 556–566.

Leester-Schädel, M., Lorenz, T., Jürgens, F., Richter, C., 2016, "Fabrication of microfuidic devices, microsystems for pharmatechnology," pp. 23-57, *Springer International Publishing Switzerland.*

Lenormand, R., 1989, "Applications of fractal concepts in petroleum engineering," *Physica D: Nonlinear Phenomena*, **38**(1-3), pp. 230–234.

Lenormand, R., Zarcone, C., and Sarr, A., 1983, "Mechanisms of the displacement of one fluid by another in a network of capillary ducts," *Journal of Fluid Mechanics*, **135**, pp. 337–353.

Lenormand, R., Touboul, E., and Zarcone, C., 1988, "Numerical models and experiments on immiscible displacements in porous media," *Journal of Fluid Mechanics*, **189**, pp. 165–187.

Lindek, S., Cremer, C., and Stelzer, E. H. K., 1996, "Confocal theta fluorescence microscopy with annular apertures," *Applied Optics*, **35**(1), pp. 126.

Lindken, R., Rossi, M., Große, S., and Westerweel, J., 2009, "Micro-particle image velocimetry (μpiv): recent developments, applications, and guidelines," *Lab on a Chip*, **9**(17), pp. 2551.

Little, W. A., 1982, "Micro miniature refrigeration-small is better," *Physica B+C*, **109-110**(3), pp. 2001-2009.

Lovoll, G., 2005, "Competition of gravity, capillary and viscous forces during drainage in a two-dimensional porous medium, a pore scale study," *Energy*, **30**(6), pp. 861–872.

Lu, C., Zhao, W., Liu, Y., and Dong, X., 2018, "Pore-scale transport mechanisms and macroscopic displacement effects of in-situ oil-in-water emulsions in porous media," *ASME Journal of Energy Resources Technology*, **140**(10).

Lu, X., Zhao, Y., and Dennis, D. J., 2018, "Flow measurements in microporous media using micro-particle image velocimetry," *Physical Review Fluids*, **3**(10), pp. 104202.

Lu, X., Zhao, Y. and Dennis, D. J., 2020, "Fluid flow characterisation in randomly packed microscale porous beds with different sphere sizes using micro-particle image velocimetry," *Experimental Thermal and Fluid Science*, **118**, pp. 110136.

Lyu, X., Liu, H., Pang, Z., and Sun, Z., 2018, "Visualized study of thermochemistry assisted steam flooding to improve oil recovery in heavy oil reservoir with glass micromodels," *Fuel*, **218**, pp. 118–126.

Mahdavi, S., and James, L. A., 2019, "Micro and macro analysis of carbonated water injection (CWI) in homogeneous and heterogeneous porous media," *Fuel*, **257**, pp. 115916.

Markov, D. A., Samson, P. C., Schaffer, D. K., Dhummakupt, A., Wikswo, J. P., and Shor, L. M., 2010, "Window on a microworld: simple microfluidic systems for studying microbial transport in porous media," *Journal of Visualized Experiments*, (39).

Mckellar, M., and Wardlaw, N., 1982, "A method of making two-dimensional glass micromodels of pore systems," *Journal of Canadian Petroleum Technology*, **21**(04).

Meakin, P., and Tartakovsky, A. M., 2009, "Modeling and simulation of pore-scale multiphase fluid flow and reactive transport in fractured and porous media," *Reviews of Geophysics*, **47**(3).

Meinhart, C. D., Wereley, S. T., and Santiago, J. G., 1999, "PIV measurements of a microchannel flow," *Experiments in Fluids*, **27**(5), pp. 414–419.

Mejia, L., Tagavifar, M., Xu, K., Mejia, M., Du, Y., and Balhoff, M., 2019, "Surfactant flooding in oil-wet micromodels with high permeability fractures," *Fuel*, **241**, pp. 1117–1128.

Melchels, F. P., Feijen, J., and Grijpma, D. W., 2010, "A review on stereolithography and its applications in biomedical engineering," *Biomaterials*, **31**(24), pp. 6121–6130.

Minsky, M., 1988, "Memoir on inventing the confocal scanning microscope," *Scanning*, **10**(4), pp. 128–138.

Mohammadzadeh, O., Sedaghat, M. H., Kord, S., Zendehboudi, S., and Giesy, J. P., 2019, "Pore-level visual analysis of heavy oil recovery using chemical-assisted water flooding process – Use of a new chemical agent," *Fuel*, **239**, pp. 202–218.

Montemagno, C. D., and Gray, W. G., 1995, "Photoluminescent volumetric imaging: A technique for the exploration of multiphase flow and transport in porous media," *Geophysical Research Letters*, **22**(4), pp. 425–428.

Morrow, N. R., 1970, "Physics and thermodynamics of capillary action in porous media," *Industrial & Engineering Chemistry*, **62**(6), pp. 32–56.

Mosavat, N., and Torabi, F., 2016, "Micro-optical analysis of carbonated water injection in irregular and heterogeneous pore geometry," *Fuel*, **175**, pp. 191–201.

Murakami, T., Kuroda, S.-I., and Osawa, Z., 1998, "Dynamics of polymeric solid surfaces treated with oxygen plasma: effect of aging media after plasma treatment," *Journal of Colloid and Interface Science*, **202**(1), pp. 37–44.

Nishihara, H., Koyama, J., Hoki, N., Kajiya, F., Hironaga, M., and Kano, M., 1982, "Optical-fiber laser Doppler velocimeter for high-resolution measurement of pulsatile blood flows," *Applied Optics*, **21**(10), pp. 1785.

Nolte, D. D., and Pyrak-Nolte, L. J., 1991, "Stratified continuum percolation: Scaling geometry of hierarchical cascades," *Physical Review A*, **44**(10), pp. 6320–6333.

Nolte, D. D., Pyrak-Nolte, L. J., and Cook, N. G. W., 1989, "The fractal geometry of flow paths in natural fractures in rock and the approach to percolation," *Fractals in Geophysics*, pp. 111–138.

Ohara, J., Asami, K., Takeuchi, Y., and Sato, K. 2010, "Development of RIE-lag reduction technique for Si deep etching using double protection layer method," *IEEJ Transactions on Electrical and Electronic Engineering*, **5**, pp. 125–130.

Park, S.-M., Huh, Y. S., Craighead, H. G., and Erickson, D., 2009, "A method for nanofluidic device prototyping using elastomeric collapse," *Proceedings of the National Academy of Sciences*, **106**(37), pp. 15549–15554.

Patil, V. A., and Liburdy, J. A., 2012, "Optical measurement uncertainties due to refractive index mismatch for flow in porous media," *Experiments in Fluids*, **53**(5), pp. 1453–1468.

Perrin, C., Sorbie, K., Tardy, P., and Crawshaw, J., 2005, "Micro-PIV – a new technology for pore scale flow characterization in micromodels (SPE94078)," *67th EAGE Conference & Exhibition*, 13-16 June, Madrid, Spain.

Philip, J. R., 1973, "Flow in porous media," *Theoretical and Applied Mechanics*, pp. 279–294.

Pyrak-Nolte, L. J., Cook, N. G. W., and Nolte, D. D., 1988, "Fluid percolation through single fractures," *Geophysical Research Letters*, **15**(11), pp. 1247–1250.

Quake, S. R., 2000, "From micro to nanofabrication with soft materials," *Science*, **290** (5496), pp. 1536–1540.

Raffel, M., Willert, C. E., Wereley, S. T., and Kompenhans, J., 2007, Particle image velocimetry a practical guide, *Springer*, Heidelberg, Berlin.

Rangel-German, E. R., and Kovscek, A. R., 2006, "A micromodel investigation of two-phase matrix-fracture transfer mechanisms," *Water Resources Research*, **42**(3).

Rogers, J. A., and Nuzzo, R. G., 2005, "Recent progress in soft lithography," *Materials Today*, **8**(2), pp. 50–56.

Roman, S., Soulaine, C., Alsaud, M. A., Kovscek, A., and Tchelepi, H., 2016, "Particle velocimetry analysis of immiscible two-phase flow in micromodels," *Advances in Water Resources*, **95**, pp. 199–211.

Romano, M., Chabert, M., Cuenca, A., and Bodiguel, H., 2011, "Strong influence of geometrical heterogeneity on drainage in porous media," *Physical Review E*, **84**(6).

Sabbagh, R., Kazemi, M. A., Soltani, H., and Nobes, D. S., 2020, "Micro-and Macro-Scale Measurement of Flow Velocity in Porous Media: A Shadow Imaging Approach for 2D and 3D," *Optics* , **1**(1), pp. 71-87.

Samel, B., Chowdhury, M. K., and Stemme, G., 2007, "The fabrication of microfluidic structures by means of full-wafer adhesive bonding using a poly(dimethylsiloxane) catalyst, *Journal of Micromechanics and Microengineering*, **17**(8), pp. 1710–1714.

Sandnes, B., Knudsen, H. A., Måløy, K. J., and Flekkøy, E. G., 2007, "Labyrinth Patterns in Confined Granular-Fluid Systems," *Physical Review Letters*, **99**(3).

Santiago, J. G., Wereley, S. T., Meinhart, C. D., Beebe, D. J., and Adrian, R. J., 1998, "A particle image velocimetry system for microfluidics," *Experiments in Fluids*, **25**(4), pp. 316–319.

Sato, Y., Irisawa, G., Ishizuka, M., Hishida, K., and Maeda, M., 2003, "Visualization of convective mixing in microchannel by fluorescence imaging," *Measurement Science and Technology*, **14**(1), pp. 114–121.

Sbragaglia, M., Benzi, R., Biferale, L., Succi, S., Sugiyama, K., and Toschi, F., 2007, "Generalized lattice Boltzmann method with multirange pseudopotential," *Physical Review E*, **75**(2).

Sedaghat, M. H., Ghazanfari, M. H., Parvazdavani, Morshedi, S., 2013, "Experimental investigation of microscopic/macroscopic efficiency of polymer flooding in fractured heavy oil five-spot systems," *Journal of Energy Resource Technology*, **135**, pp. 032901-1.

Sedaghat, M., Mohammadzadeh, O., Kord, S., and Chatzis, I., 2016, "Heavy oil recovery using ASP flooding: A pore-level experimental study in fractured five-spot micromodels," *The Canadian Journal of Chemical Engineering*, **94**(4), pp. 779–791.

Semwogerere, D., and Weeks, E., 2005, Confocal microscopy, in encyclopedia of biomaterials and biomedical engineering, ed. Second, *Taylor and Francis, New York.*

Sen, D., Nobes, D. S., and Mitra, S. K., 2012, "Optical measurement of pore scale velocity field inside microporous media," *Microfluidics and Nanofluidics*, **12**(1-4), pp. 189–200.

Senn, T., Esquivel, J. P., Lörgen, M., Sabaté, N., and Löchel, B., 2010, "Replica molding for multilevel micro-/nanostructure replication," *Journal of Micromechanics and Microengineering*, **20**(12), pp. 129804.

Sharma, J., Inwood, S. B., and Kovscek, A., 2012. "Experiments and analysis of multiscale viscous fingering during forced imbibition," *Society of Petroleum Engineers Journal*, **17**(04), pp. 1142–1159.

Shinohara, K., Sugii, Y., Okamoto, K., Madarame, H., Hibara, A., Tokeshi, M., and Kitamori, T., 2004, "Measurement of pH field of chemically reacting flow in microfluidic devices by laser-induced fluorescence," *Measurement Science and Technology*, **15**(5), pp. 955–960.

Shor, L. M., Kosson, D. S., Rockne, K. J., Young, L. Y., and Taghon, G. L., 2004, "Combined effects of contaminant desorption and toxicity on risk from PAH contaminated sediments," *Risk Analysis*, **24**(5), pp. 1109–1120.

Sirivithayapakorn, S., and Keller, A., 2003, "Transport of colloids in saturated porous media: A pore-scale observation of the size exclusion effect and colloid acceleration," *Water Resources Research*, **39**(4).

Stöhr, M., Roth, K., and Jähne, B., 2003, "Measurement of 3D pore-scale flow in index-matched porous media," *Experiments in Fluids*, **35**(2), pp. 159–166.

Stoner, D. L., Watson, S. M., Stedtfeld, R. D., Meakin, P., Griffel, L. K., Tyler, T. L., Pegram, L. M., Barnes, J. M., and Deason, V. A., 2005, "Application of stereolithographic custom models for studying the impact of biofilms and mineral precipitation on fluid flow," *Applied and Environmental Microbiology*, **71**(12), pp. 8721–8728.

Suga, K., 2013, "Lattice Boltzmann methods for complex micro-flows: applicability and limitations for practical applications," *Fluid Dynamics Research*, **45**(3), pp. 034501.

Sugii, Y., and Okamoto, K., 2004, "Quantitative visualization of micro-tube flow using micro-PIV," *Journal of Visualization*, **7**(1), pp. 9–16.

Sugii, Y., Nishio, S., and Okamoto, K., 2002, "In vivo PIV measurement of red blood cell velocity field in microvessels considering mesentery motion," *Physiological Measurement*, **23**(2), pp. 403–416.

Tallakstad, K. T., Løvoll, G., Knudsen, H. A., Ramstad, T., Flekkøy, E. G., and Måløy, K. J., 2009, "Steady-state, simultaneous two-phase flow in porous media: An experimental study," *Physical Review E*, **80**(3).

Theodoropoulou, M., Sygouni, V., Karoutsos, V., and Tsakiroglou, C., 2005, "Relative permeability and capillary pressure functions of porous media as related to the displacement growth pattern," *International Journal of Multiphase Flow*, **31**(10-11), pp. 1155–1180.

Thielicke, W., and Stamhuis, E. J., 2014, "PIVlab – towards user-friendly, affordable and accurate digital particle image velocimetry in MATLAB," *Journal of Open Research Software*, **2**.

Thompson, L. F., Willson, C. G., and Bowden M. J., 1994, Introduction to microlithography, *American Chemical Society*, Washington DC.

Thompson, L.F., Wilson and Bowden M. J., "1983, Introduction to microlithography," ACS symposium series no. **219**, *American Chemical Society*, Washington DC.

Tóth, T., Horváth, D., and Tóth, Á., 2007, "Density fingering in spatially modulated Hele-Shaw cells," *The Journal of Chemical Physics*, **127**(23), pp. 234506.

Tsakiroglou, C. D., and Avraam, D. G., 2002, "Fabrication of a new class of porous media models for visualization studies of multiphase flow processes," *Journal of Materials Science*, **37**(2), pp. 353–363.

Tsakiroglou, C., Avraam, D., and Payatakes, A., 2007, "Transient and steady-state relative permeabilities from two-phase flow experiments in planar pore networks," *Advances in Water Resources*, **30**(9), pp. 1981–1992.

Tsakiroglou, C., Theodoropoulou, M., Karoutsos, V., Papanicolaou, D., and Sygouni, V., 2003, "Experimental study of the immiscible displacement of shear-thinning fluids in pore networks," *Journal of Colloid and Interface Science*, **267**(1), pp. 217–232.

Vayenas, D., Michalopoulou, E., Constantinides, G., Pavlou, S., and Payatakes, A., 2002, "Visualization experiments of biodegradation in porous media and calculation of the biodegradation rate," *Advances in Water Resources*, **25**(2), pp. 203–219.

Verma, M. K. S., Majumder, A., and Ghatak, A., 2006, "Embedded template-assisted fabrication of complex microchannels in PDMS and design of a microfluidic adhesive," *Langmuir*, **22**(24), pp. 10291–10295.

Wan, J., and Wilson, J. L., 1994, "Visualization of the role of the gas-water interface on the fate and transport of colloids in porous media," *Water Resources Research*, **30**(1), pp. 11–23.

Wan, J., Tokunaga, T. K., Tsang, C.-F., and Bodvarsson, G. S., 1996, "Improved glass micromodel methods for studies of flow and transport in fractured porous media," *Water Resources Research*, **32**(7), pp. 1955–1964.

Wang, J. S. Y., 1991, "Flow and transport in fractured rocks," *Reviews of Geophysics*, **29**(S1), pp. 254–262.

Wang, W., Shor, L. M., Leboeuf, E. J., Wikswo, J. P., and Kosson, D. S., 2005, "Mobility of protozoa through narrow channels," *Applied and Environmental Microbiology*, **71**(8), pp. 4628–4637.

Wegner, M. W., and Christie, J. M., 1983, "Chemical etching of deformation sub-structures in quartz," *Physics and Chemistry of Minerals*, **9**(2), pp. 67–78.

Wei, Z. A., Zheng, Z. C., and Yang, X., 2014, "Computation of flow through a three-dimensional periodic array of porous structures by a parallel immersed-boundary method," *ASME Journal of Fluids Engineering*, **136**(4).

Weidman, T. W., and Joshi, A. M., 1993, "New photo definable glass etch masks for entirely dry photolithography: Plasma deposited organosilicon hydride polymers," *Applied Physics Letters*, **62**(4), pp. 372–374.

Wereley, S. T., and Meinhart, C. D., 2010, "Recent advances in micro-particle image velocimetry," *Annual Review of Fluid Mechanics*, **42**(1), pp. 557–576.

Wereley, S. T., and Meinhart C. D., 2005, Micron-resolution particle image velocimetry, in microscale diagnostic techniques, *Springer-Verlag, New York.*

Wörner, M., 2012, "Numerical modeling of multiphase flows in microfluidics and micro process engineering: a review of methods and applications," *Microfluidics and Nanofluidics*, **12**(6), pp. 841–886.

Wu, Y.-shu, 2015, Multiphase fluid flow in porous and fractured reservoirs, *Gulf Professional Publishing, Amsterdam*.

Xia, Y., and Whitesides, G. M., 1998, "Soft lithography," *Annual Review of Materials Science*, **28**(1), pp. 153–184.

Xu, K., Liang, T., Zhu, P., Qi, P., Lu, J., Huh, C., and Balhoff, M., 2017, "A 2.5-D glass micromodel for investigation of multi-phase flow in porous media," *Lab on a Chip*, **17**(4), pp. 640–646.

Yeom, J., Wu, Y., Selby, J. C., and Shannon, M. A., 2005, "Maximum achievable aspect ratio in deep reactive ion etching of silicon due to aspect ratio dependent transport and the microloading effect," *Journal of Vacuum Science & Technology B: Microelectronics and Nanometer Structures*, **23**(6), pp. 2319.

Yu, F., Jiang, H., Xu, F., Fan, Z., Su, H., and Li, J., 2019, "New insights into flow physics in the EOR process based on 2.5D reservoir micromodels," *Journal of Petroleum Science and Engineering*, **181**, pp. 106214.

Yun, W., Ross, C. M., Roman, S., and Kovscek, A. R., 2017, "Creation of a dual-porosity and dual-depth micromodel for the study of multiphase flow in complex porous media," *Lab on a Chip*, **17**(8), pp. 1462–1474.

Zampieri, M. F., and Moreno, R. B. Z. L., 2013, "Water injection, polymer injection and polymer alternating water injection for enhanced oil recovery: a laboratory study," volume 6: *Polar and Arctic Sciences and Technology; Offshore Geotechnics; Petroleum Technology Symposium*, June 9–14, Nantes, France.

Zang, W., 1998, "Application of photo-luminescent volumetric imaging in multiphase dynamics in porous media", Ph.D. thesis, Cornell University.

Zhang, C., Dehoff, K., Hess, N., Oostrom, M., Wietsma, T. W., Valocchi, A. J., Fouke, B. W., and Werth, C. J., 2010, "Pore-scale study of transverse mixing induced $caco_3$ precipitation and permeability reduction in a model subsurface sedimentary system," *Environmental Science & Technology*, **44**(20), pp. 7833–7838.

Zhang, C., Oostrom, M., Grate, J. W., Wietsma, T. W., and Warner, M. G., 2011, "Liquid CO_2 displacement of water in a dual-permeability pore network micromodel," *Environmental Science & Technology*, **45**(17), pp. 7581–7588.

Zhou, J., Ellis, A. V., and Voelcker, N. H., 2010, "Recent developments in PDMS surface modification for microfluidic devices," *Electrophoresis*, **31**(1), pp. 2–16.

List of Publications

Journals

1. **Haque N,** Singh A, and Saha UK, (2019), "A noble method for rapid prototyping of porous micromodels applicable to enhanced oil recovery," *Journal of Physics: Conference Series*, Vol. 1276, pp. 012022.

2. **Haque N,** Singh A, and Saha UK, (2022), "Experimental visualization and analysis of multiphase immiscible flow in fractured micromodels using micro-particle image velocimetry," *ASME Journal of Energy Resources Technology,* Vol. 144, Issue 2, pp. 024501.

3. **Haque N,** Singh A, and Saha UK, (2020), "A new method to develop homogeneous and heterogeneous porous micromodels applicable to enhanced oil recovery and flow visualization experiments," *Communicated to ASME Journal of Energy Resources Technology.*

Conferences

4. **Haque N**, Singh A, and Saha UK, (2018), A noble method for rapid prototyping of porous micromodels applicable to enhanced oil recovery**,** ***I**nternational **C**onference on **R**ecent **A**dvances in **F**luid and **T**hermal Sciences*, December 5 – 7, Dubai, UAE. This paper appeared in Journal of Physics: Conference Series.

5. **Haque N,** Singh A, and Saha UK, (2018), Particle image velocimetry investigation of fluid flow in fractured porous media**,** *7th International and 45th National Fluid Mechanics and Fluid Power Conference* (FMFP-2018), December 10 -12, IIT Bombay, Mumbai.